Oxides for thermoelectricity

Sylvie Hébert
Laboratoire CRISMAT
UMR6508 CNRS et ENSICAEN

Collège de France
Avril 2013

Oxides for thermoelectricity

Aim of this seminar :
Best thermoelectric oxides / Show the specificities of oxides

Introduction :

Oxides specificities / Models for oxides /

Best thermoelectric oxides
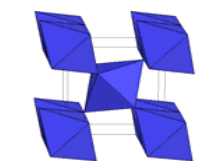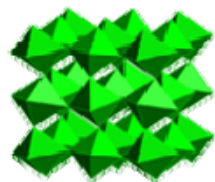
Increase
of the
carrier
density

- Semi – conductors : the Heikes formula
- Degenerate semi-conductors : best n type oxides
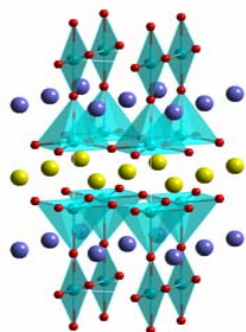- Na_xCoO_2 and misfit compounds
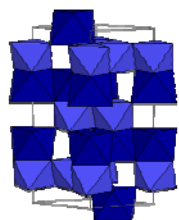
- Conclusion

Introduction

Why oxides?

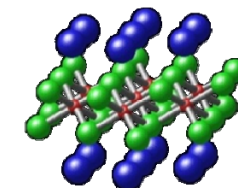## Strong interplay between spin/charge/lattice

Rutile, TiO$_2$

YBa$_2$Cu$_3$O$_7$

LiNbO$_3$
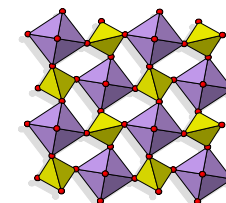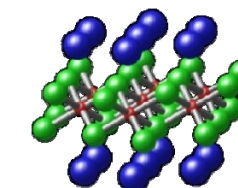
Property	Materials
Metals	CrO$_2$, Fe$_3$O$_4$, SrRuO$_3$
Insulators	Cr$_2$O$_3$, CoO, Fe$_2$O$_3$, Al$_2$O$_3$
Metal-Insulator Transition	VO$_2$, V$_2$O$_3$
Superconductors	Ba(Bi,Pb)O$_3$, YBa$_2$Cu$_3$O$_7$
Piezo- and Ferroelectrics	Pb(Zr,Ti)O$_3$, BaTiO$_3$
Catalysts (chemical, photo-)	TiO$_2$, LaCoO$_3$, BiMoO$_4$
Ferro-, Antiferro-, Ferrimagnets	CrO$_2$, MnO, MnFe$_2$O$_4$
Pigments	TiO$_2$, CoAl$_2$O$_4$, Co$_3$(PO$_4$)$_2$
Sensors	Ca$_x$Zr$_{1-x}$O$_{2-x}$, SnO$_2$
Negative Thermal Expansion	ZrW$_2$O$_8$
Ionic Conductors (battery, SOFC)	Li$_x$MnO$_2$, Ca$_x$Zr$_{1-x}$O$_{2-x}$
Thermoelectrics	Na$_x$CoO$_2$
Non-Linear Optics	LiNbO$_3$

LiMnO$_2$

ZrW$_2$O$_8$

Na$_x$CoO$_2$

From M. Subramanian, OSU

Large family of compounds,
Can be cheap, environment friendly and resistant in air

High Tc superconductors

PRB46, 14928 (1992)

Systematics in the thermoelectric power of high-T_c oxides

S. D. Obertelli and J. R. Cooper*

Interdisciplinary Research Centre in Superconductivity, Madingley Road, Cambridge CB3 0HE, United Kingdom

J. L. Tallon

New Zealand Institute for Industrial Research and Development,
P.O. Box 31310, Lower Hutt, New Zealand

Many superconducting cuprates show a parabolic variation of T_c with hole concentration p, there being a minimum and a maximum hole concentration for superconductivity. Thermoelectric power (TEP) measurements reported here as a function of p for a number of oxides reveal several important trends: (1) close similarities in the TEP of several compounds and a change in sign of the room-temperature TEP near the maximum T_c, (2) continuity in the TEP when doping across the two superconducting-nonsuperconducting boundaries, and (3) a universal correspondence of the room-temperature TEP with p over the whole range of doping.
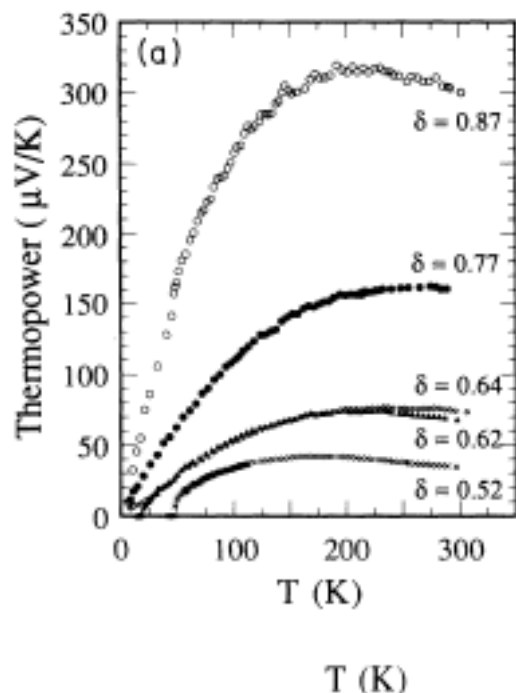
Correlation between Seebeck / doping / Critical temperature

$YBa_2Cu_3O_{7-\delta}$

FIG. 2. (a) Thermoelectric power vs temperature for underdoped $YBa_2Cu_3O_{7-\delta}$ with $0.52 \leq \delta \leq 0.87$. For $\delta > 0.5$ the estimated uncertainty in S relative to other preparation batches
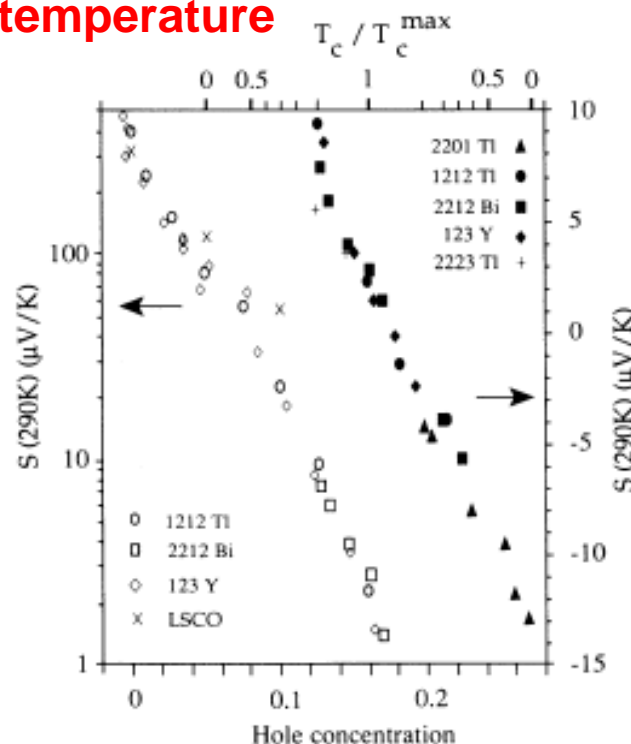
FIG. 3. Room-temperature thermoelectric power $S(290 \text{ K})$ vs hole concentration (and T_c/T_c^{max}) for various high-T_c cuprates in both the underdoped (logarithmic scale) and overdoped (linear scale) regions. $La_{2-x}Sr_xCuO_4$ (LSCO) data from Ref. 33.
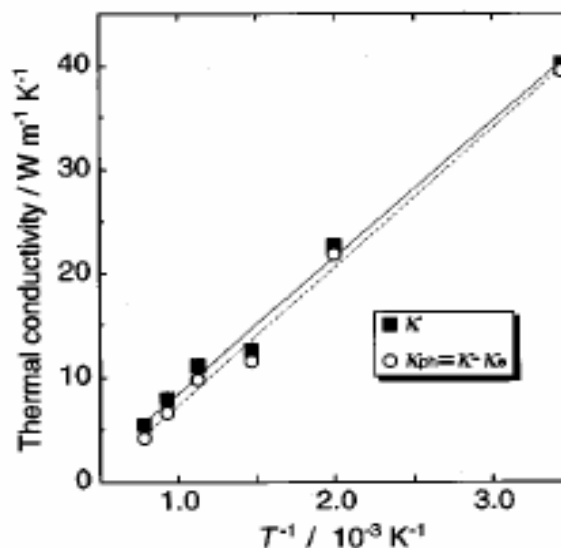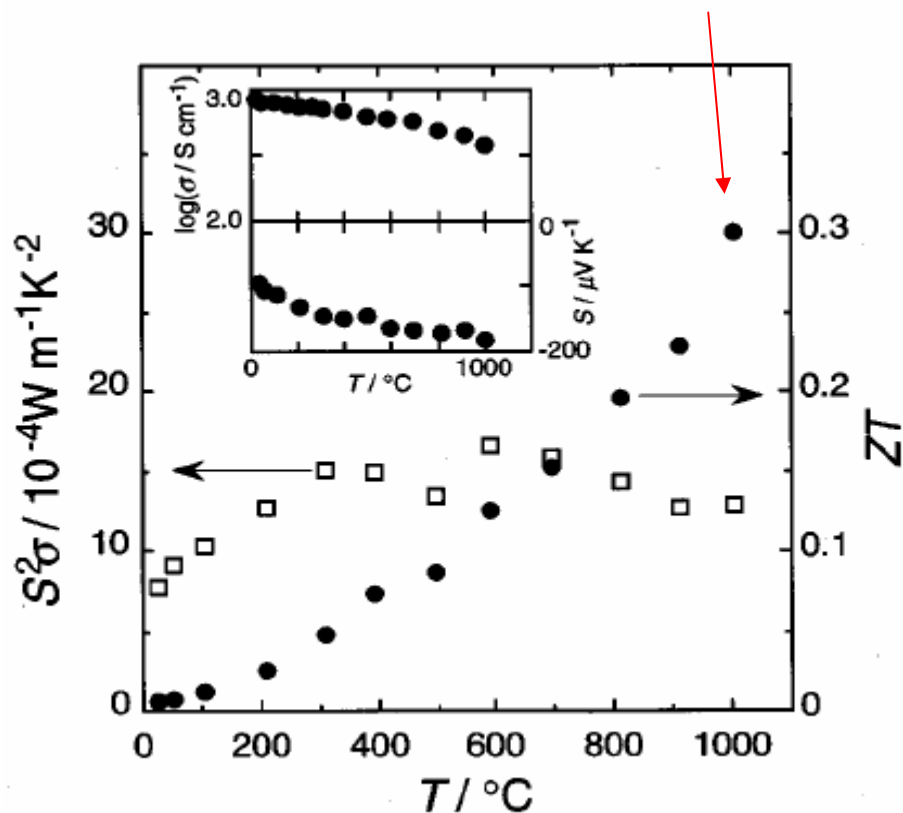
Zn$_{1-x}$Al$_x$O (x = 0 – 0.1)

ZT = 0.3

Broadband model for extrinsic n type semiconductor

$$\sigma = ne\mu,$$

$$S = -(k/e)[\ln(N_v/n) + A],$$

Large mobility of the carriers : 3 – 7cm^2/Vs

= 40Wm^{-1}K^{-1} at 300K
=5.4 Wm^{-1}K^{-1} at 1000°C

But κ is too high !!!

In conclusion, this is the first time that an ionic material such as oxide exhibits the thermoelectric performance comparable to those of the conventional thermoelectric materials.

M. Ohtaki et al., JAP79, 1816 (1996)

$Na_{0.7}CoO_2$
' Phonon Glass / Electron crystal '

I. Terasaki et al., Phys. Rev. B 56, R12685 (1997)

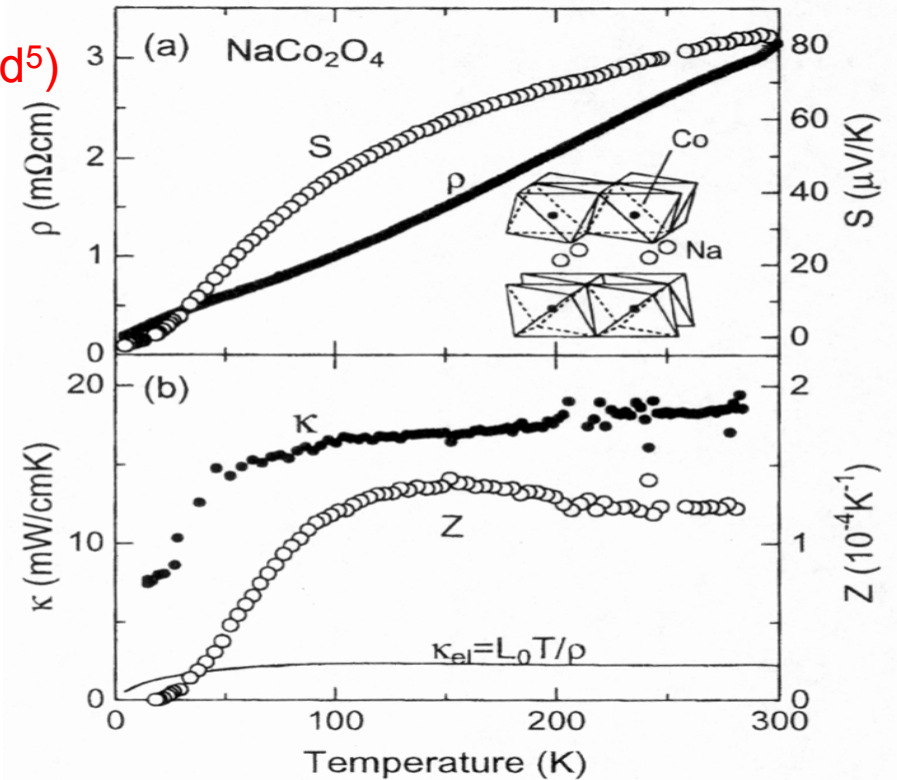$Na_xCoO_2 : Na^+_x Co^{3+}_x Co^{4+}_{1-x} O_2$
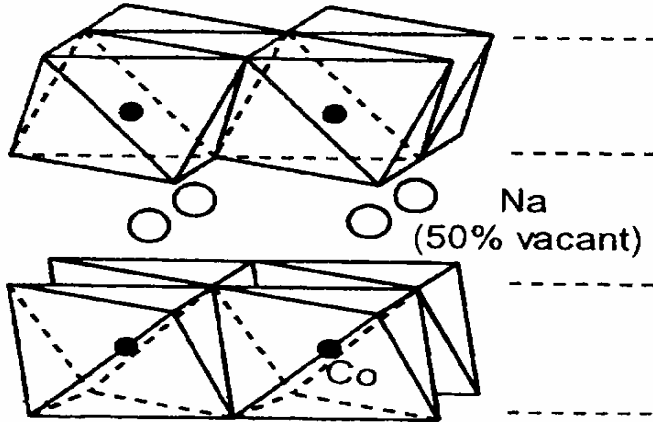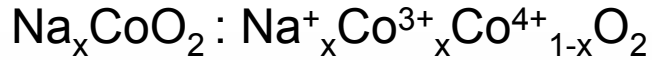
$Co^{3+} (3d^6) / Co^{4+} (3d^5)$

Measurements on polycrystals

At 300K
Metallicity (crystals) $\rho \sim 0.2\ m\Omega\ cm$
Large S $S \sim +80\ \mu V/K$
Small κ (polycrystals) $\kappa \sim 2 Wm^{-1}K^{-1}$
        (crystals) $\kappa \sim 5 Wm^{-1}K^{-1}$

Power factor $P = S^2/\rho$ at 300K

$Na_{0.7}CoO_2$

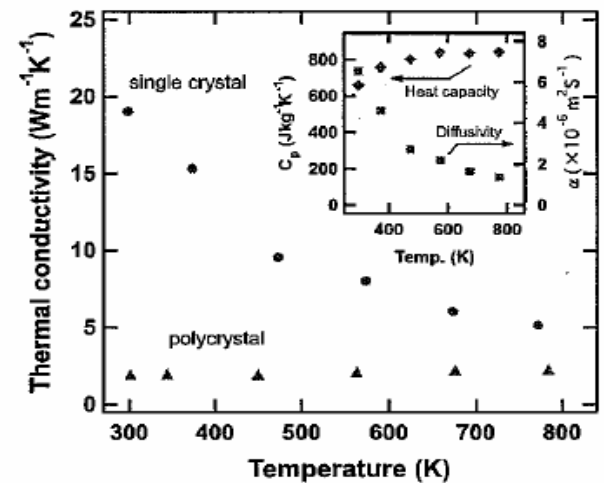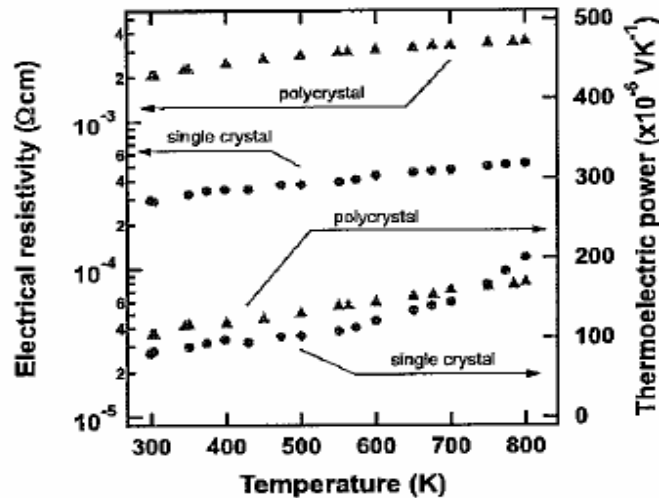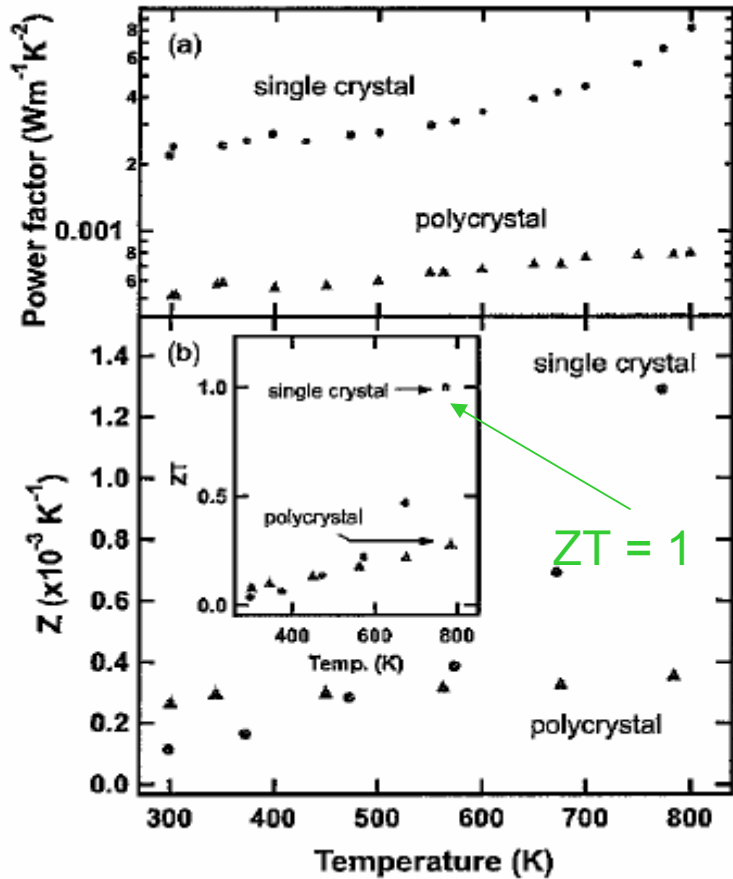$P = 50\ 10^{-4}\ WK^{-2}m^{-1}$

Bi_2Te_3

$P = 40\ 10^{-4}\ WK^{-2}m^{-1}$

High T properties of Na_xCoO_2

K. Fujita et al. JJAP40, 4644 (2001)

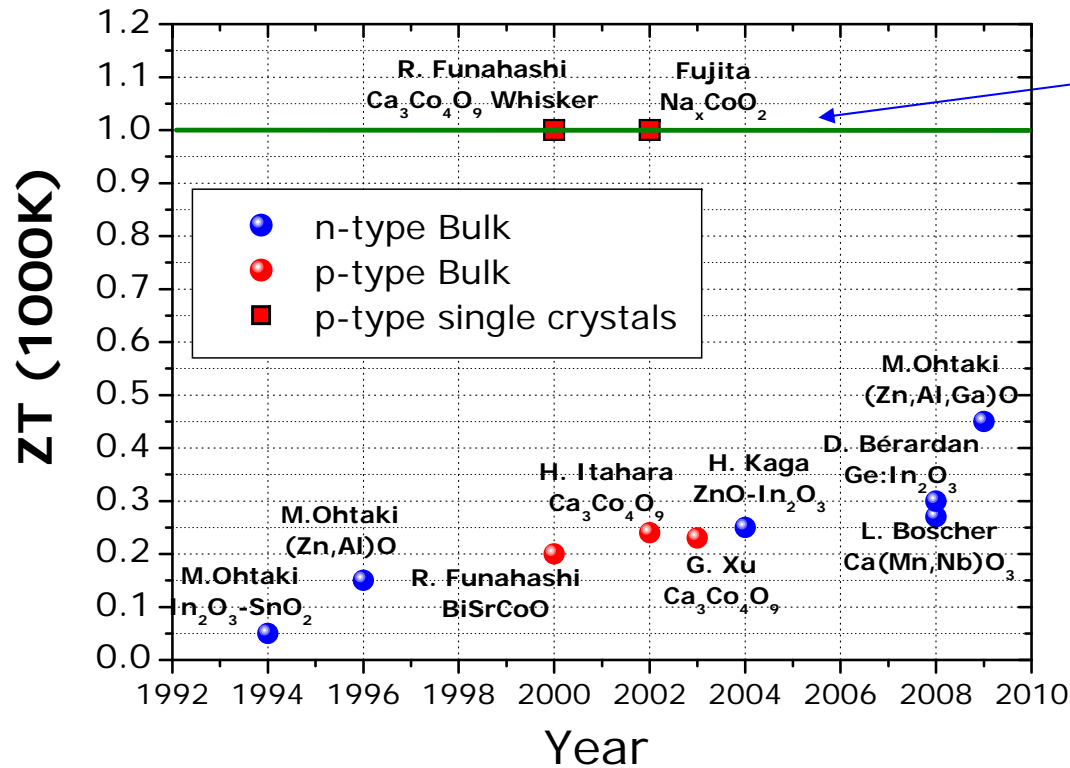Crystal and polycrystal measurements

Crystals : 1.5 ×1.5 × 0.03 mm³

ZT ~ 1 (for crystals only) at 800K

ZT of oxides

2 different families for the best thermoelectric oxides
• Type p : oxides related to Na_xCoO_2, metallic <u>and</u> large S
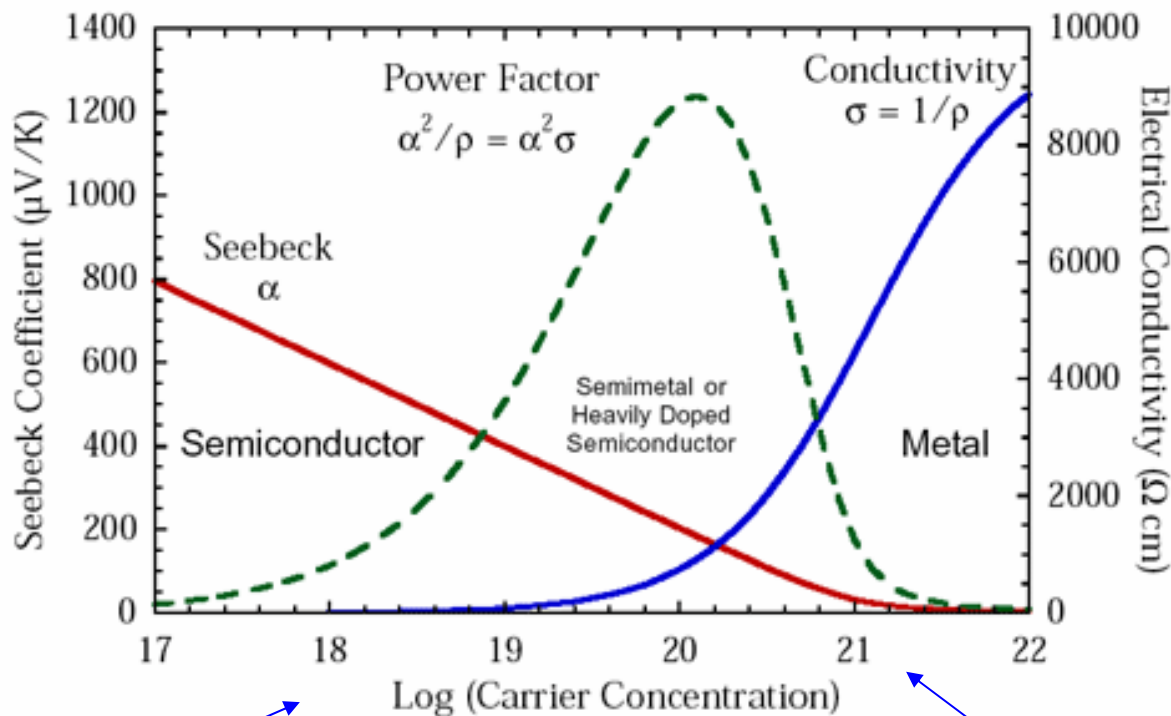• Type n : 'transparent conducting oxides', degenerate semi-conductors

ZT (type p single crystals) > ZT (type n)

p type : Na_xCoO_2, Misfit oxides

n type : TCOs

Oxides

Plot: Seebeck Coefficient (μV/K) vs Log (Carrier Concentration) with Electrical Conductivity (Ω cm) on the right axis.

- Power Factor $\alpha^2/\rho = \alpha^2\sigma$
- Conductivity $\sigma = 1/\rho$
- Seebeck α
- Semiconductor
- Semimetal or Heavily Doped Semiconductor
- Metal

Semi-conductors
Large
S, large ρ
n and p type
Increase of S
through Heikes?

Transparent conductors, Delafossites
Large S, small ρ
Large κ
Mostly n type (some p type)
Reduction of κ
through nanostructuration?

Misfits
Na_xCoO_2
Large S
+ metallic ρ
small κ
p type
Model system
Texturation problems

Specificities of oxides

Low T limit : Mott's formula

$$S = \frac{\pi^2 k_B^2}{3e} T \left(\frac{\partial \ln \sigma(E)}{\partial E} \right)_{E=E_F}$$
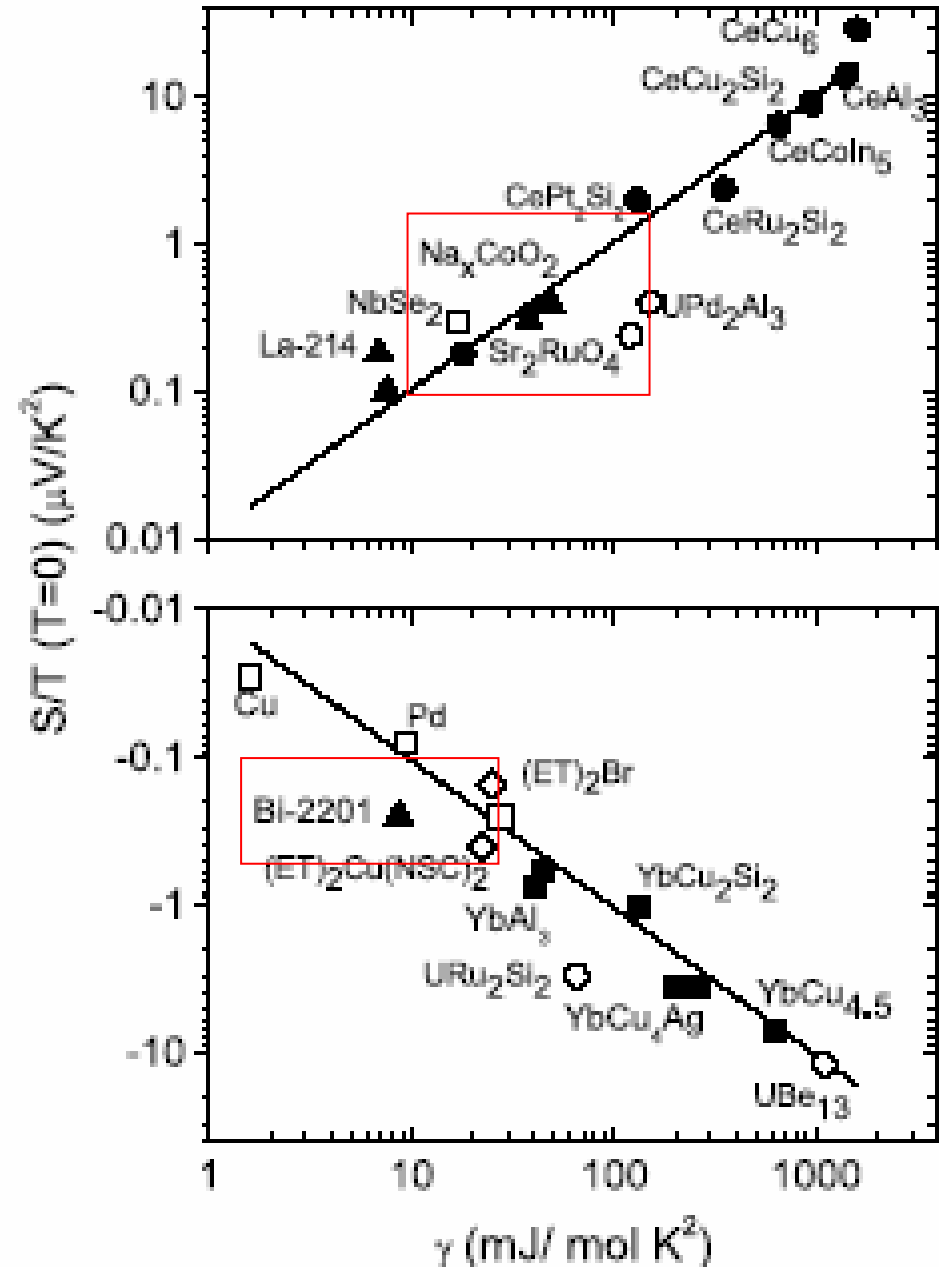
$$S = -\frac{\pi^2}{3} \frac{k_B^2 T}{e} \frac{N(E_F)}{n}$$

$$C_{el} / T = \gamma = \frac{\pi^2}{3} k_B^2 N(E_F)$$

Universal value for the ratio of S / γ

Limit T $\rightarrow$ 0

$$q = \frac{S}{T} \frac{N_{Av} e}{\gamma} = \text{cste}$$

$$0.5 < |q| < 2$$

K. Behnia et al. JPCM 16, 5187 (2004)

Models

The Heikes formula

High T limit

Thermopower in the correlated hopping regime

P. M. Chaikin*

Department of Physics, University of California, Los Angeles, California 90024

G. Beni

Bell Laboratories, Murray Hill, New Jersey 07974
(Received 16 June 1975)

The high-temperature limit for the thermopower of a system of interacting localized carriers is governed entirely by the entropy change per added carrier. The calculation of this quantity reduces to a simple combinatorial problem dependent only on the density of carriers and the interactions stronger than the thermal energy. We have thus been able to generalize the Heikes formula to include several cases of interacting Fermi systems with spin.

'Simple combinatorial problem'
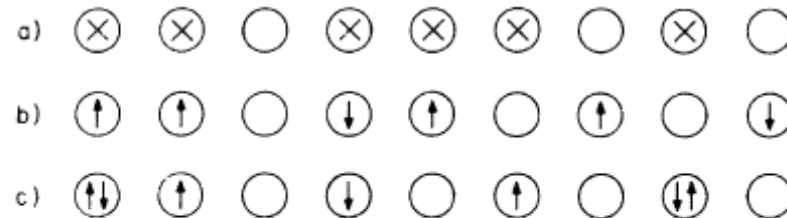
Calculated for organic thermoelectrics

FIG. 1. Possible high–temperature site configuration of (a) spinless fermions; (b) electrons with an infinite on-site repulsion; and (c) electrons with no interactions.

P. M. Chaikin et al. Phys. Rev. B 13, 647 (1976)

The Heikes formula

The Hubbard model

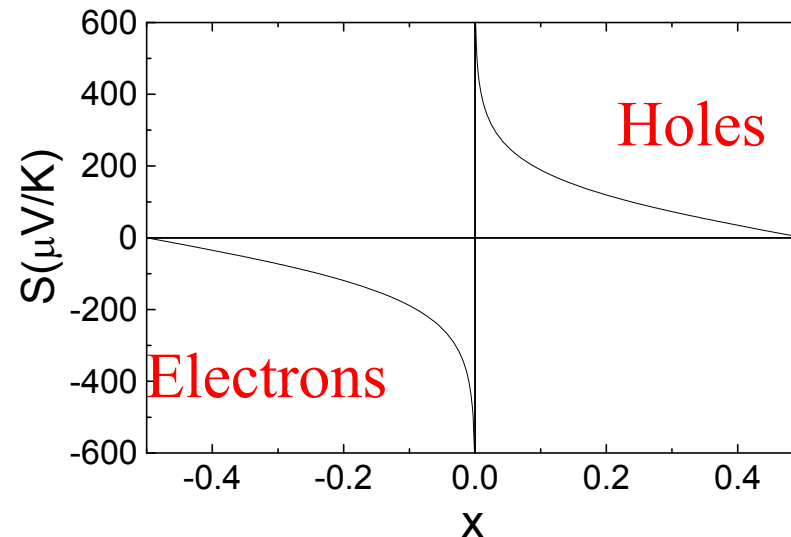$$S = \frac{-S^{(2)}/S^{(1)} + \mu/|e|}{T} \rightarrow \frac{\mu/|e|}{T} \qquad \text{for } T \rightarrow \infty$$

$S^{(1)}$, $S^{(2)}$: depend on v and Q, velocity and energy operators

Valid for narrow band systems (localized correlated particles)

Limit $T \rightarrow \infty$: S ~ entropy / carrier

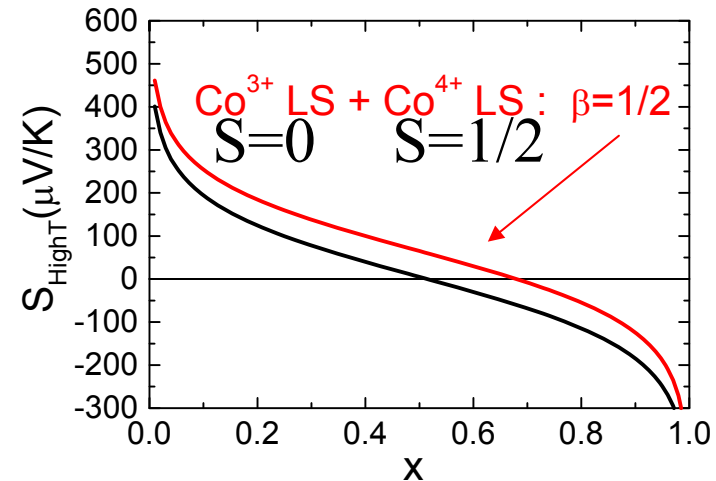$$S = \frac{-k_B}{|e|} \ln(\frac{1-x}{x})$$

x = concentration of carriers

P. M. Chaikin et al. Phys. Rev. B 13, 647 (1976)

Spin entropy

Extra term in the Heikes formula due to the spin degeneracy

Mixed valency cation M^{n+} / $M^{(n+1)+}$:

$$\beta = \frac{2S_n + 1}{2S_{n+1} + 1}$$

$$S = -\frac{k_B}{|e|} \ln(\beta \frac{1-x}{x})$$

J. P. Doumerc JSSC 110, 419 (1994)

Na_xCoO_2 :

Spin and orbital degeneracy Co^{3+} ($3d^6$)/Co^{4+} ($3d^5$)

J. P. Doumerc JSSC 109, 419 (1994)
W. Koshibae et al., Phys. Rev. B 62, 6869 (2000)

$$S = -\frac{k_B}{e} \ln\left(\frac{g_3}{g_4} \frac{x}{1-x}\right)$$

(a)
Co³⁺ e_g === 1   Co⁴⁺ e_g === 6
LS state, S=0   LS state, S=1/2

(b)
Co³⁺ e_g 18   Co⁴⁺ e_g 24
IS state, S=1   IS state, S=3/2

(c)
Co³⁺ e_g 15   Co⁴⁺ e_g 6
HS state, S=2   HS state, S=5/2

$g_4/g_3 = 6$

LS+LS
LS+(HS+LS)
HS+HS
(HS+LS)+HS
(HS+LS+IS)+(HS+LS+IS)

$S_{HT}(\mu V/K)$

x : Co^{4+} concentration
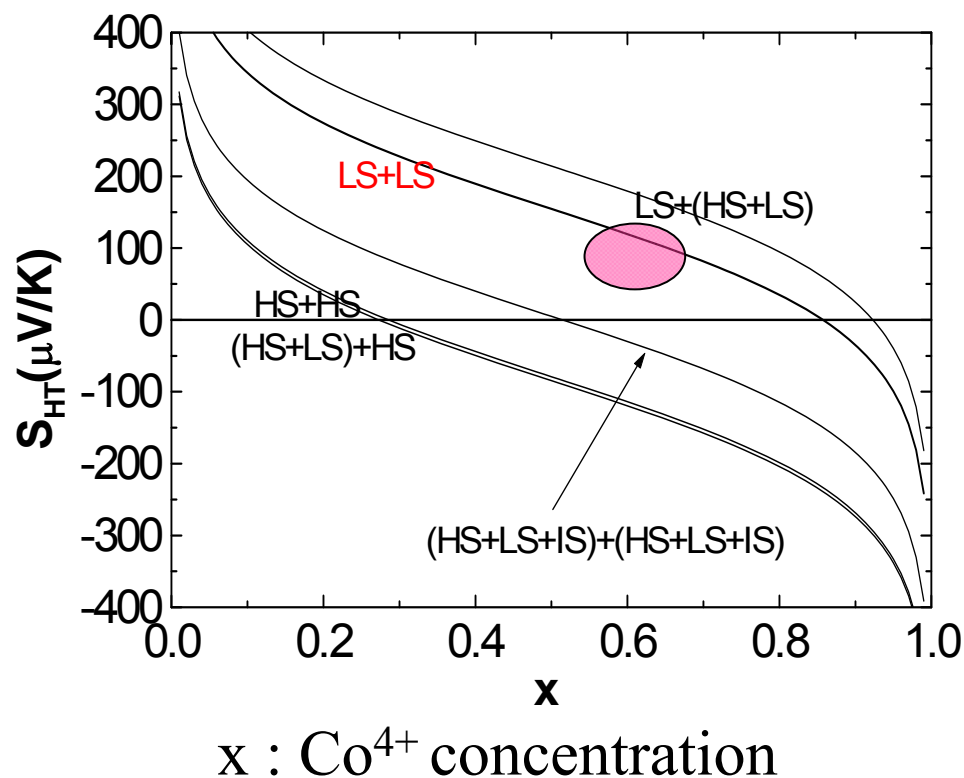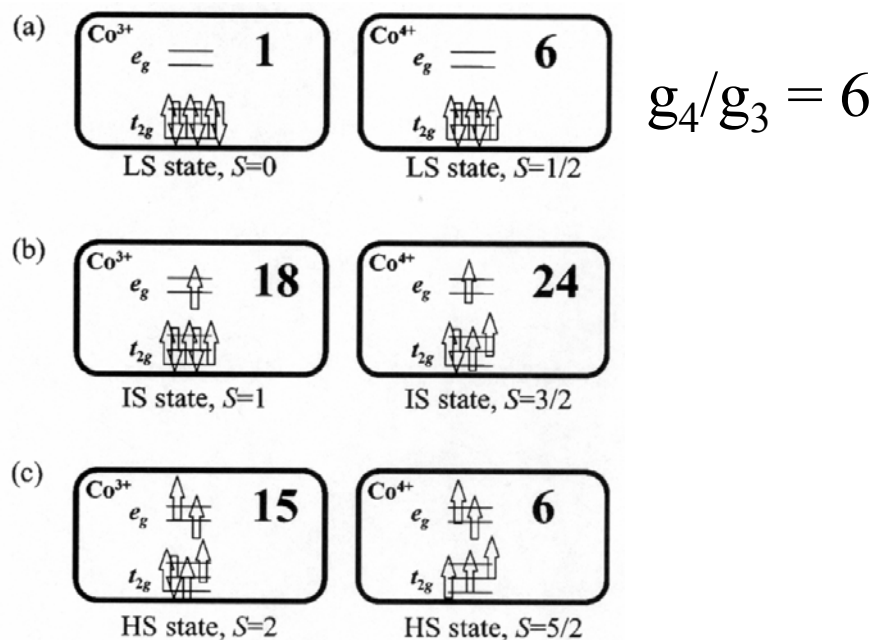
Large S in Na_xCoO_2
Origin of the metallicity ?

Models
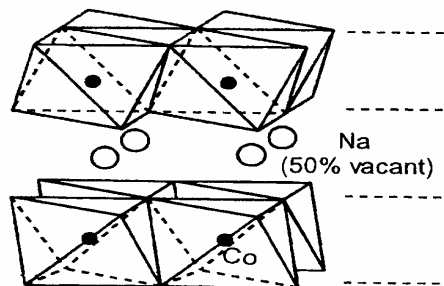
Band structure?

Rhombohedral crystalline field
Lifting of the t_{2g} levels degeneracy

D. J. Singh, Phys. Rev. B 61, 13397 (2000)

Na (50% vacant)

Co

ε

DOS

ε_F

t_{2g} orbitals {

a_{1g} : narrow band (localized)

e'_g : broad band (itinerant)

Metallic <u>and</u> large S
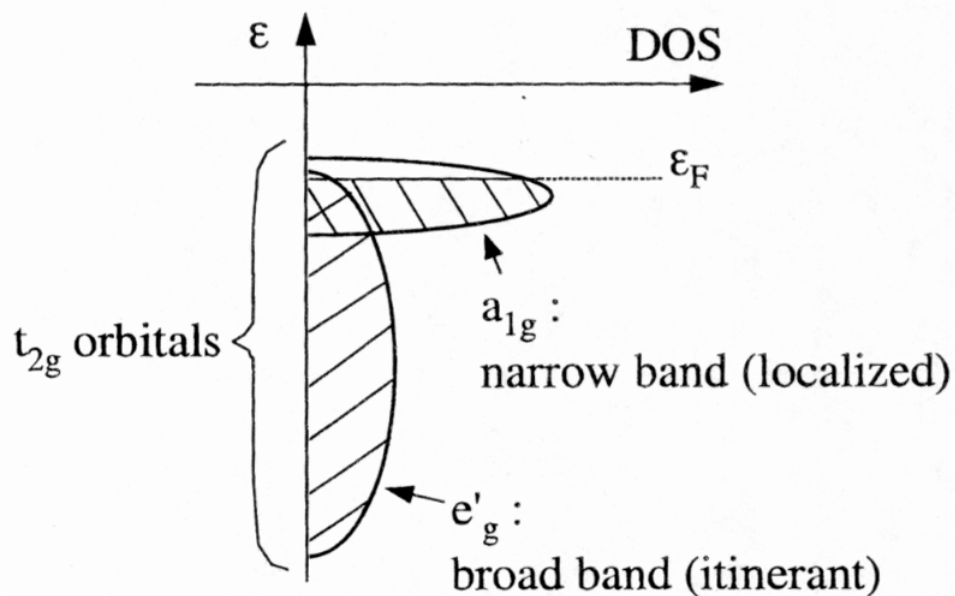
Peak of $N(E_F)$

$$\frac{S}{T} = \frac{\pi^2 k^2}{3e}\left(\frac{d\ln(\sigma)}{dE}\right)_{E=E_F}$$

avec $\sigma = N(E)<v_F(E)^2>$

⇨ **S = +110µV/K** at 300K
calculated for $NaCo_2O_4$

a_{1g} : localized moments / heavy holes
e'_g : mobile carriers / light holes

T. Yamamoto et al., Phys. Rev. B 65, 184434 (2002)

'Pudding mold model' : K. Kuroki et al., JPSJ76, 083707 (2007)

'Thermoelectric effects in a strongly correlated model for Na_xCoO_2'

t-J model : t = hopping and J = spin coupling
Kubo formalism
Valid at any T (different from the limit $T \to \infty$)
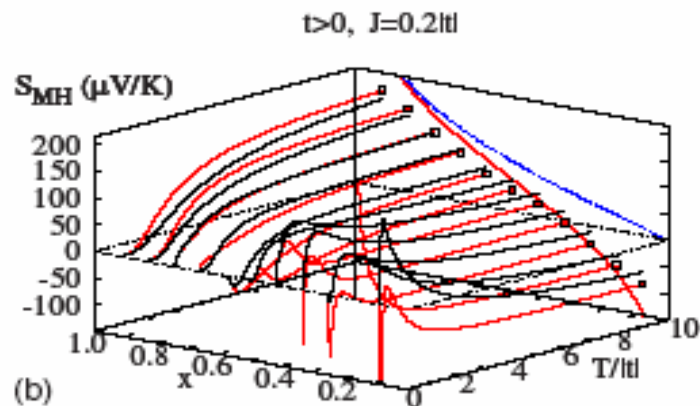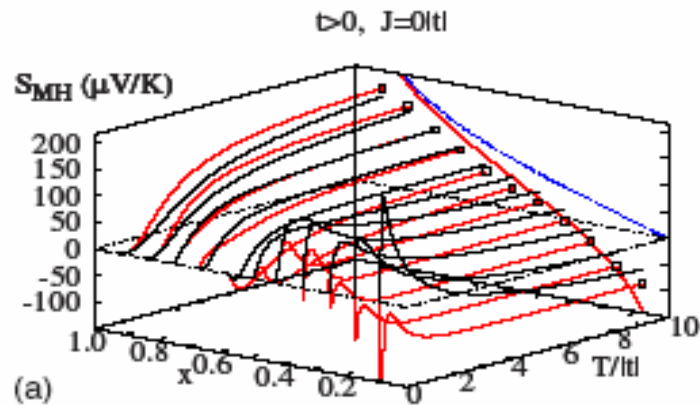
$$S = S_{transport} + S_{Heikes}$$

Black : Heikes formula
Red : $S = S_{transport} + S_{Heikes}$

In a large part of the phase diagram (x, T, t), the Heikes formula gives a good estimate of S

M. R. Peterson et al., PRB76, 165118 (2007)
M. R. Peterson et al., PRB82, 195105 (2010)

Semi-conducteurs : The Heikes formula
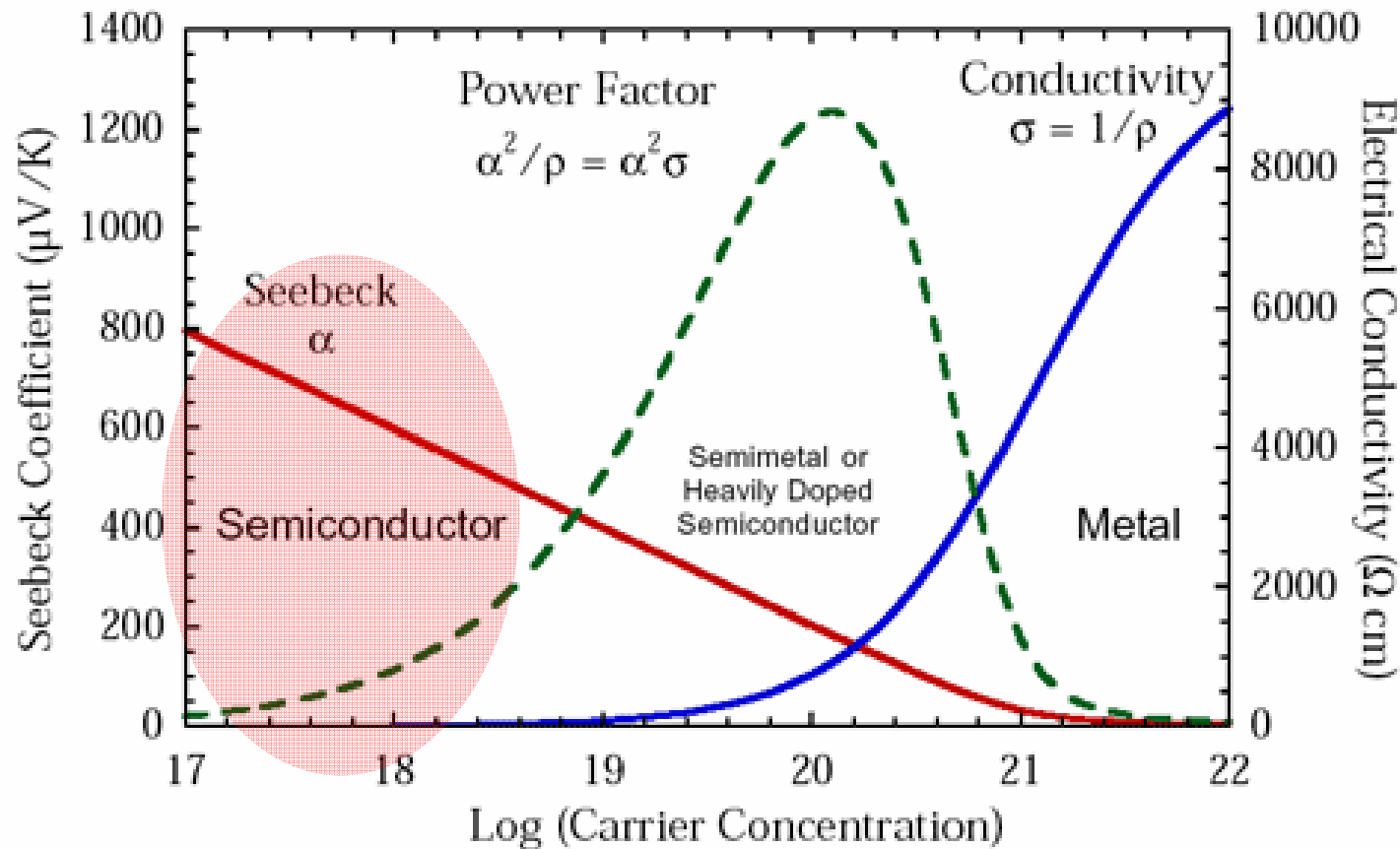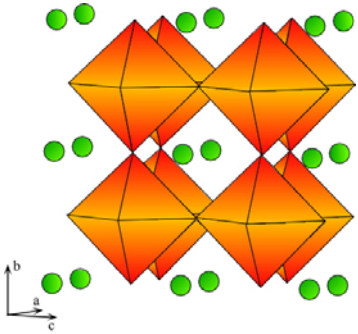
LaCoO$_3$

Heikes formula : possible change of sign

$$S = -\frac{k_B}{e}\ln\left(\frac{1-x}{x}\right)$$

x = carrier concentration
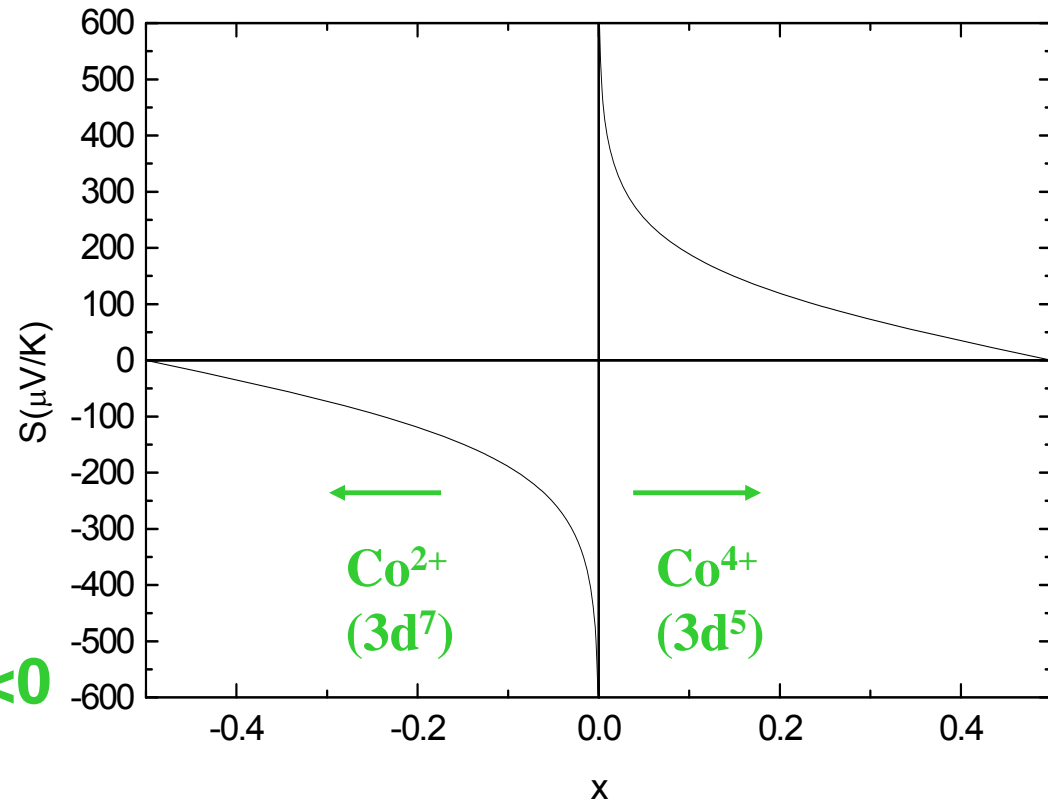
Depending on x, S>0 or S<0

Small x ➡ |S| very large

S(μV/K)

Co^{2+}
(3d^7)

Co^{4+}
(3d^5)

x

LaCoO$_3$: A site substitution

LaCoO$_3$ x~0 : La^{3+}Co^{3+}O$_3$

Sr^{2+} x>0 : La$_{1-x}$Sr$_x$(Co^{3+}/Co^{4+})O$_3$

Ce^{4+} x<0 : La$_{1-x}$Ce$_x$(Co^{3+}/Co^{2+})O$_3$
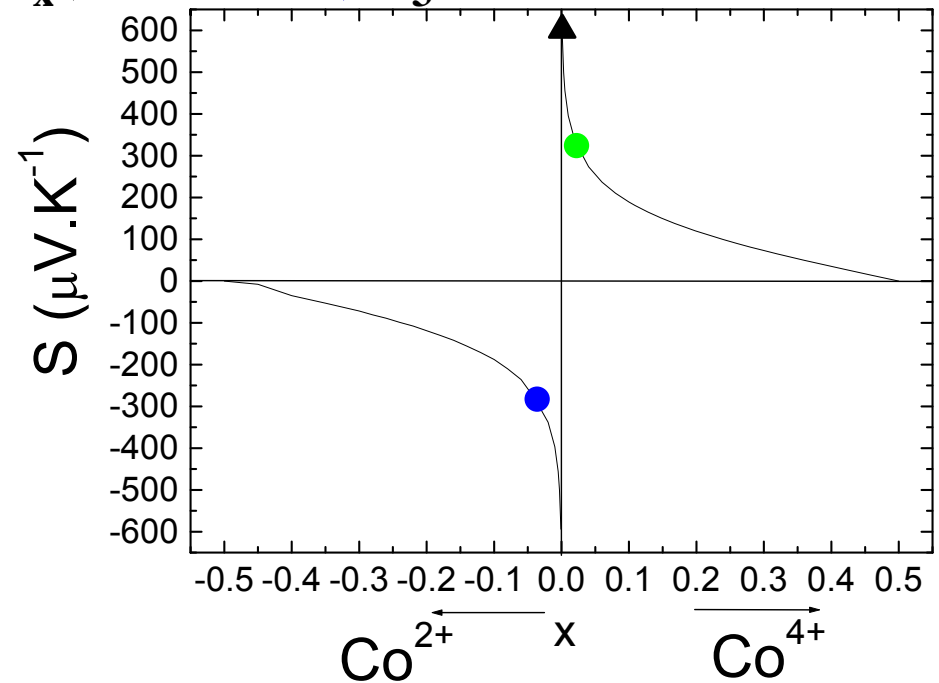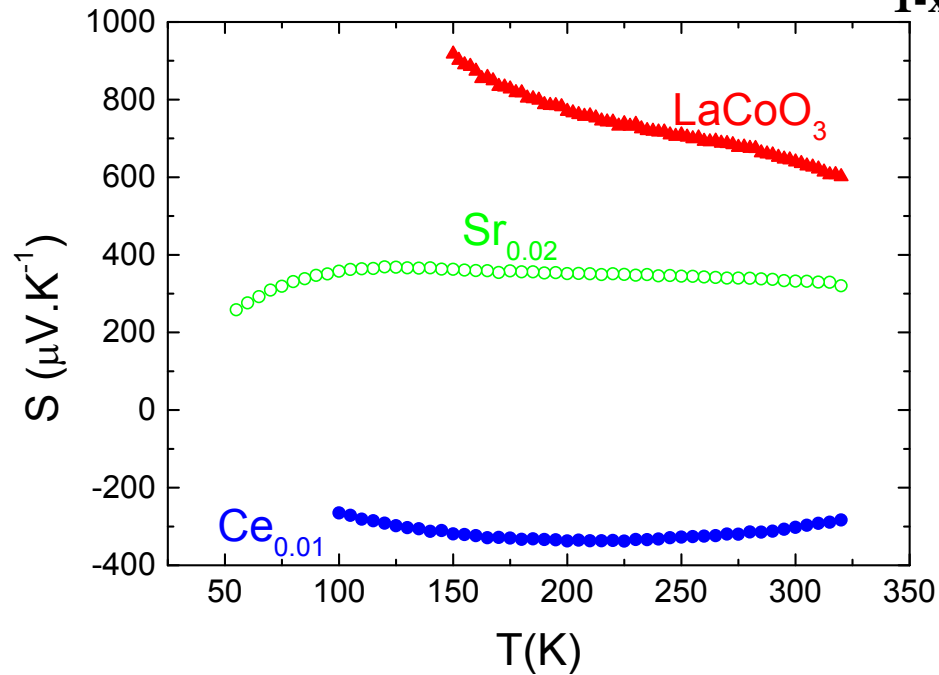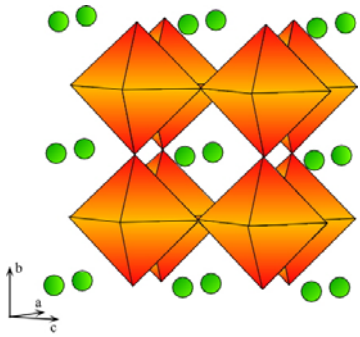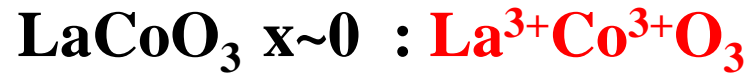
A. Maignan et al., EPJB 39, 145 (2004)

LaCoO$_3$
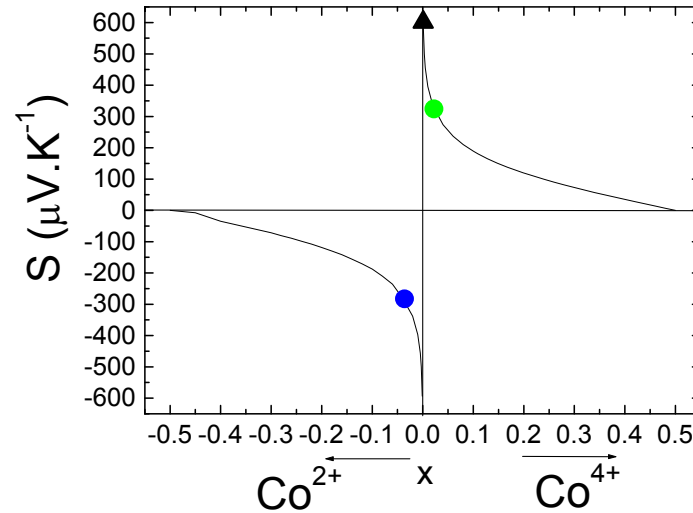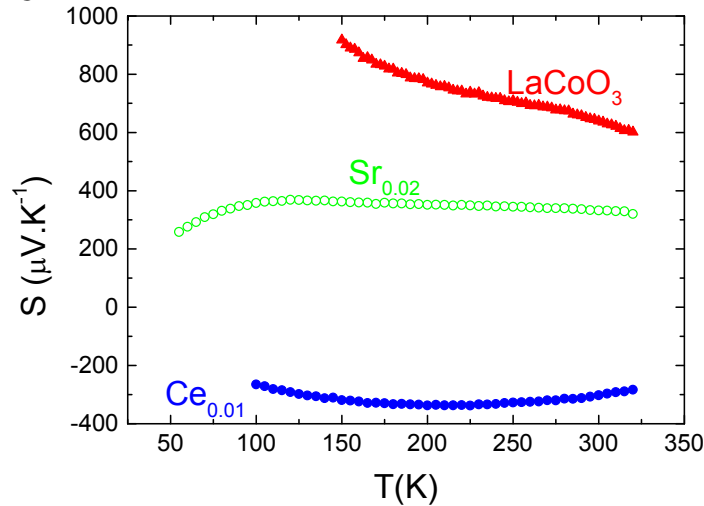
A. Maignan et al., EPJB 39, 145 (2004)

Formule de Heikes pour S, avec

$$S = -\frac{k_B}{e} \ln\left(\frac{g_3}{g_4} \frac{x}{1-x}\right)$$

Co^{4+} LS

Co^{3+} IS
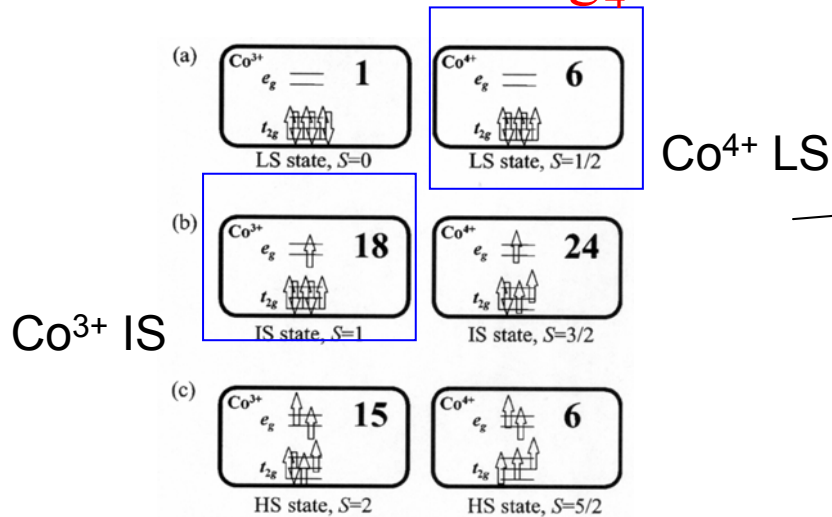
Spin only degeneracy
g$_3$ = 3 / g$_4$ = 2
(experimentally 1.8)

g$_2$ = 4
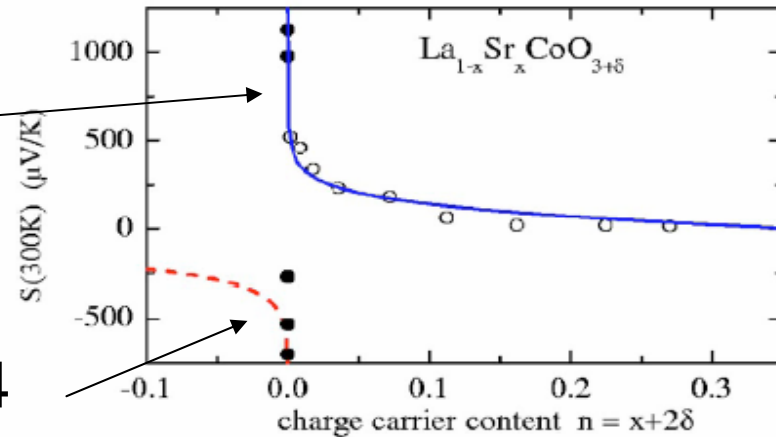
Cobaltites '112' :
A. A. Taskin et al., PRB73, 121101 (2006)

K. Berggold et al., PRB72, 155116 (2005)

LaCoO$_3$

Single crystals measurements
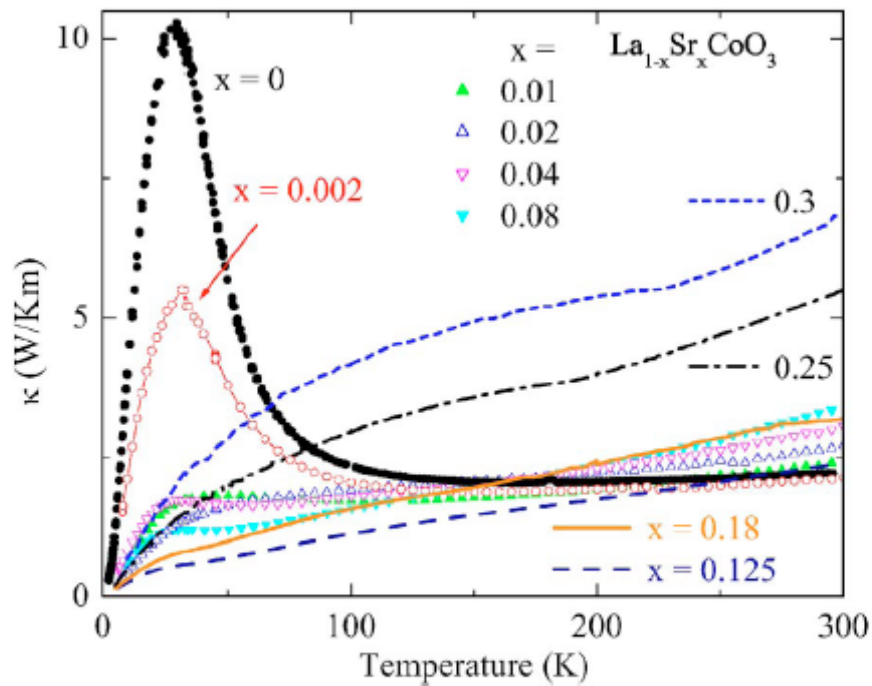
FIG. 1. (Color online) Thermal conductivity of La$_{1-x}$Sr$_x$CoO$_3$ a function of temperature for different doping x.

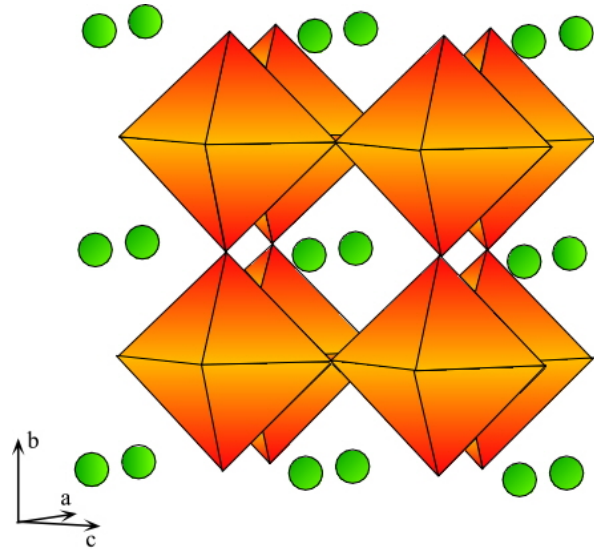FIG. 5. (Color online) Figure of merit of La$_{1-x}$Sr$_x$CoO$_3$ as a function of temperature for different doping x.

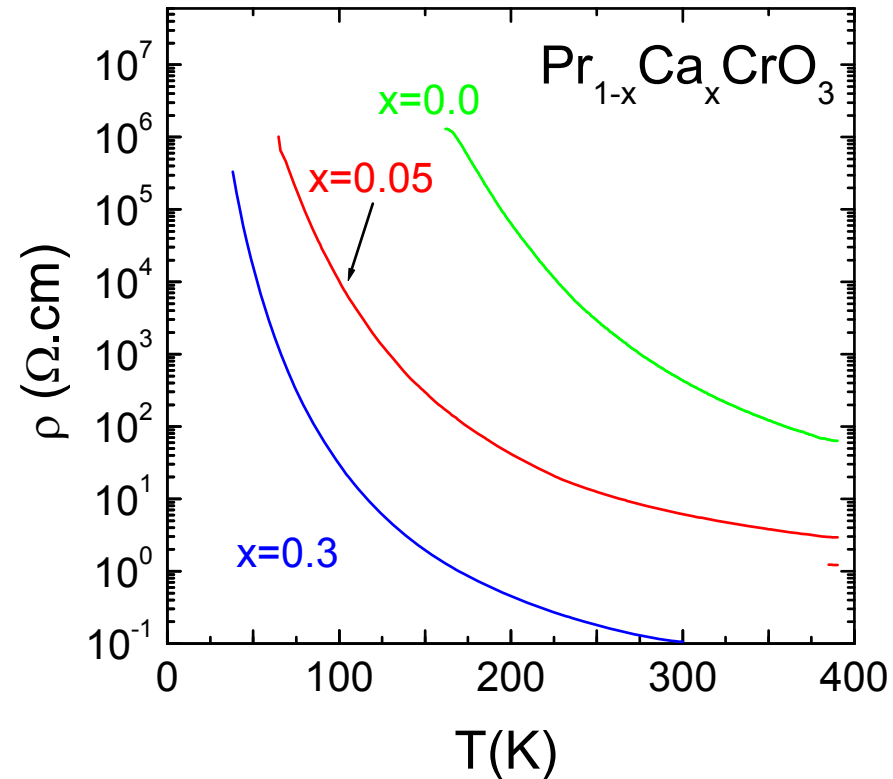*K. Berggold et al., PRB72, 155116 (2005)*

Orthochromites

Type p : $Pr_{1-x}Ca_xCrO_3$

Perovskite structure

$$Pr^{3+}_{1-x}Ca^{2+}_xCr^{3+/4+}O_3 : 3d^3/3d^2$$

Introduction of holes :
Activated behavior with
a decrease of ρ

S. Pal et al., Eur. Phys. J. B 53, 5 (2006)

Orthochromites

Type p : $Pr_{1-x}Ca_xCrO_3$

$$Pr^{3+}_{1-x}Ca^{2+}_xCr^{3+/4+}O_3 : 3d^3/3d^2$$
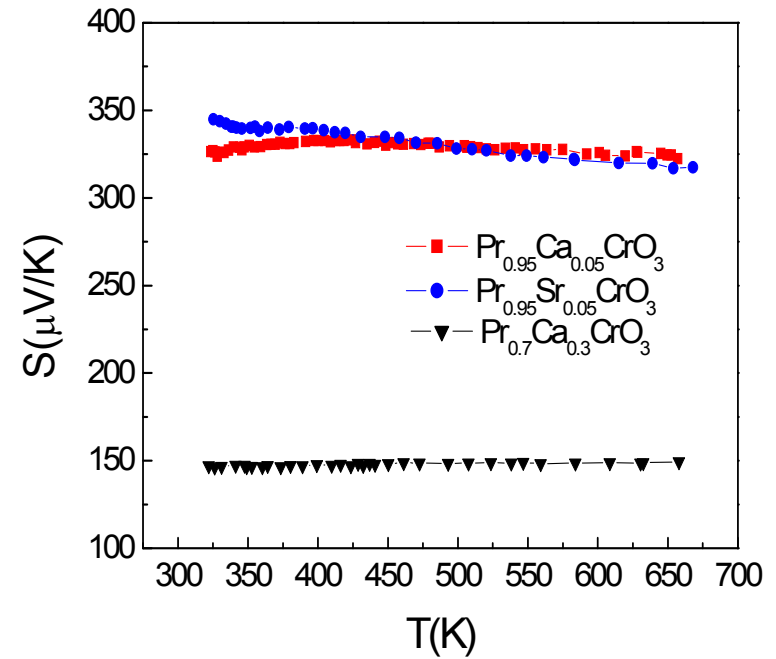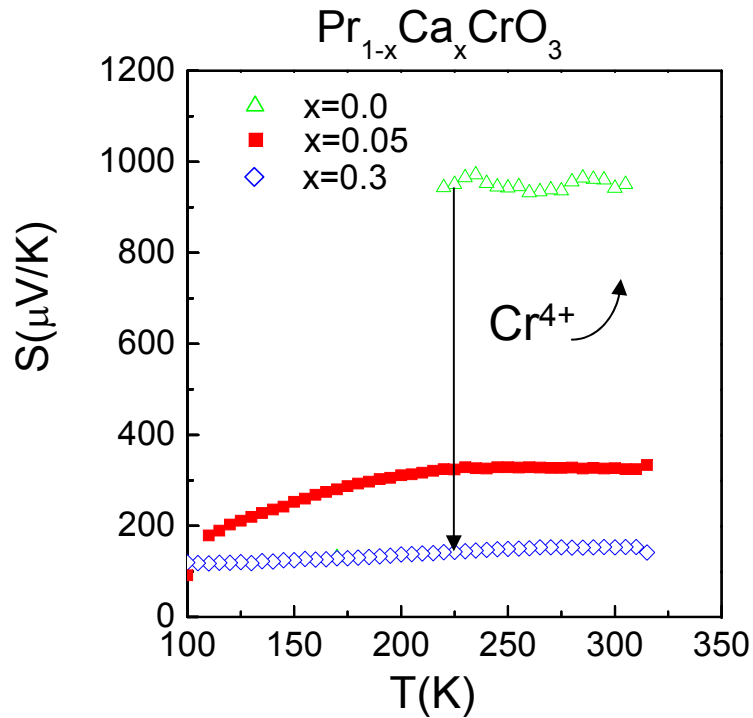
Decrease of S induced by doping

S constant from 200K to high T

S. Pal et al., Eur. Phys. J. B 53, 5 (2006)
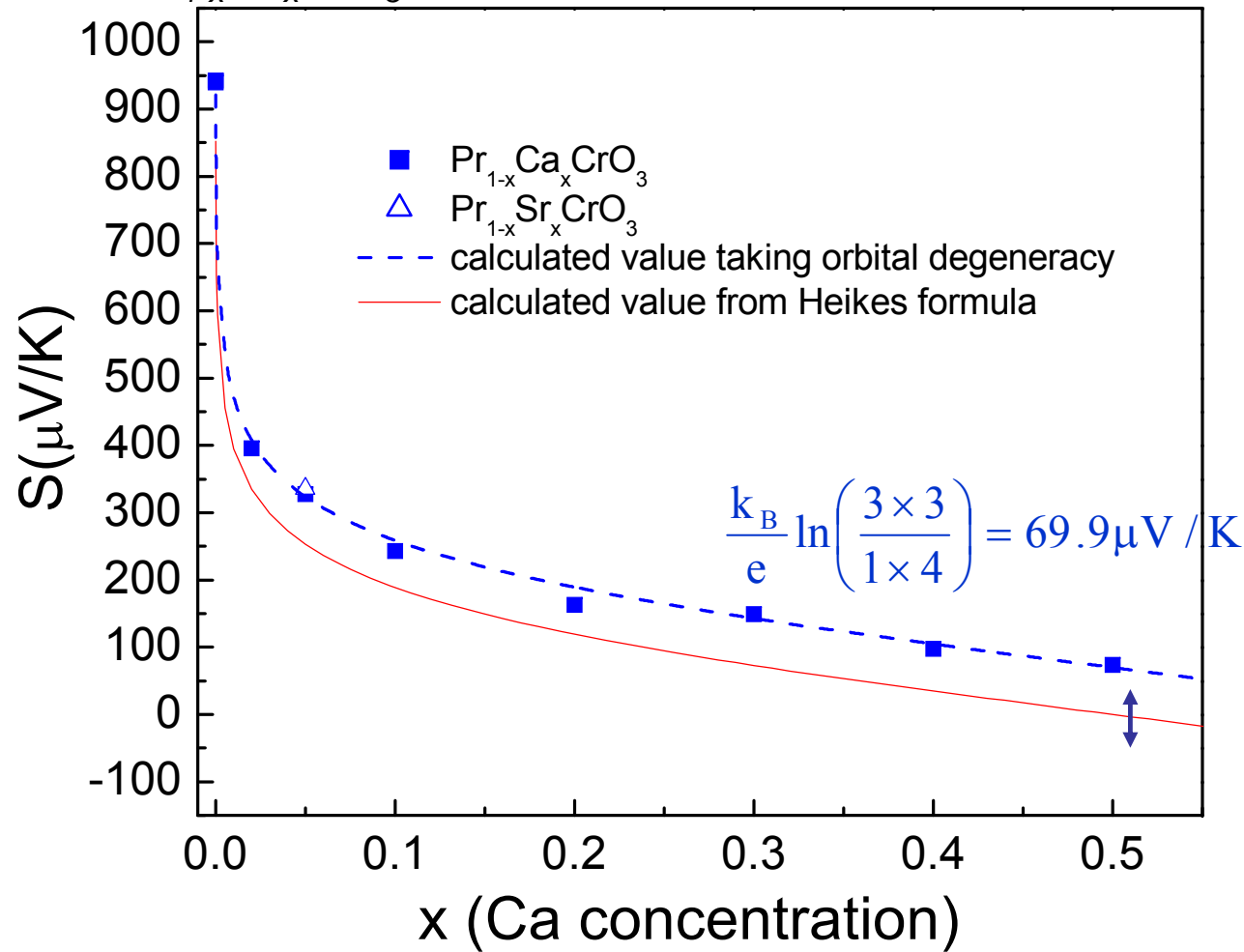
Type p : $Pr_{1-x}Ca_xCrO_3$

Heikes formula with spin and orbital degeneracies

Legend:
- ■ $Pr_{1-x}Ca_xCrO_3$
- △ $Pr_{1-x}Sr_xCrO_3$
- - - - calculated value taking orbital degeneracy
- —— calculated value from Heikes formula

$$\frac{k_B}{e}\ln\left(\frac{3\times 3}{1\times 4}\right) = 69.9\,\mu V\,/\,K$$

Y-axis: $S(\mu V/K)$

X-axis: x (Ca concentration)

$3d^3$, $S = 3/2$
$\Gamma_{orb}=1$
$\Gamma_{spin} = 4$
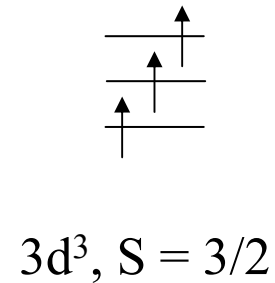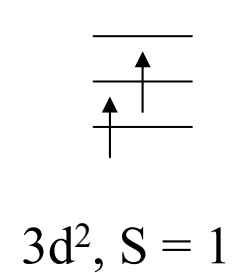
$3d^2$, $S = 1$
$\Gamma_{orb}=3$
$\Gamma_{spin} = 3$

$$S = \frac{-k_B}{|e|}\ln\left(\frac{1-x}{x}\right) + \frac{k_B}{|e|}\ln(\Gamma_{orb}\Gamma_{spin})$$

Marsh and Parris, Phys. Rev. B 54, 7720 (1996)
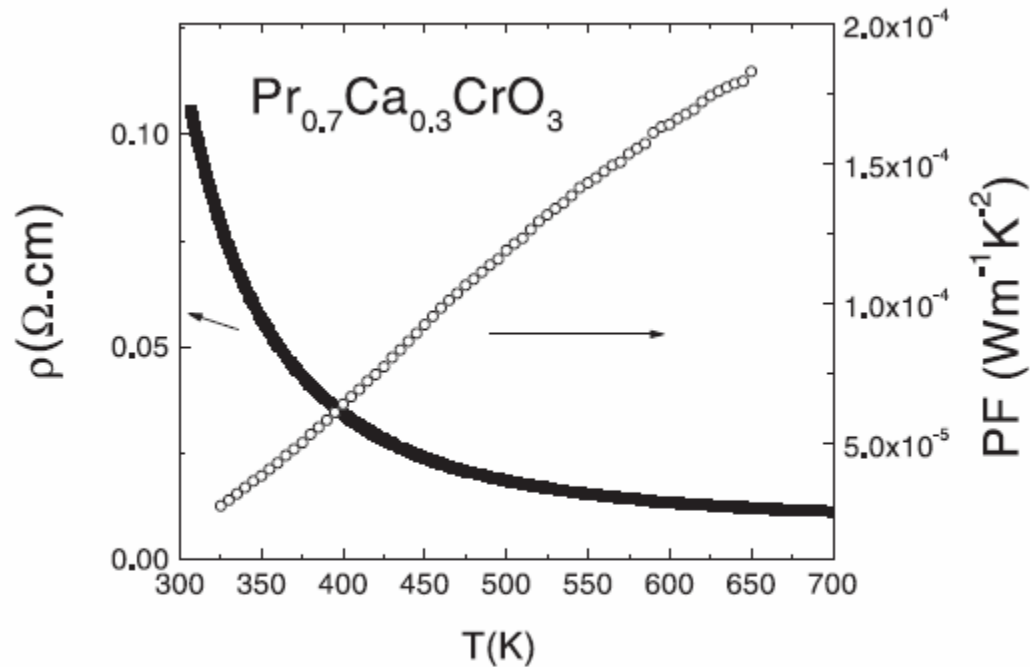
Type p : Pr$_{1-x}$Ca$_x$CrO$_3$

Power factor

Fig. 6. ρ vs. T (left scale) and Power Factor ($PF = S^2/\rho$) (right scale) of Pr$_{0.7}$Ca$_{0.3}$CrO$_3$ measured up to 700 K.

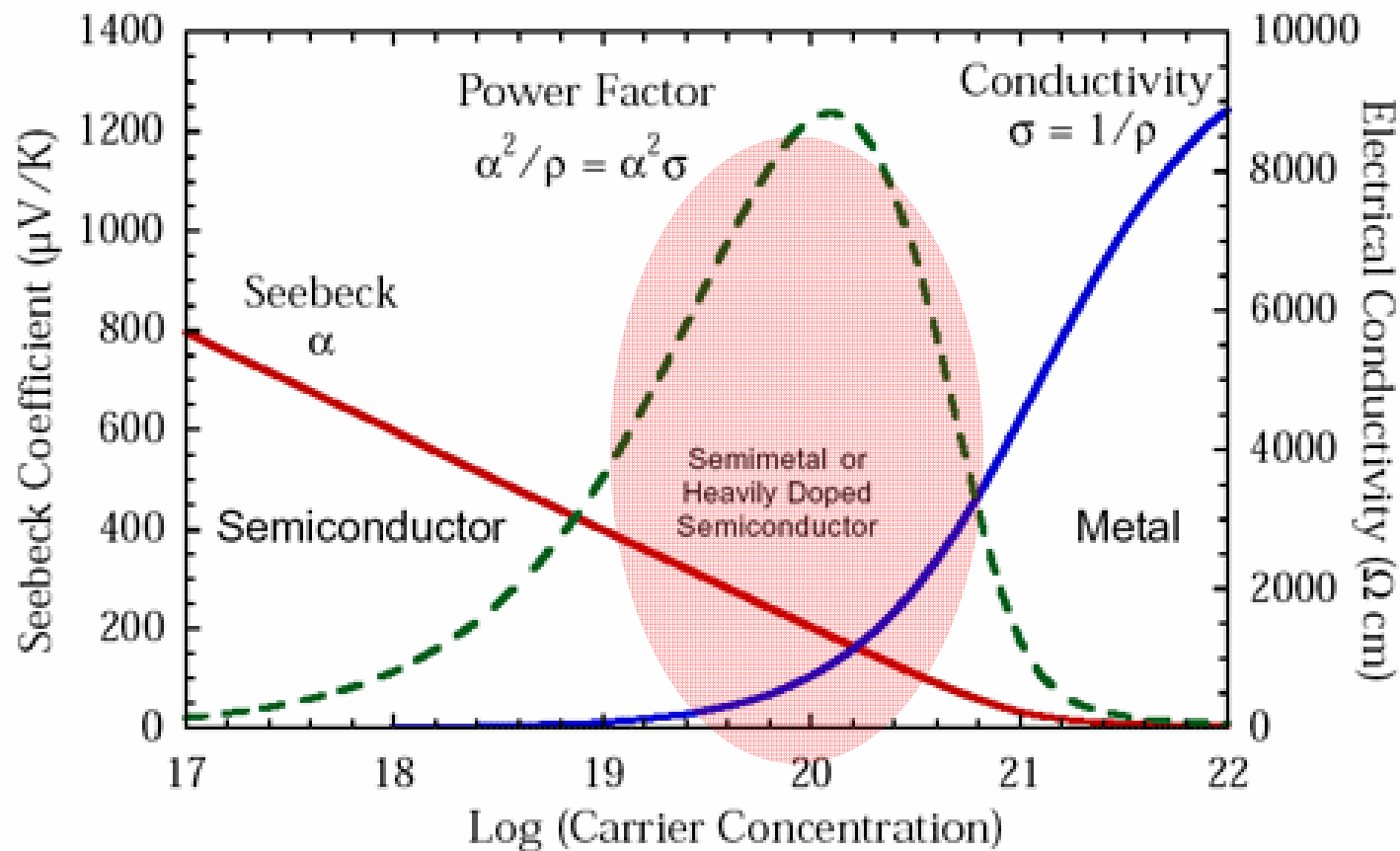PF ~ 2.10^{-4} Wm^{-1}K^{-1}
Typical for oxides

Semi – conducting oxides

The Heikes formula

→ Possibility to get p and n type oxides

→ Spin and/or orbital degeneracies have to be taken into account for a quantitative analysis

→ Explains the asymmetry between n and p type

But too large resistivity !

Degenerate semi-conductors : Best n type oxides

Type n : ZnO

$Zn_{1-x}Al_xO$ (x = 0 – 0.1)

ZT = 0.3
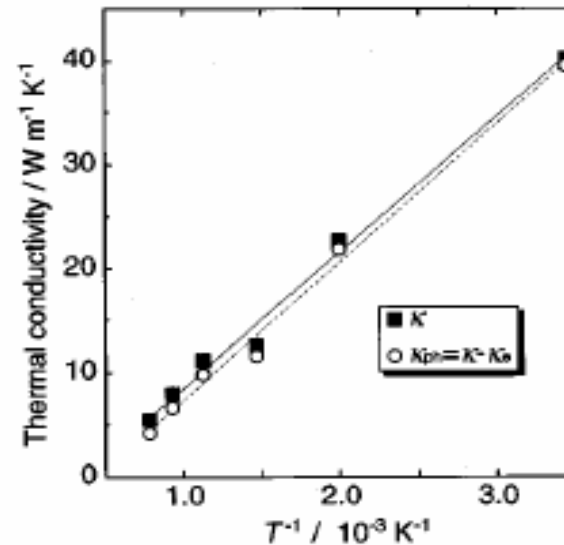
Broadband model for extrinsic n type semiconductor

$$\sigma = n e \mu,$$

$$S = -(k/e)[\ln(N_v/n) + A],$$

Large mobility of the carriers : 3 – 7cm^2/Vs
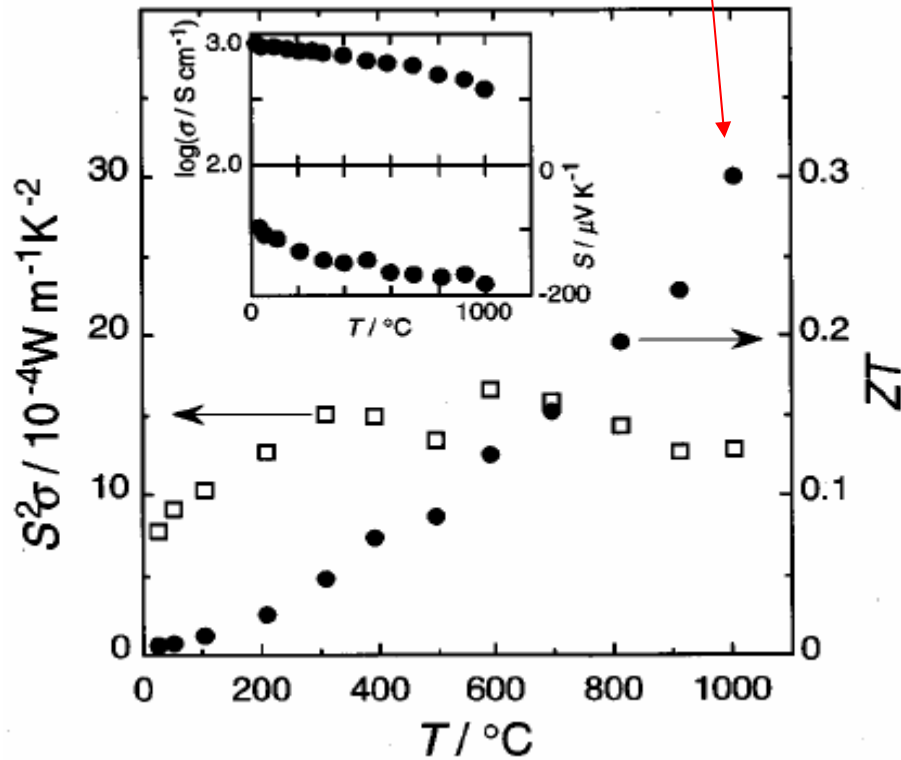
κ too high!

M. Ohtaki et al., JAP79, 1816 (1996)

κ = 40Wm^{-1}K^{-1} at 300K
κ=5.4 Wm^{-1}K^{-1} at 1000°C

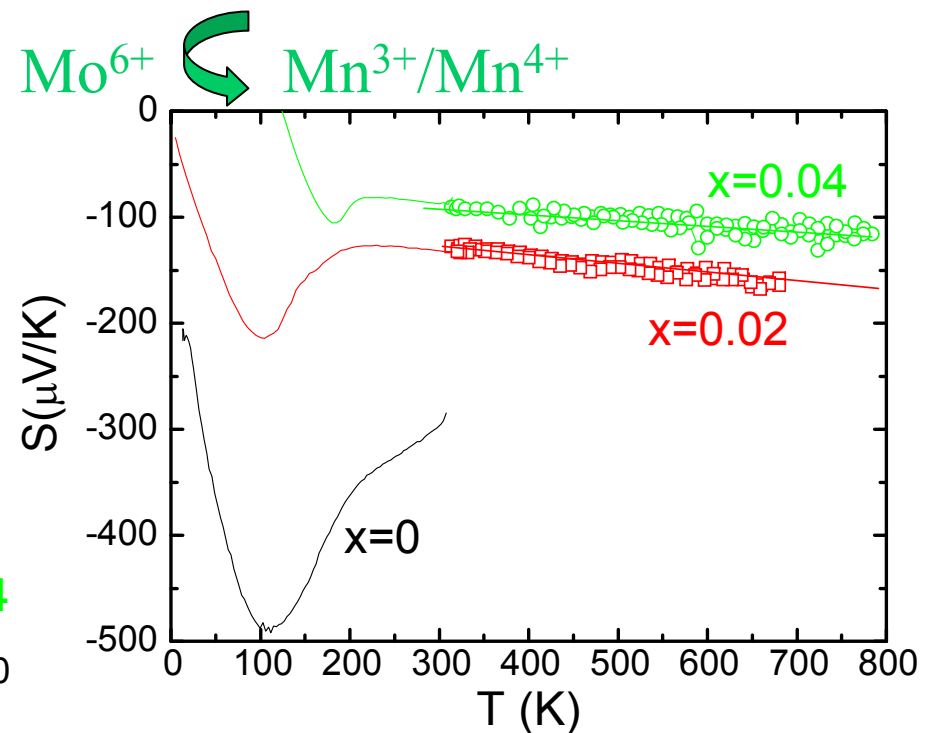*Type n : CaMnO₃*

Perovskite $Ca_{1-x}Sm_xMnO_3$
$SrMn_{1-x}Mo_xO_3$

Partially filled 3d levels

Mn^{3+} $t_{2g}^3 e_g^1$, HS JT

$V(Mn) = 4-x$

Hund J_H

Crystal field

Jahn-Teller Distorsion

$d_{x^2-y^2}$

d_{z^2}

$3d^4$

e_g

x2

S=3/2

t_{2g}
(e⁻ localized)

d_{xy}

d_{yz} d_{xz}
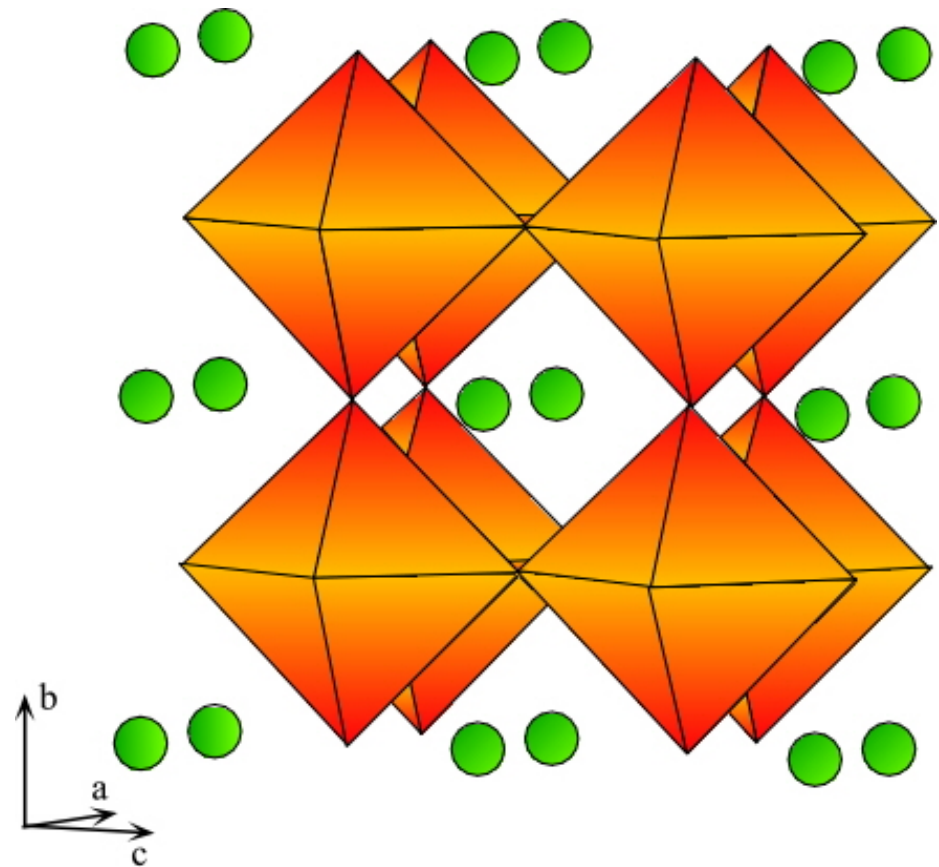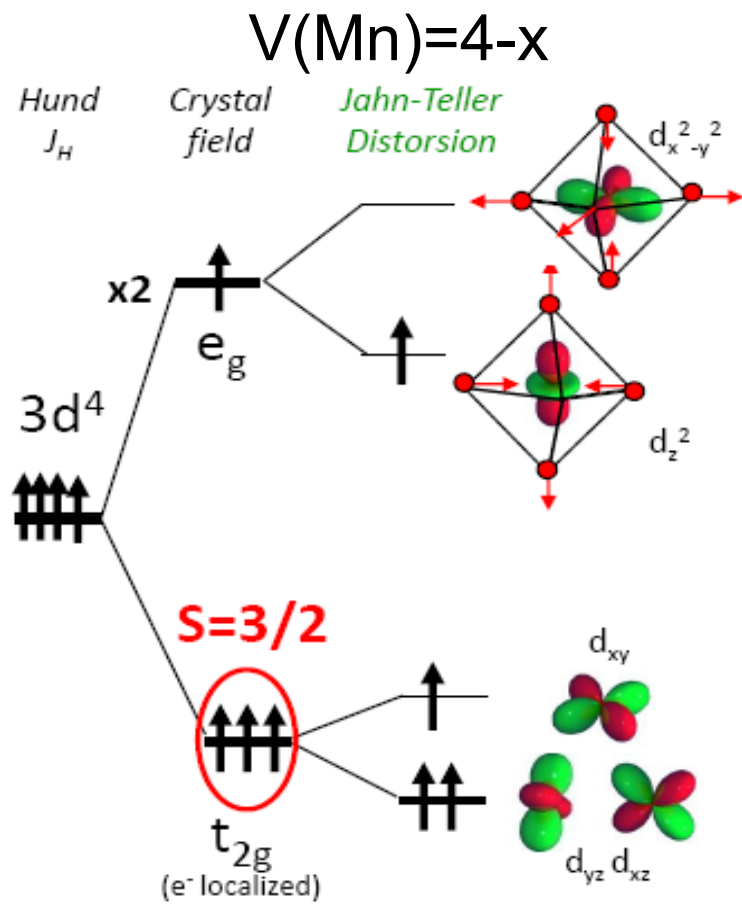
Manganese oxides
n type SrMn$_{1-x}$Mo$_x$O$_3$

3d^3 t$_{2g}$^{3} / 3d^4 t$_{2g}$^{3}e$_g$^{1} SrMnO$_3$: Mn^{4+}

Mo^{6+} Mn^{3+}/Mn^{4+}
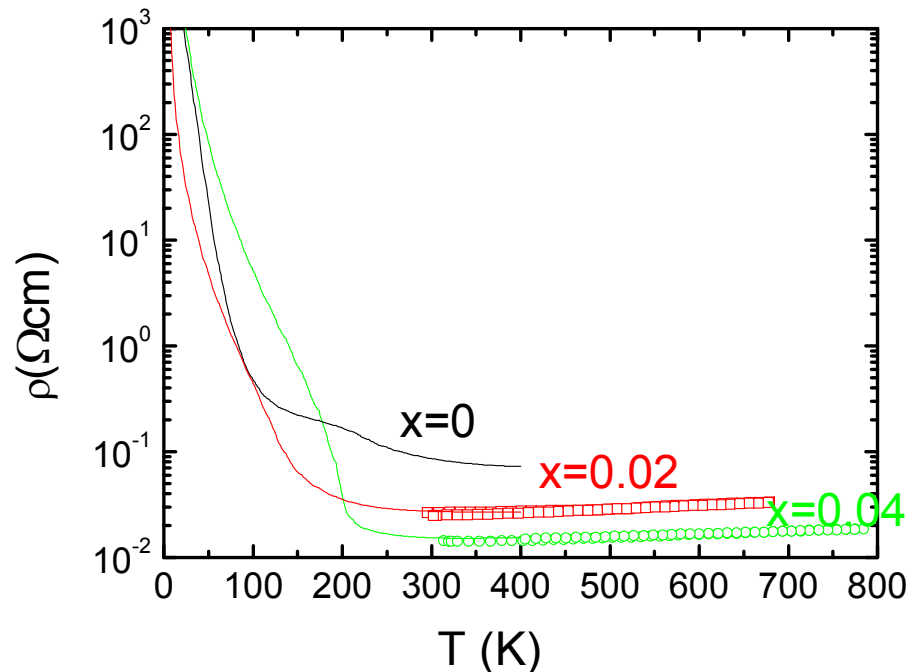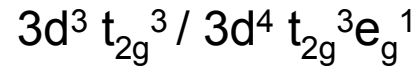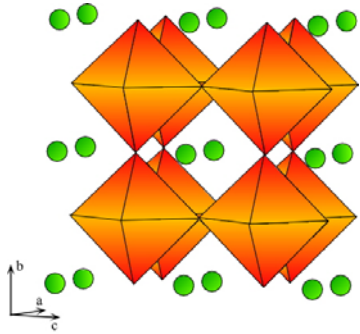
Metallic up to high T / S linear in T

Power factor increases as T increases : PF = 9.10^{-4}Wm^{-1}K^{-2} for x=0.02 at 800K

$$S = \pi^2 \times k_B/3e \times k_B T (\partial \ln \sigma(E)/\partial E)$$

Measurements by J. Hejtmanek (Prague)

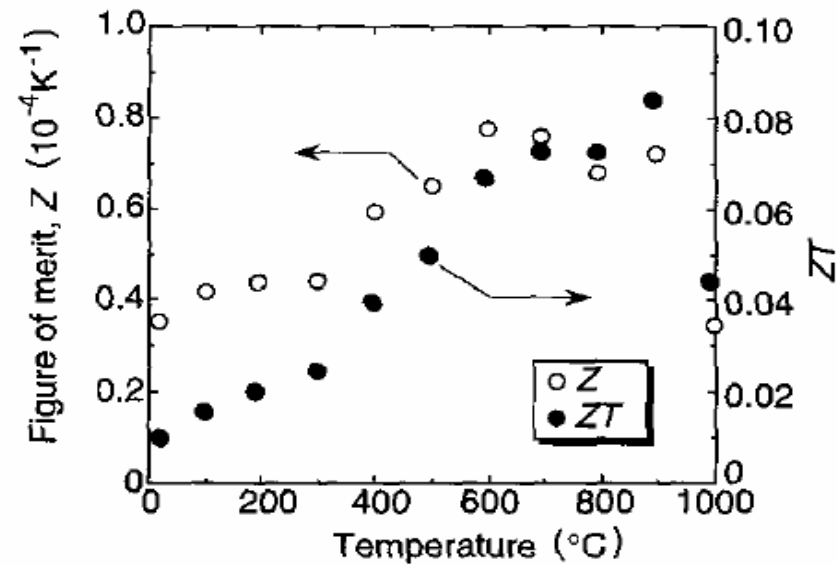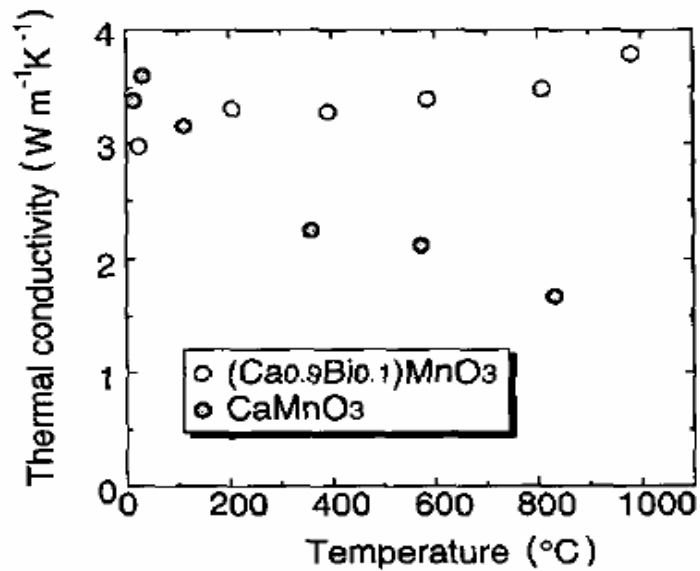J. Hejtmanek et al., PRB60, 14057 (1999)

Type n : CaMnO$_3$

Ca$_{0.9}$M$_{0.1}$MnO$_3$

FIG. 7. The temperature dependence of the figures of merit Z and the dimensionless figures of merit ZT for (Ca$_{0.9}$Bi$_{0.1}$)MnO$_3$.
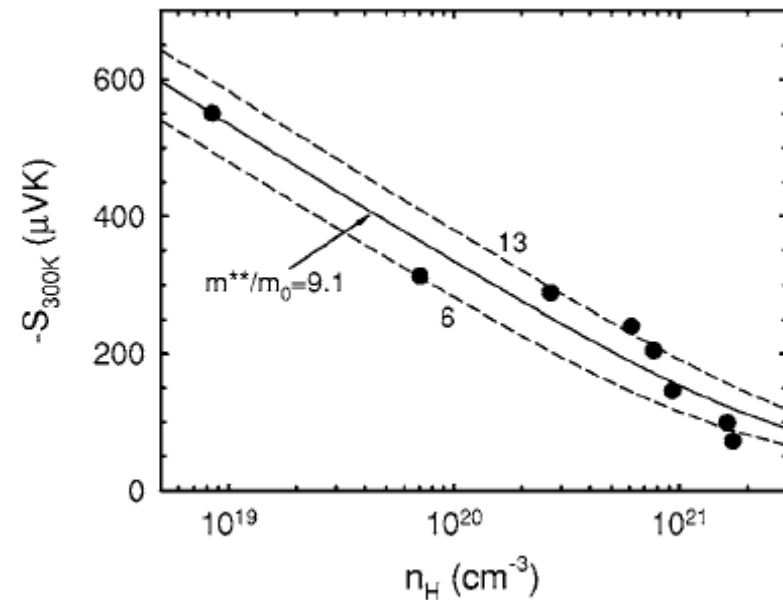
ZT ~ 0.1 à 900°C

M. Ohtaki et al., JSSC120, 105 (1995)

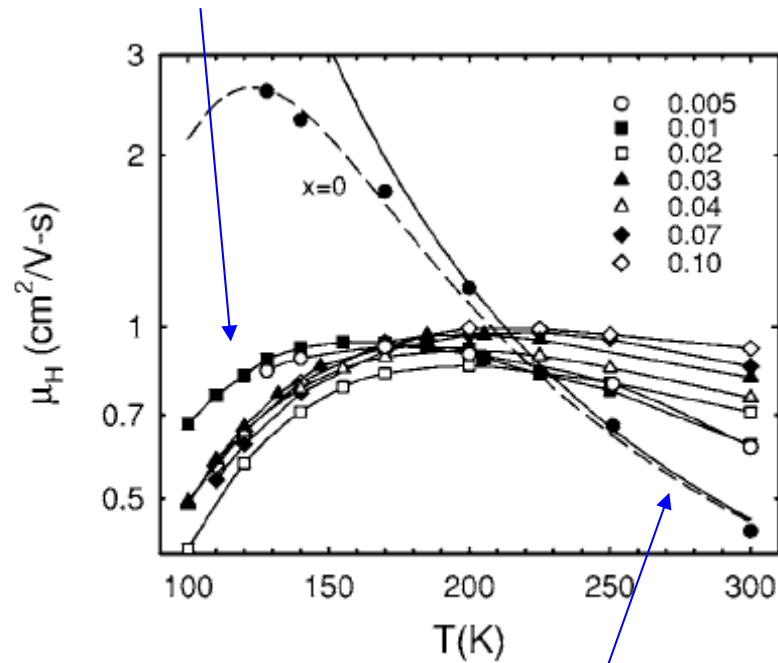*Type n : CaMnO₃*

Polarons transport in CaMnO₃

Carrier concentration
~ 10^{20} cm^{-3}

Charged impurity scattering

Smaller mobility than in ZnO

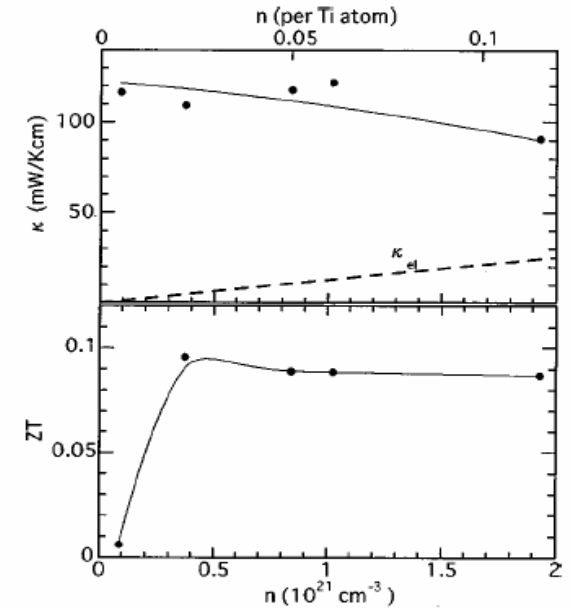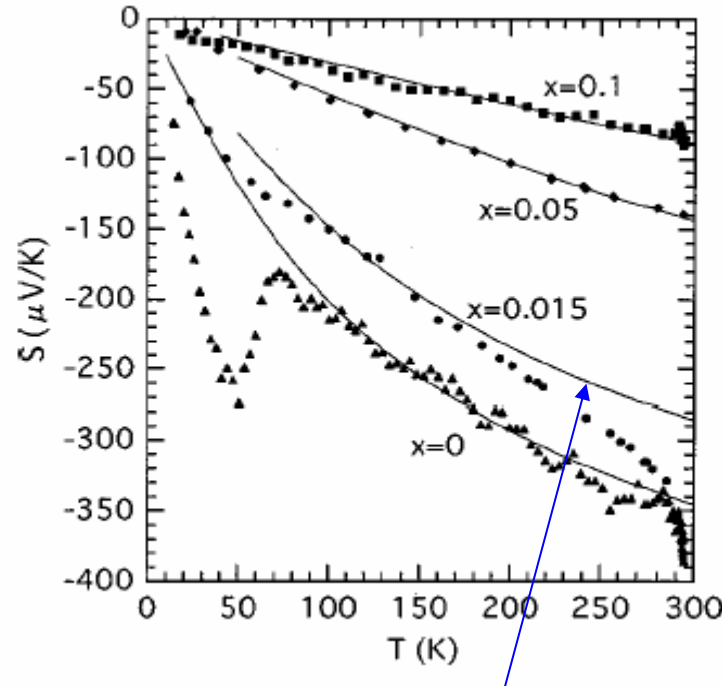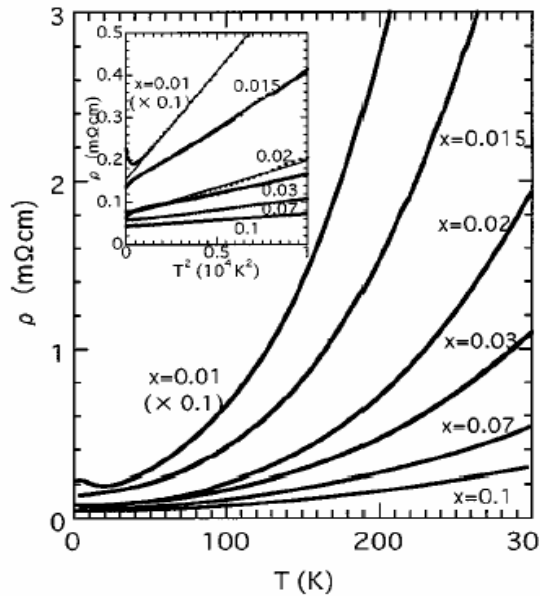Phonon scattering

J. L. Cohn et al., PRB72, 024422 (2006)

n type : SrTiO$_3$

Sr$_{1-x}$La$_x$TiO$_3$

SrTiO$_3$ = non magnetic insulator
La^{3+} : doping of Ti^{3+} in a matrix of Ti^{4+}

3d^0 / 3d^1

$\sigma \sim n$
(Constant mobility
~ 1 -10cm^2/Vs)

PF = 28 -36 10^{-4} WK^{-2}m^{-1}
But thermal conductivity too large!!

T. Okuda et al., PRB63, 113104 (2001)

Boltzmann model for a parabolic band
Degenerate semi-conductor

n ~10^{20} – 10^{21} cm^{-3}

ZT = 0.22 for Sr$_{0.9}$Dy$_{0.1}$TiO$_3$
at 573K
H. Muta et al., J. Alloys and Comp.350, 292 (2003)

n type : SrTiO$_3$

Sr$_{1-x}$La$_x$TiO$_3$

TABLE I. Various physical quantities derived from measurements of the resistivity, specific heat, Hall, and Seebeck coefficients (S) in Sr$_{1-x}$La$_x$TiO$_3$ crystals; n is the carrier (electron) density, A is the T^2 coefficient of resistivity, γ is the electronic specific heat coefficient, m^* is the carrier effective mass, T_F is the Fermi temperature, Θ_D is the Debye temperature, and μ is the chemical potential. S_r represents the calculated Seebeck coefficient with use of the scattering parameter r [see Eq. (1) in the text]. n, μ, S, and S_r are the values at 300 K.

x	n (1/Ti)	n (10^{20} cm^{-3})	A (Ω cm/K^2)	γ (mJ/K^2 mol)	m^*/m_b	T_F (K)	Θ_D (K)	μ (eV)	$-S$ (μV/K)	$-S_0$ (μV/K)	$-S_1$ (μV/K)	$-S_2$ (μV/K)
0	0.0052	0.877	3.68×10^{-7}	0.63	1.17	343	402	0.0061	380	190	268	345
0.015	0.014	2.31	2.58×10^{-8}						350			
0.02	0.022	3.73	1.21×10^{-8}	1.04	1.51	697	378	0.0488	260	150	182	247
0.04	0.05	8.41	6.69×10^{-9}						162			
0.05	0.061	10.23	5.14×10^{-9}	1.96	1.62	1273	380	0.102	147	93	118	168
0.1	0.11	19.31	3.08×10^{-9}						88.7			

Carrier concentration
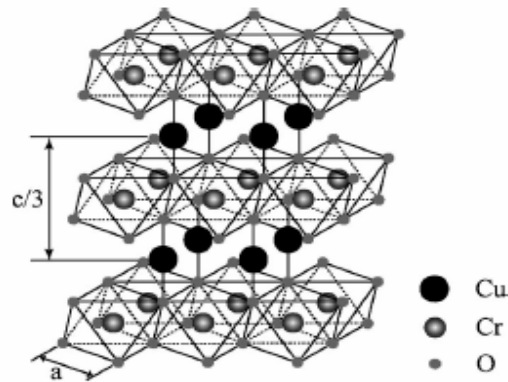10^{19} -10^{21} cm^{-3}

γ smaller than for p type oxides
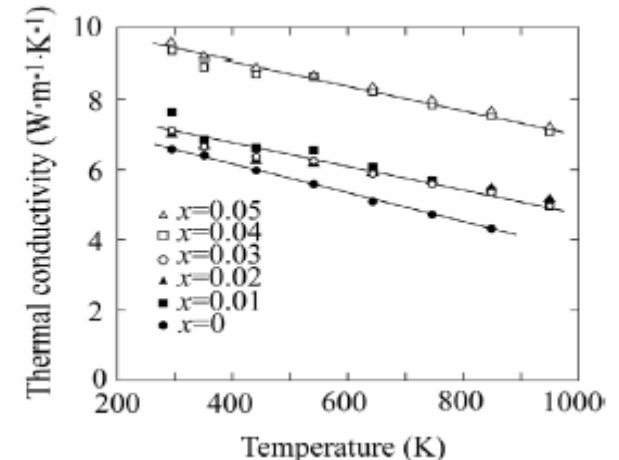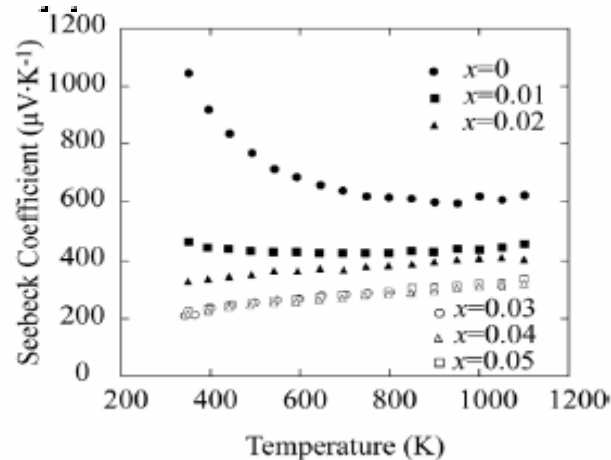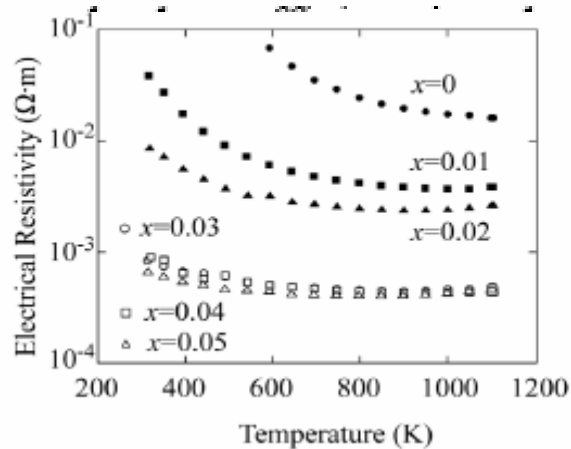Less sensitive to correlation effects?

T. Okuda et al., PRB63, 113104 (2001)

Type p : delafossites

$CuCr_{1-x}Mg_xO_2$

CrO_2 layers : edge shared octahedra

ZT = 0.04 at 950K

$Cu^+[Cr^{3+}]_{1-2x}[Cr^{4+}]_x[Mg^{2+}]_x O_2$

T. Okuda et al., PRB72, 144403 (2005), Y. Ono et al., ICT 2006
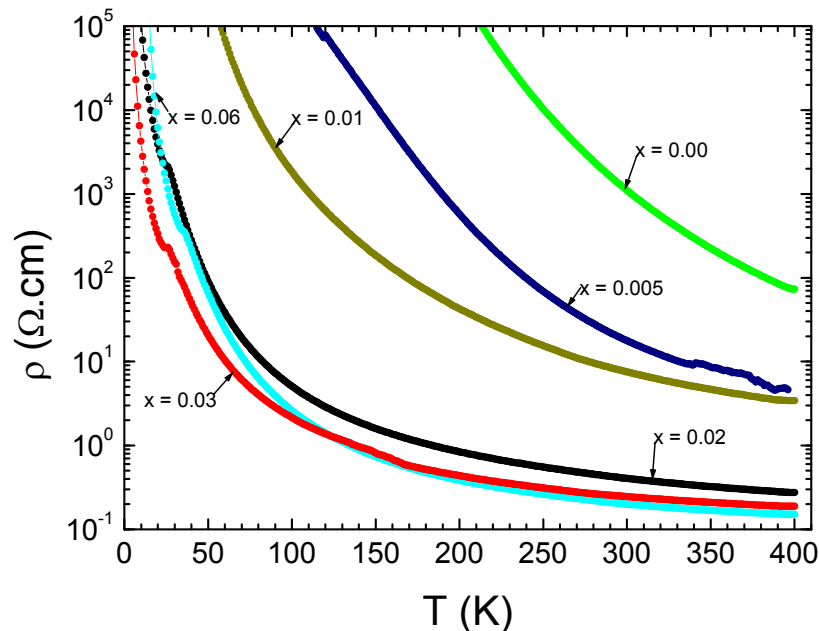
$CuRh_{0.9}Mg_{0.1}O_2$: ZT = 0.15 à 1000K
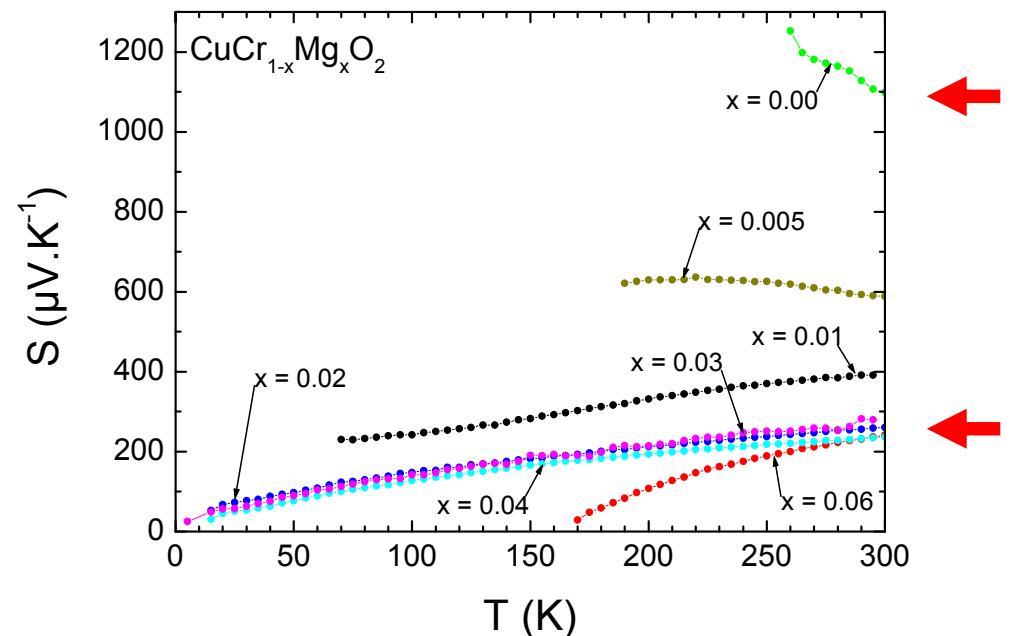
H. Kuriyama et al., ICT2006

Type p : delafossites

Transport properties of CuCr$_{1-x}$Mg$_x$O$_2$

Trivalent Cr S=3/2

Large resistivity drop up to x=0.02

Large S drop up to x=0.02

Activated (x=0.00) to small polaron (x>0.01)

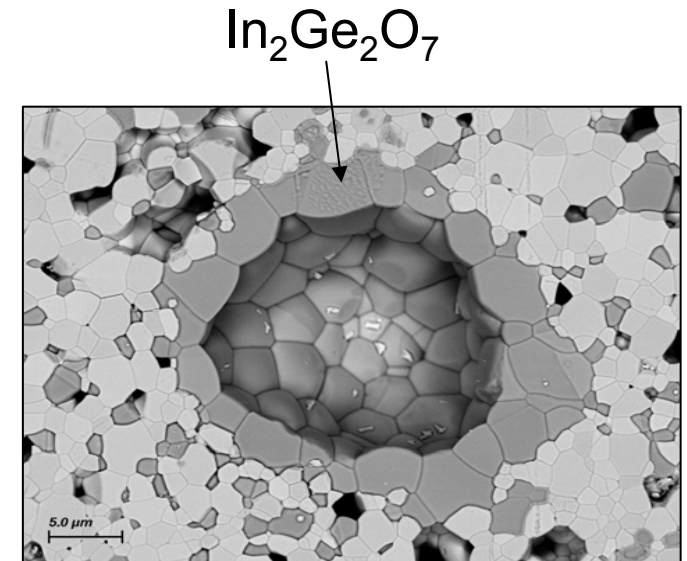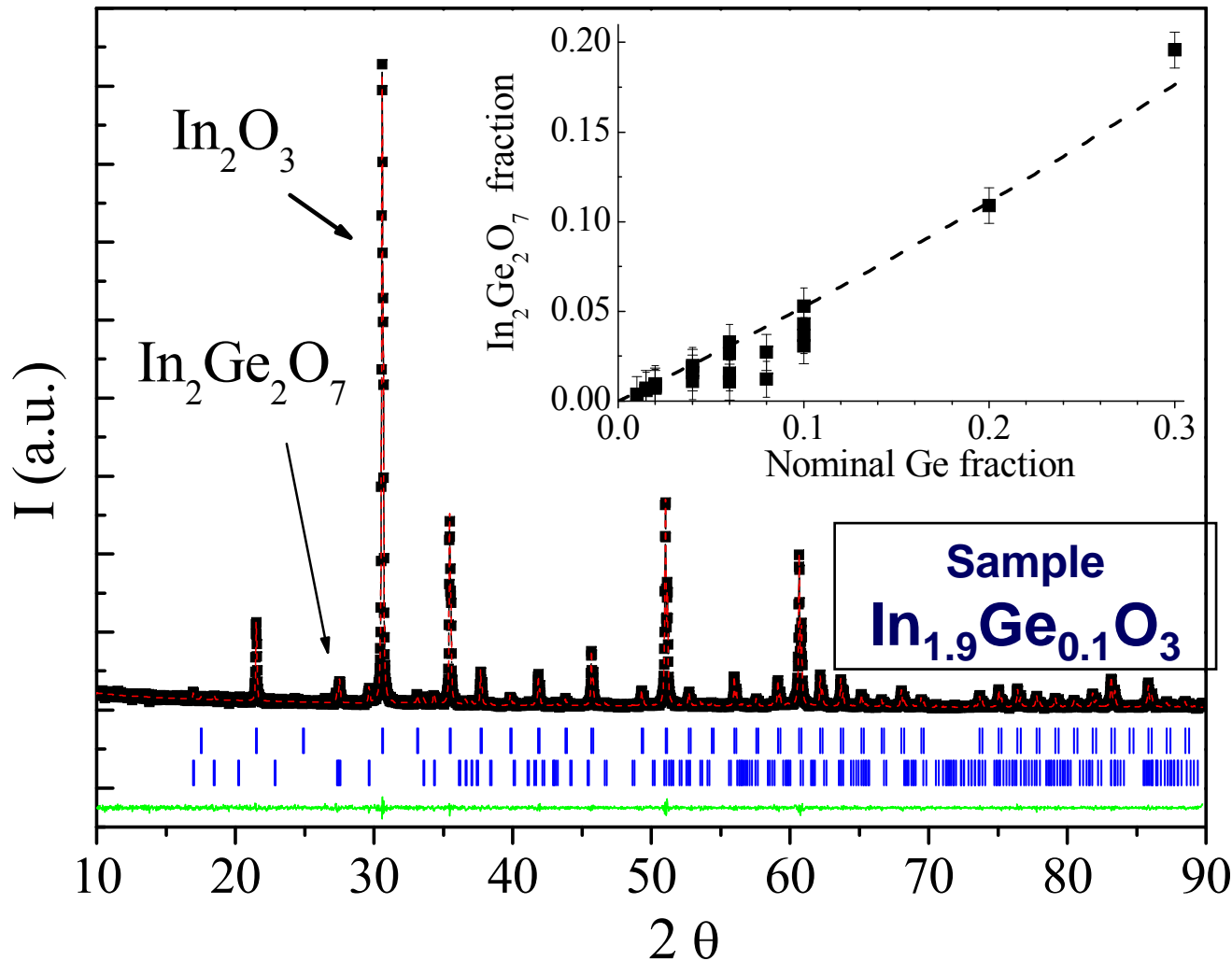TEM/ED/EDX/XRD: x$_{max}$ =0.01

Holes : Cr^{4+}

E. Guilmeau et al. SSC151, 1798 (2011)

$In_{2-x}Ge_xO_3$

XRD

Doping or microstructure effect??
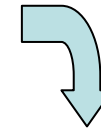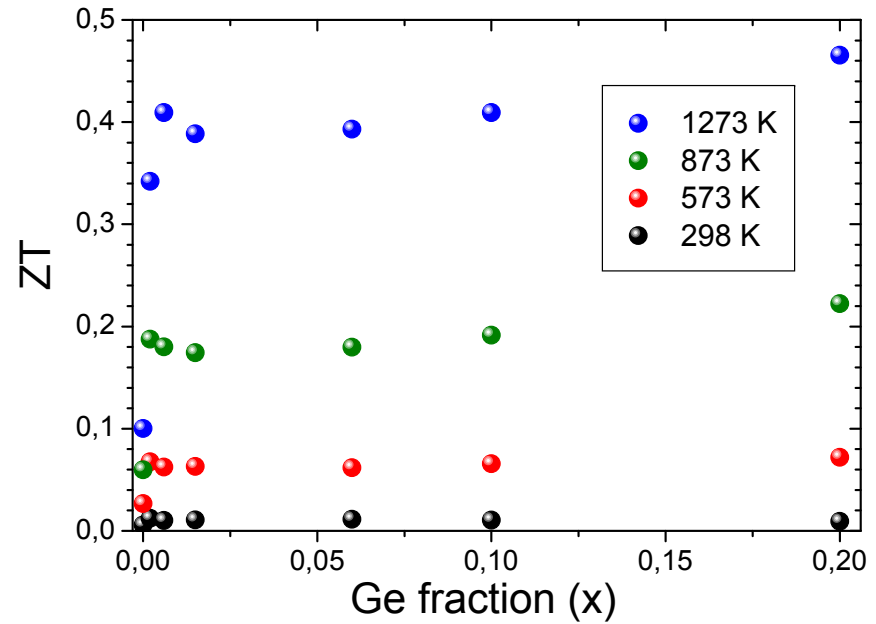
No substitution occurs
or
Small Ge solubility limit

In_2O_3

$In_2Ge_2O_7$

0.20
0.15
0.10
0.05
0.00

$In_2Ge_2O_7$ fraction

0.0   0.1   0.2   0.3
Nominal Ge fraction

I (a.u.)

Sample
$In_{1.9}Ge_{0.1}O_3$

10   20   30   40   50   60   70   80   90

2θ

$In_2Ge_2O_7$

5.0 µm

Sample
$In_{1.8}Ge_{0.2}O_3$

$R_{Bragg}= 2.98$, Chi2=1.28

D. Bérardan et al., Solid Stat. Comm. 146 (2008) 97.

Type n : In₂O₃

In₂O₃ doped with Ge

In₂₋ₓGeₓO₃

ZT = 0.4 à 1273K

D. Bérardan et al., Solid Stat. Comm. 2008
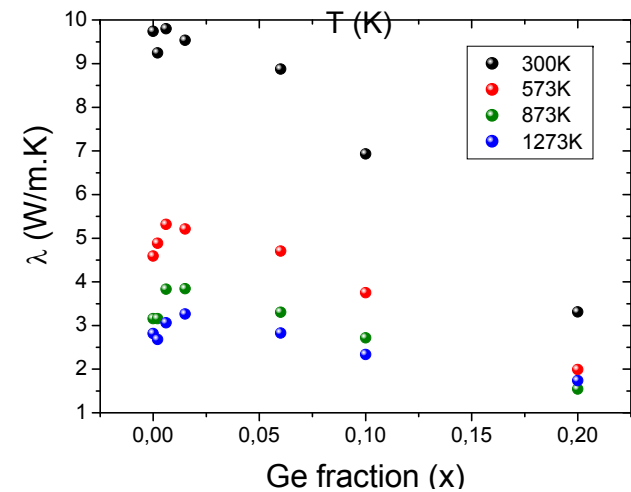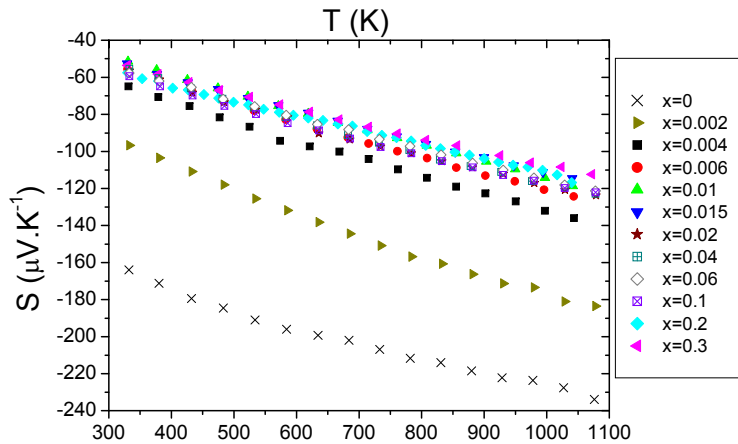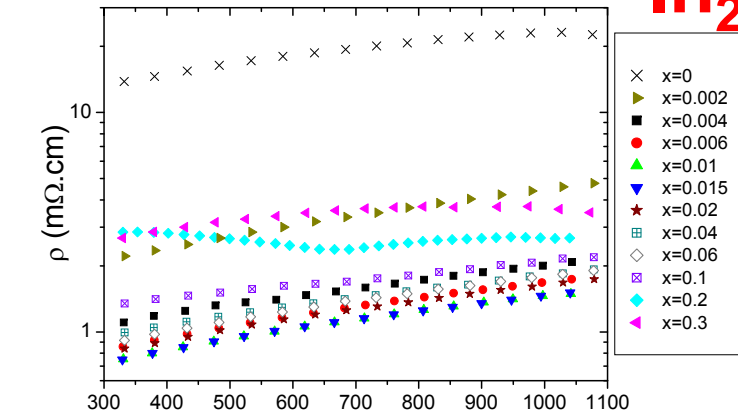
Degenerate semi - conductors

- Classical behavior which can be described by the Boltzmann model
Small enhancement of the effective mass
Polaronic transport

- Mostly n type (p type in delafossites)

- Problem : too large thermal conductivity
Microstructure modification is necessary to enhance ZT

Doped CaMnO$_3$:
New preparation techniques

Soft chemistry techniques

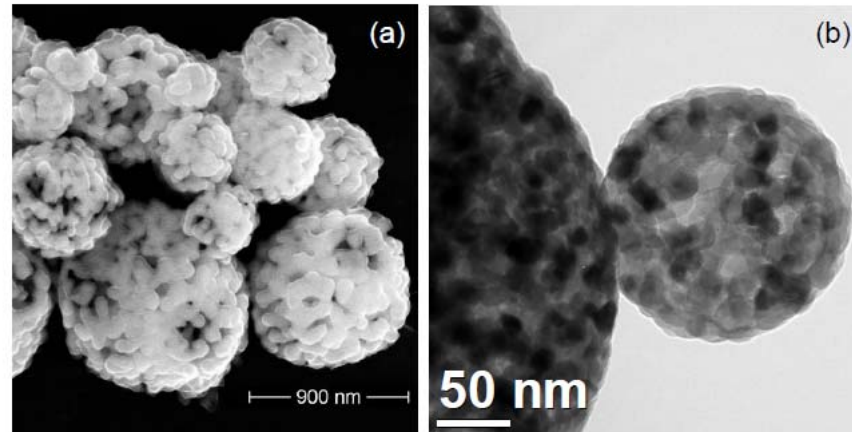*L. Bocher et al., Inorg. Chem. 47, 8077 (2008)*

Reduction of κ
Possible size effect?

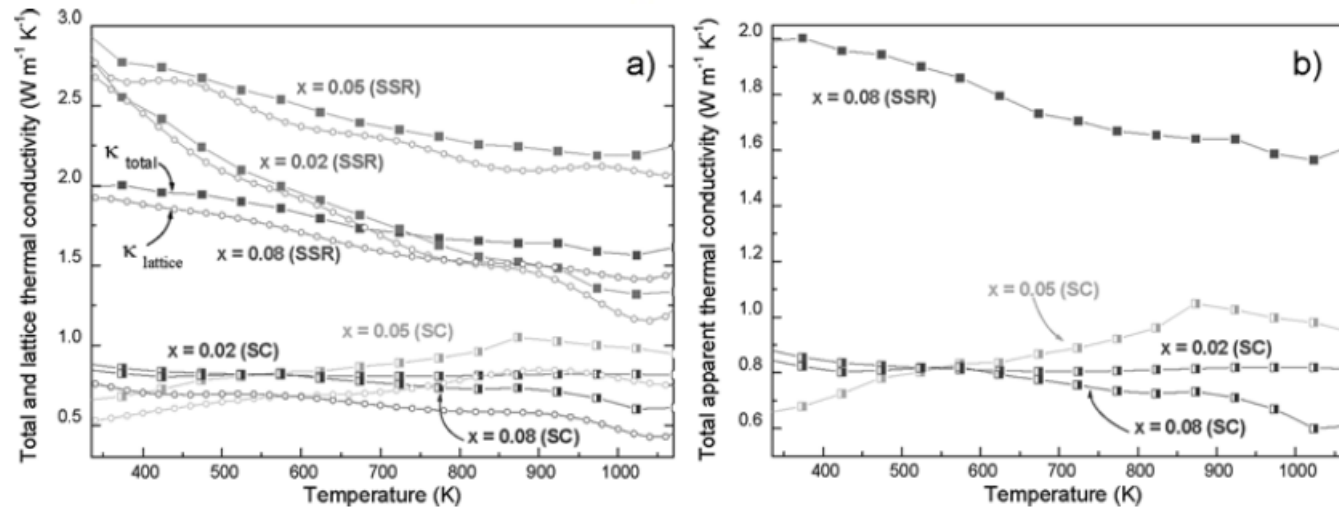Fig. 1. a) SEM picture and b) low resolution TEM of hollow perovskite spheres

Figure 8. (a) Total thermal conductivity κ_{total} of CaMn$_{1-x}$Nb$_x$O$_3$ ($x = 0.02$, 0.05, and 0.08) synthesized by both SSR (closed symbols) and SC (half-open symbols) methods and lattice contribution κ_l (open symbols) versus T and (b) highlight in the low thermal conductivity range.

Nb doped TiO$_2$

Polaronic transport
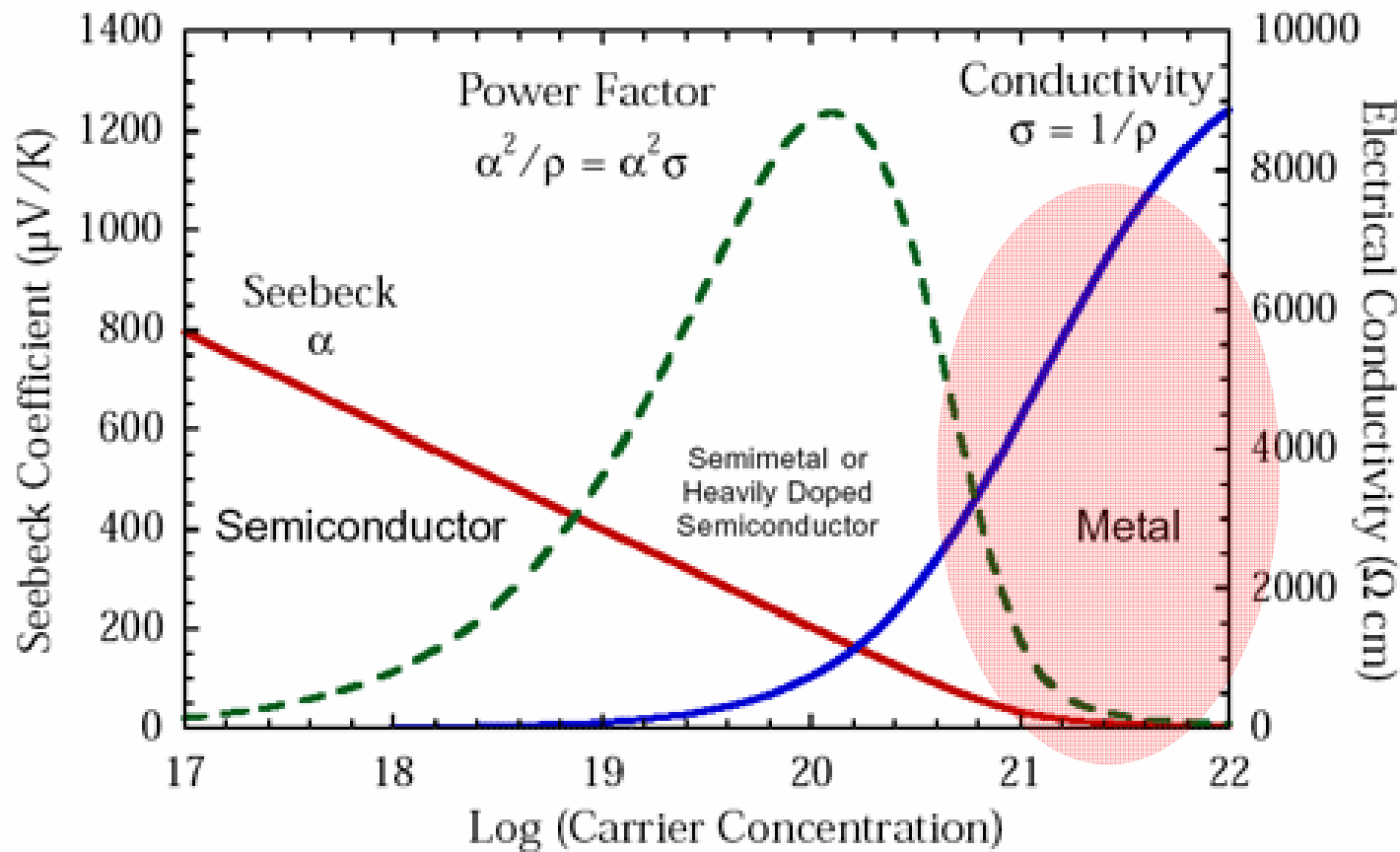Measurements for thin films
J. Jacimovic et al., APL102, 013901 (2013)
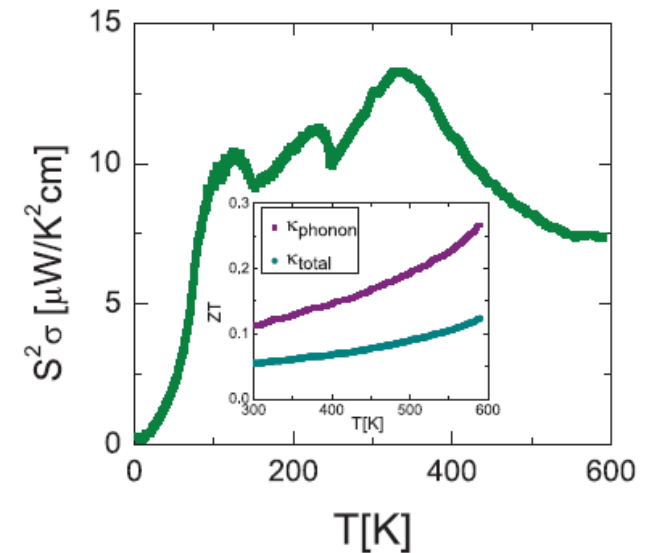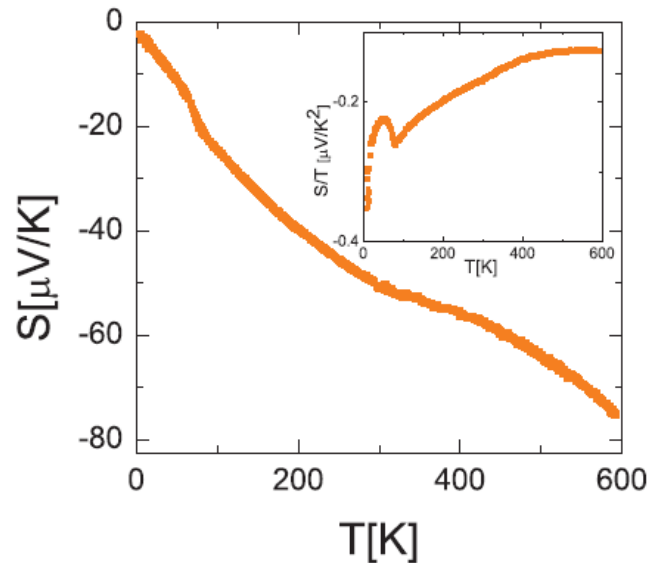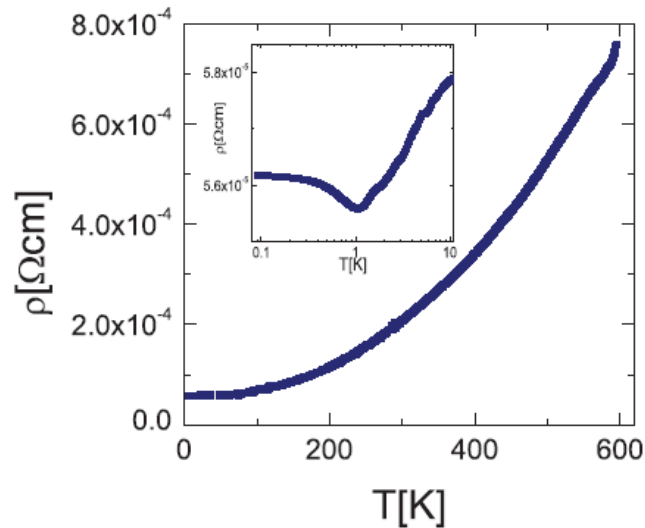
Search for other materials in the 'TCO' family
Critical role of doping through vacancies
Calculations for Cu$_2$O (D. J. Singh et al.), …

Na$_x$CoO$_2$ and related metallic compounds (p type)

Na_xCoO_2
Misfits

Cobalt bronzes family of Na_xCoO_2

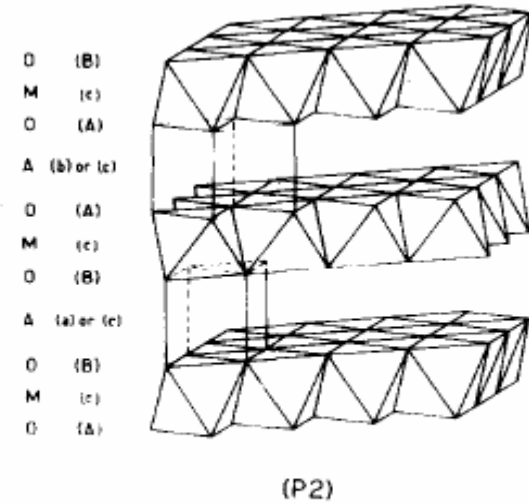*C. Fouassier et al., JSSC6, 532 (1973)*

0	(B)
M	(c)
0	(A)
A	(b) or (c)
0	(A)
M	(c)
0	(B)
A	(a) or (c)
0	(B)
M	(c)
0	(A)

(P2)

Fig. 1. Layer structure of $Na_{0.70}CoO_{2-y}$.
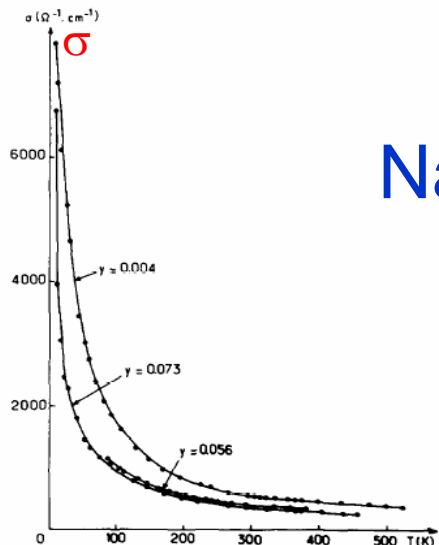
$Na_{0.7}CoO_{2-\gamma}$

Fig. 6. Temperature dependence of the electrical conductivity of quenched pellets.
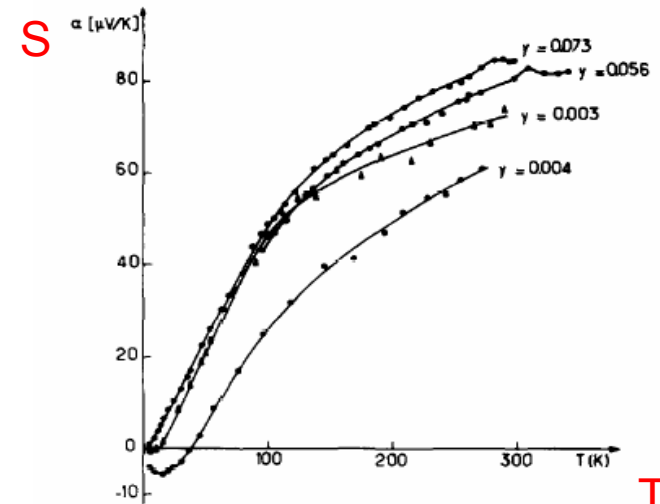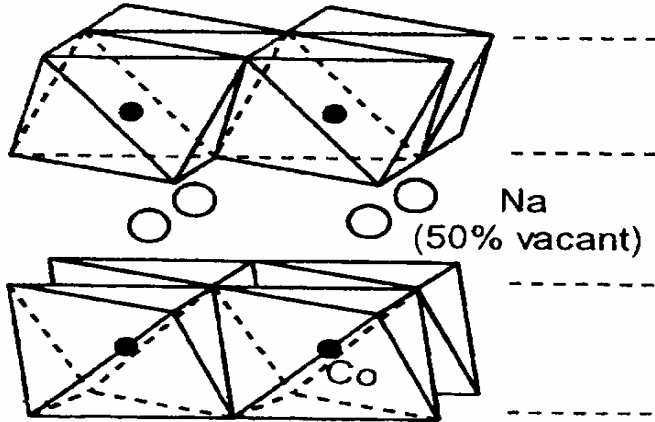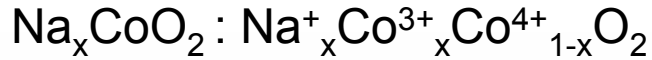

Fig. 7. Temperature dependence of the thermoelectric power of quenched pellets.

J. Molenda, C. Delmas, P. Dordor, A. Stoklosa,
Solid Stat. Ionics 12, 473 (1989)

$Na_{0.7}CoO_2$
' Phonon Glass / Electron crystal '
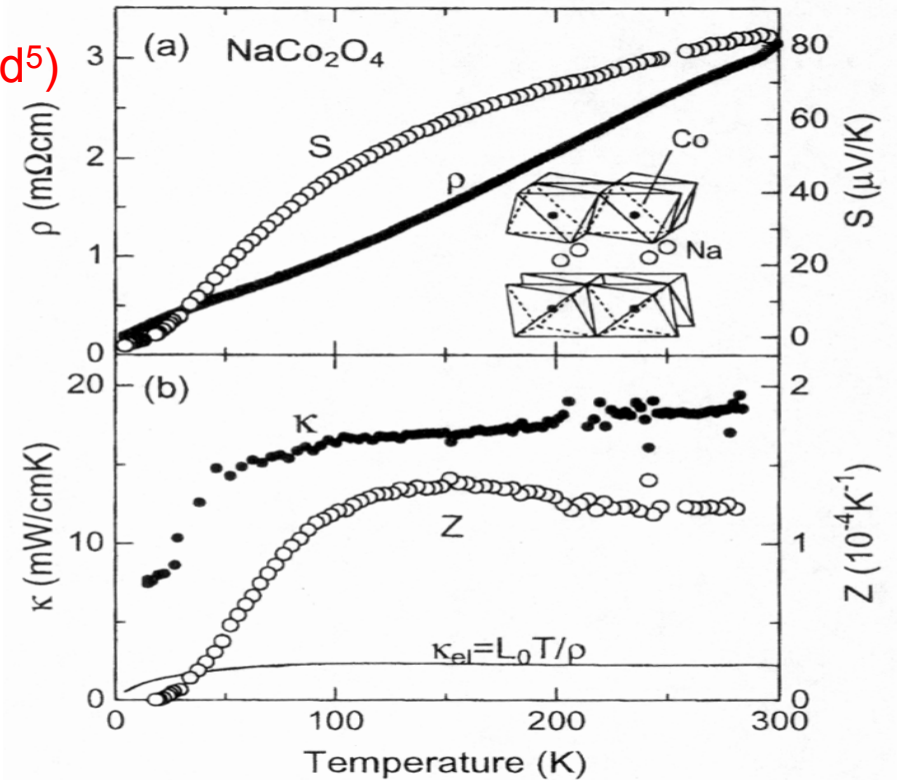
I. Terasaki et al., Phys. Rev. B 56, R12685 (1997)

$Na_xCoO_2 : Na^+_x Co^{3+}_x Co^{4+}_{1-x} O_2$

Measurements on polycrystals

Co^{3+} ($3d^6$) / Co^{4+} ($3d^5$)

At 300K

Metallicity (crystals) $\rho \sim$ **0.2 mΩ cm**

Large S **S $\sim$ +80 μV/K**

Small κ (polycrystals) $\kappa \sim$ **2Wm^{-1}K^{-1}**

(crystals) $\kappa \sim$ **5Wm^{-1}K^{-1}**

Power factor $P = S^2/\rho$ at 300K

$Na_{0.7}CoO_2$

Bi_2Te_3

P= 50 10^{-4} WK^{-2}m^{-1}

P= 40 10^{-4} WK^{-2}m^{-1}

The misfit family

- n = 4 $[Bi_2A'_2O_4]^{RS}[CoO_2]_{b1/b2}$
  A' = Ca^{2+}, Sr^{2+} or Ba^{2+}
- n = 3 $[A'_2CoO_3]^{RS}[CoO2]_{b1/b2}$
  A' = Ca^{2+} or Sr^{2+}
- n = 2 $[Sr_2O_2]^{RS}[CoO2]_{b1/b2}$
  $[Ca_2(OH)_2]^{RS}[CoO_2]_{b1/b2}$

$a_1 = a_2$
$c_1 = c_2$ $b_1 \neq b_2$
$\beta_1 = \beta_2$
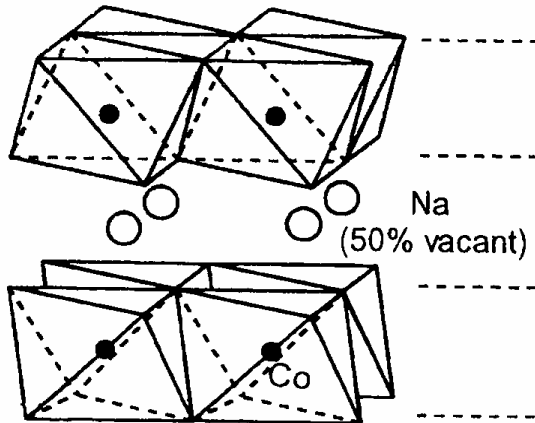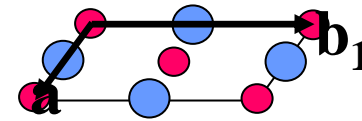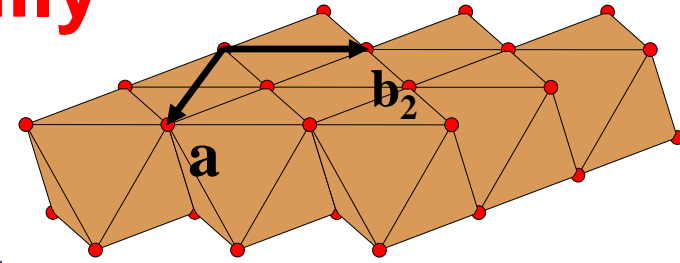
Na_xCoO_2
K_xCoO_2, …

NaCl-like triple layer (RS)

Na (50% vacant)

Co

i0.7 Å
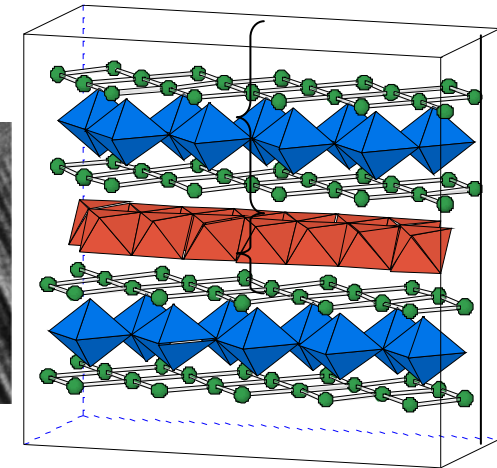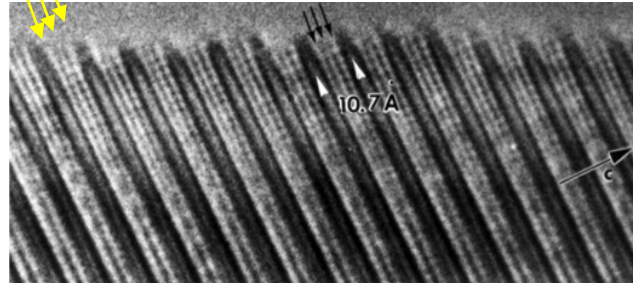
CoO₂ (type CdI₂)
Heikes formula : doping influence?
Band structure influence : peculiarity of CoO_2 layers ?
Role of separating block layers?

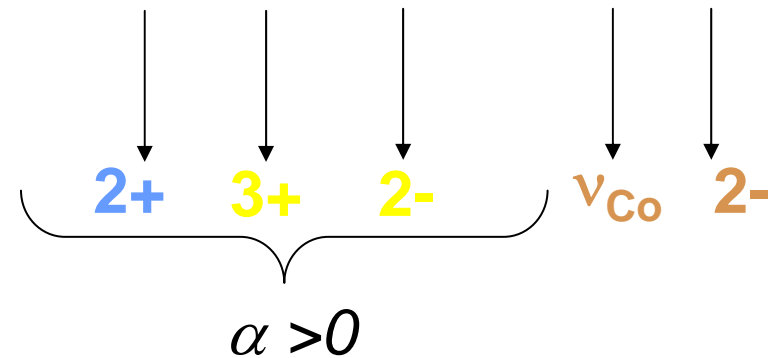*Leligny et col., C. R. Acad. Sci. Paris, t. 2, Série II c, 409 (1999)*
Boullay et col., Chem. Mater. 8, 1482 (1996)

Masset et col., Phys. Rev. B 62, 166 (2000)
Yamauchi et col., Chem. Mater. 18, 155 (2005)

Doping effect in the misfit family

$Ca_3Co_4O_9$

Ca_2CoO_3 NaCl-like	
CoO_2 CdI_2-like	

Electronic neutrality :

$$[Ca_2CoO_{3\pm\delta}]^{RS}[CoO_2]_{b1/b2}$$

2+ 3+ 2- ν_{Co} 2-

$\alpha > 0$
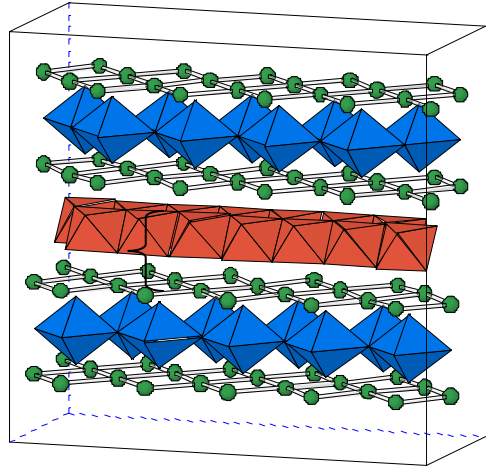
$$\boxed{\nu_{Co} = 4 - \frac{\alpha}{b_1/b_2}}$$

Modification of ν_{Co} via α and b_1/b_2

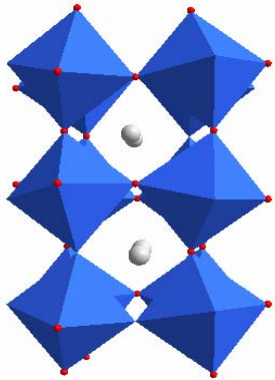Link between ν_{Co} and S?

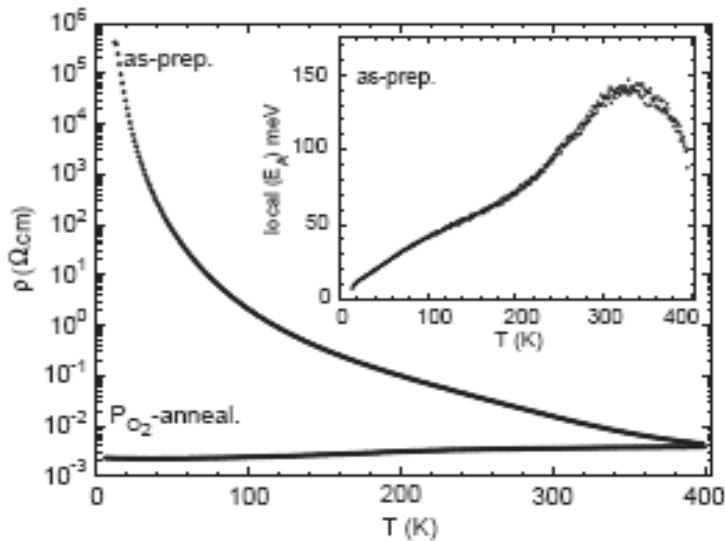# Modification of the block layers

Misfits
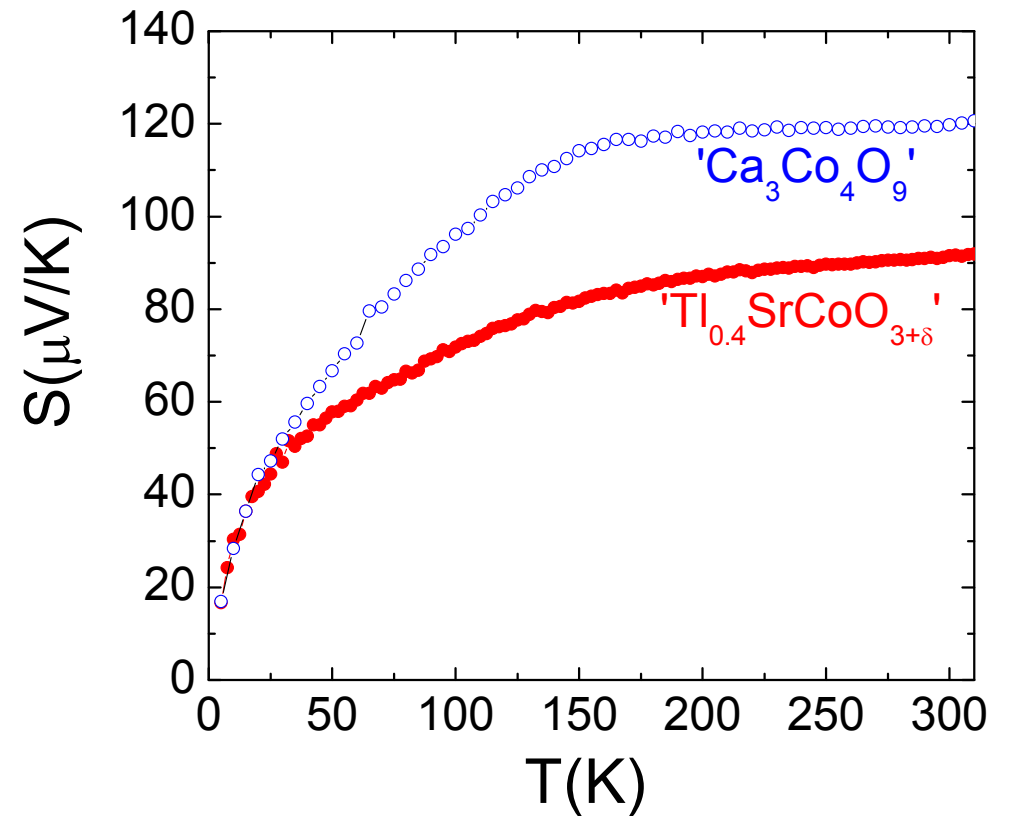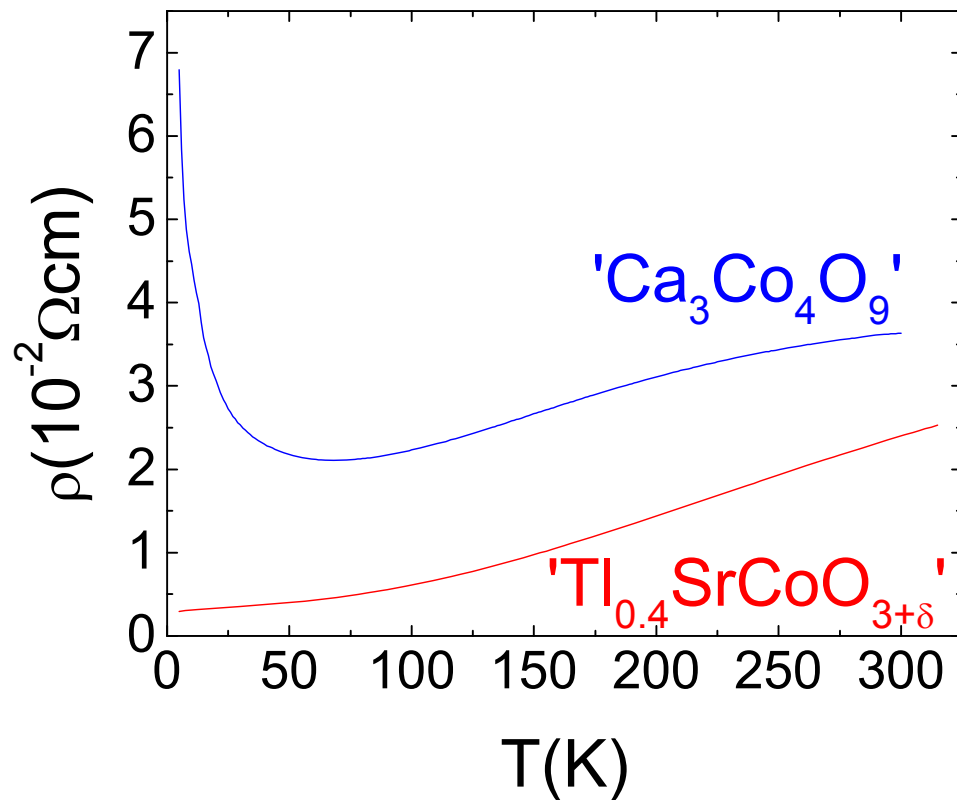
Na$_x$CoO$_2$
Misfits

Unique behavior of CdI$_2$ type layers: Comparison with other oxides
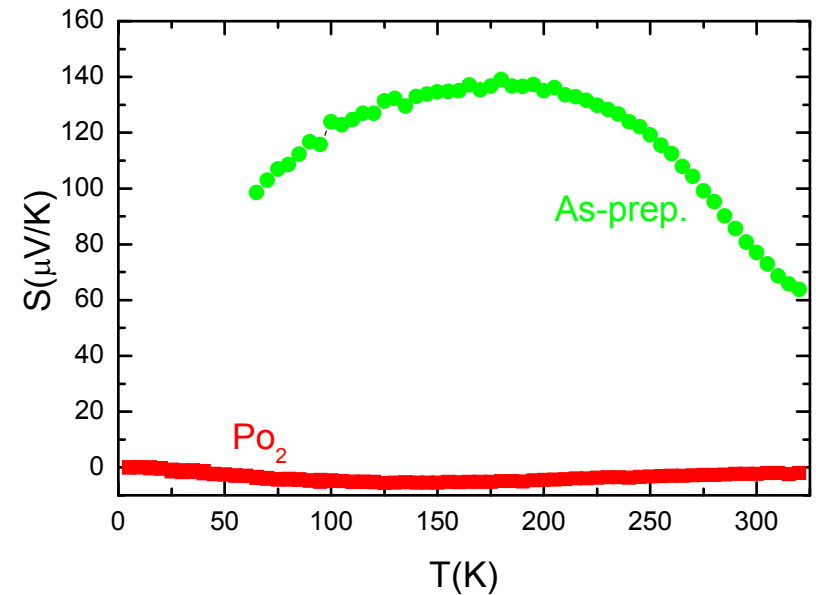

Perovskite Sr$_{2/3}$Y$_{1/3}$CoO$_{8/3+\delta}$

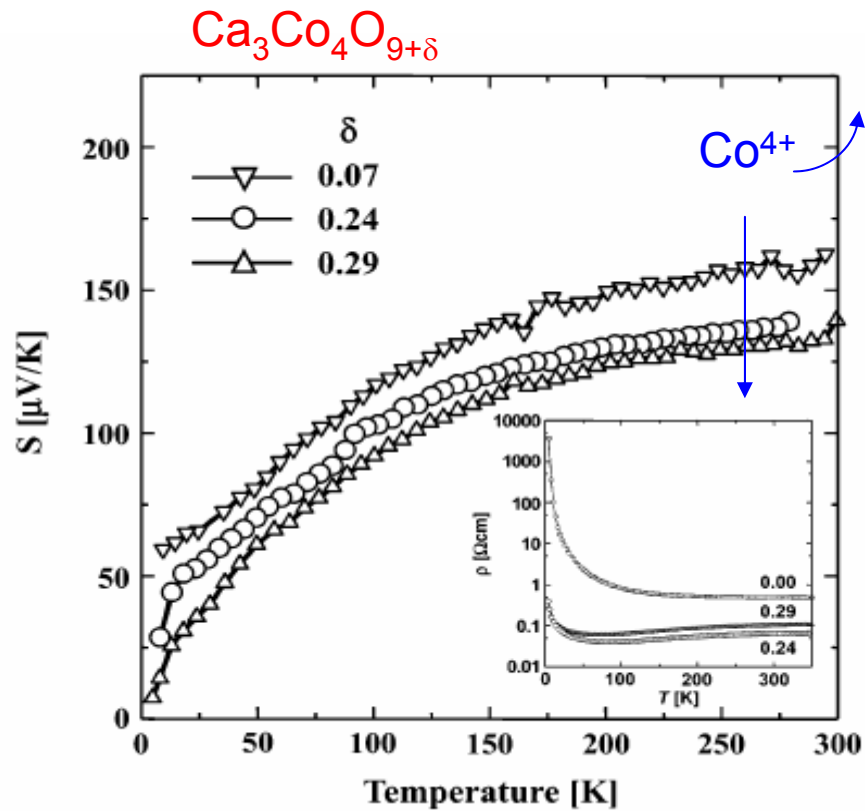Corner shared octahedra

$\neq$ edge shared octahedra

Metallicity

Seebeck ≈ 0

A. Maignan et al., JSSC178, 868 (2005)

Na$_x$CoO$_2$
Misfits

Influence du taux d'oxygène

Ca$_3$Co$_4$O$_{9+\delta}$

Co^{4+}

M. Karppinen et al., Chem. Mater. 16, 2790 (2004)

Famille BiCaCoO,
Polycristaux préparés sous air,
ou en tube scellé

Co^{4+}

Misfits : S le plus élevé
pour le taux de 'Co^{4+}'
le plus faible
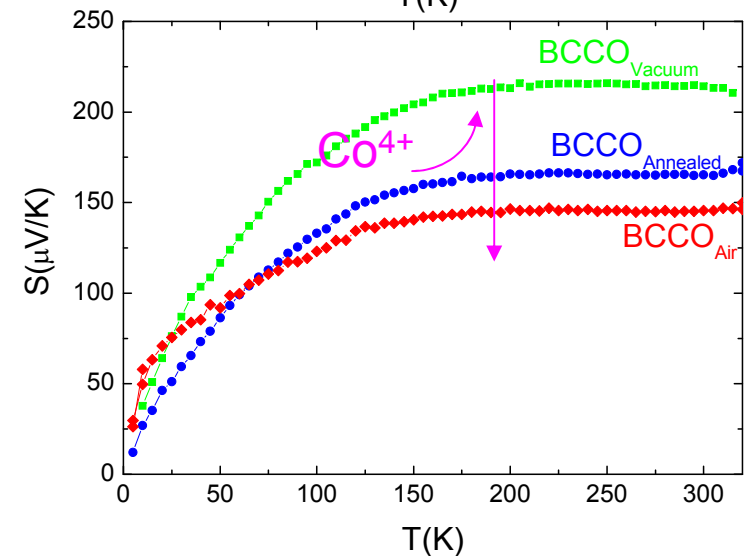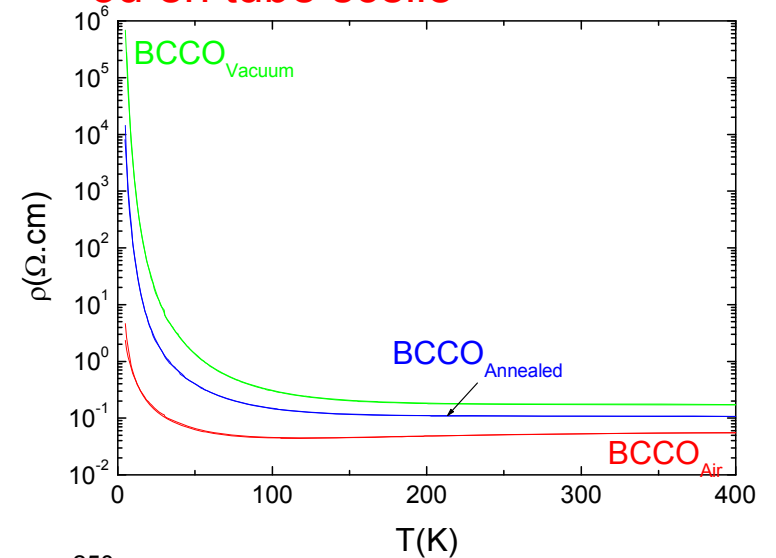
S. Hébert et al.

BiSrPbCoO single crystals : modification of α

$$v_{Co} = 4 - \frac{\alpha}{b_1 / b_2}$$

$[Bi_{1.74}Sr_2O_4][CoO_2]_{1.82}$

$[Bi_{1.5}Pb_{0.5}Sr_2O_{4-\delta}][CoO_2]_{1.86}$
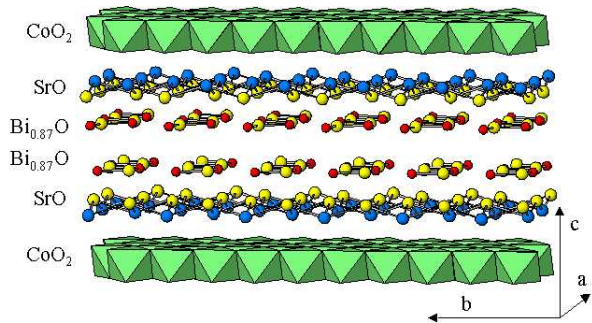
Substitution of Bi^{3+} by Pb^{2+} : decrease of α
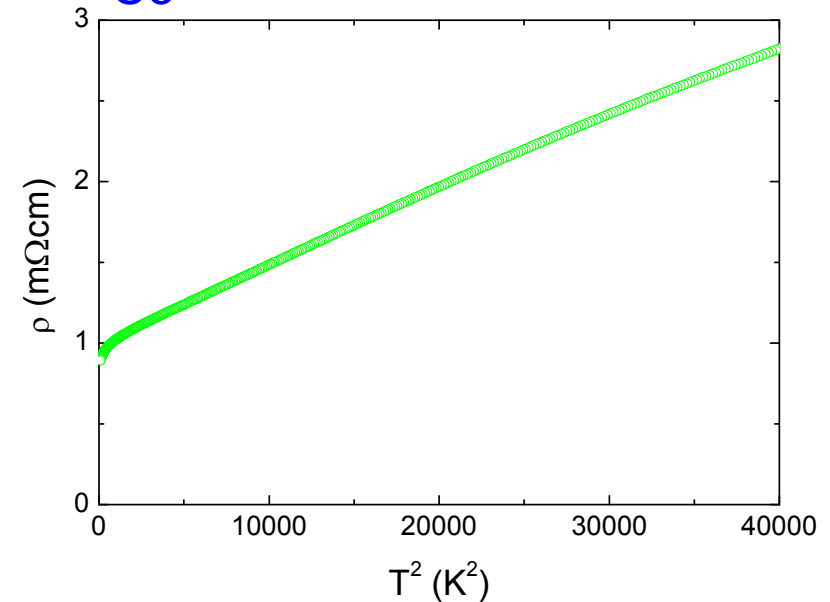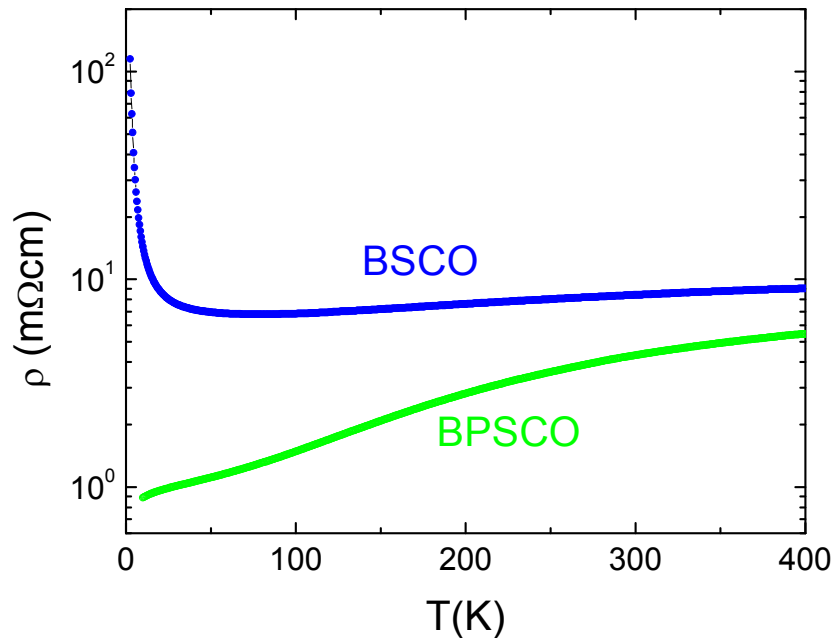
Increase of v_{Co}

Metallic behavior down to 5K with $\rho = AT^2$

BiSrPbCoO single crystals : modification of α
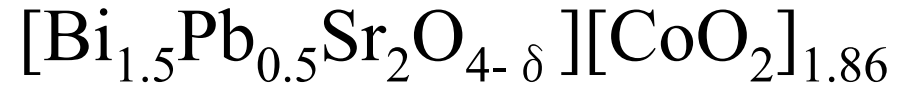

$$S = -\frac{k_B}{e}\ln\left(\frac{g_3}{g_4}\frac{x}{1-x}\right)$$

Increase of 'Co^{4+}' associated to a decrease of S

Generalized Heikes formula : increase of v_{Co}

3.59 for BSCO and 3.65 for BPSCO

Na$_x$CoO$_2$
Misfits

BiSrPbCoO single crystals : modification of α
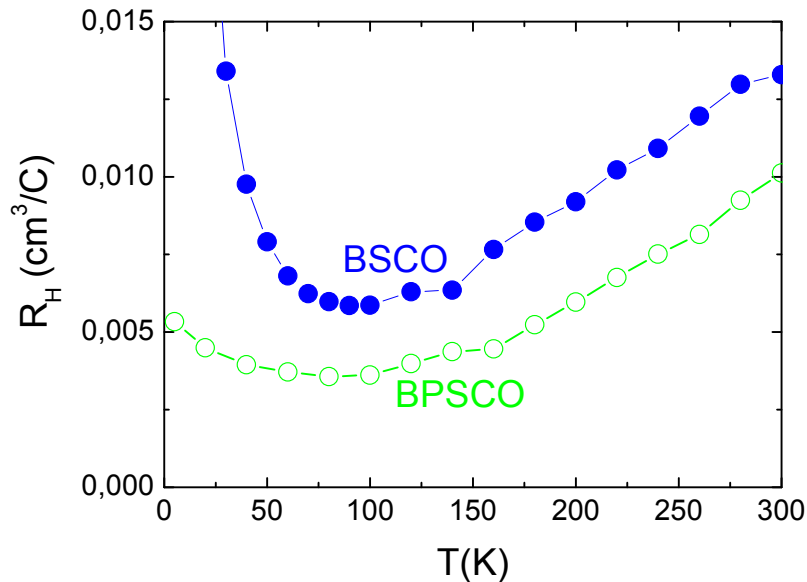
At 100K
1.06 $\times$ 10^{21} cm^{-3} for BSCO
1.73 $\times$ 10^{21} cm^{-3} for BPSCO

Increase of v$_{Co}$
3.11
3.18

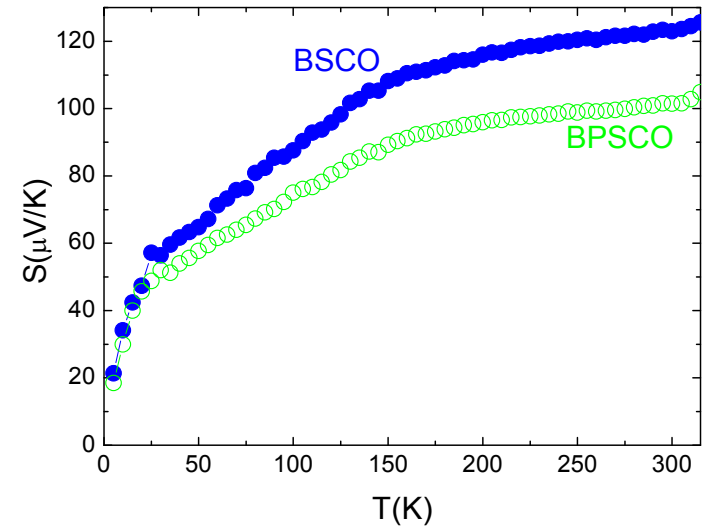t- J model : Linear T dependence of R$_H$
t ~10 – 40K
Justifies the Heikes formula?
B. Kumar et al., PRB68, 104508 (2003)
Y. Wang et al., cond-mat/0305455
G. Leon et al. , PRB78, 085105 (2008)

W. Kobayashi et al., JPCM21, 235404 (2009)

Influence du b_1/b_2

Na_xCoO_2
Misfits

b_1 : plans NaCl / b_2 : plans CoO_2
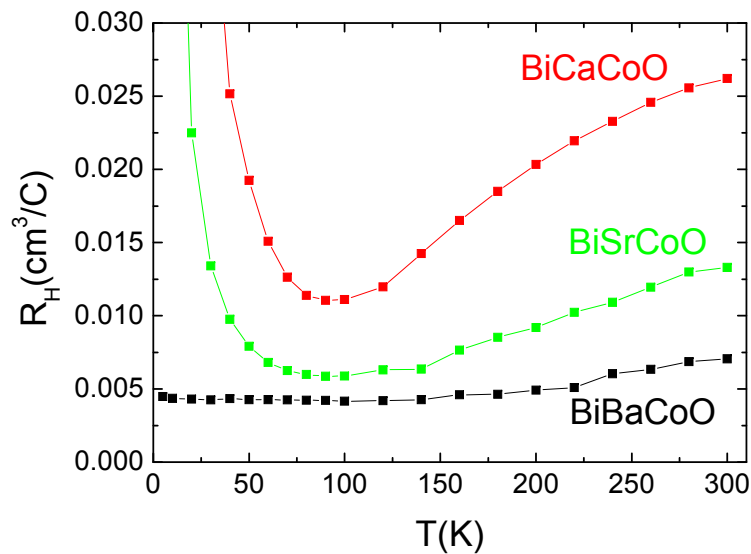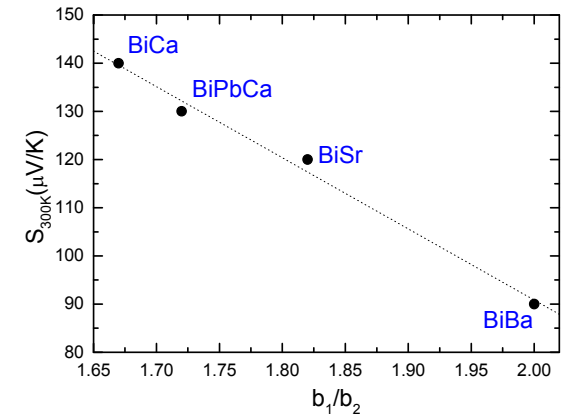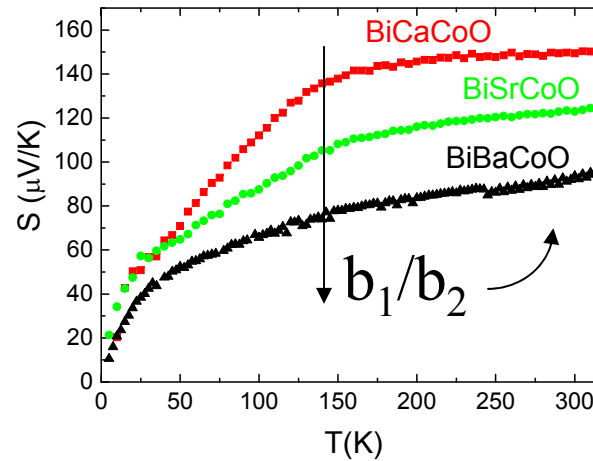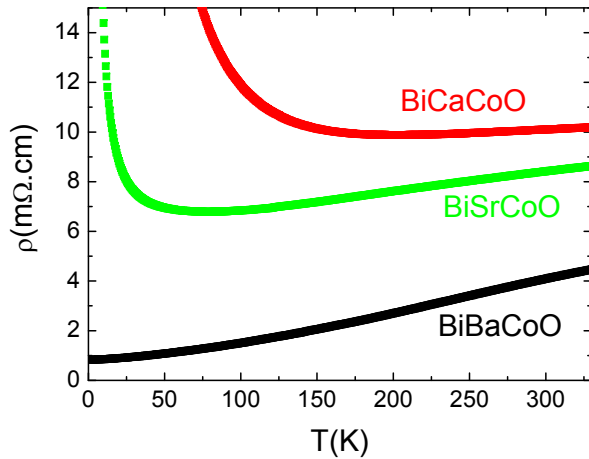
Si $b_1/b_2 \nearrow$, concentration en Co^{4+}

$$v_{Co} = 4 - \frac{\alpha}{b_1/b_2}$$

⇨ **S à 300K dépend du taux de Co^{4+} modifié via le b_1/b_2**

Taux de porteurs ~ 10^{21} cm^{-3}, plus élevé que pour les matériaux conventionnels

S. Hébert et al., PSSA210, 69 (2013)

Heikes formula

$$S = -\frac{k_B}{|e|} \ln(\frac{g_4}{g_3} \frac{1-x}{x})$$

Co valency in BiCaCoO/ BiSrCoO / BiBaCoO?

Spin and orbital degeneracy
Co^{3+} LS + Co^{4+} LS : β=1/6

Heikes β = 0

Spin degeneracy
Co^{3+} S = 1/2 + Co^{4+} S=0 : β=1/2
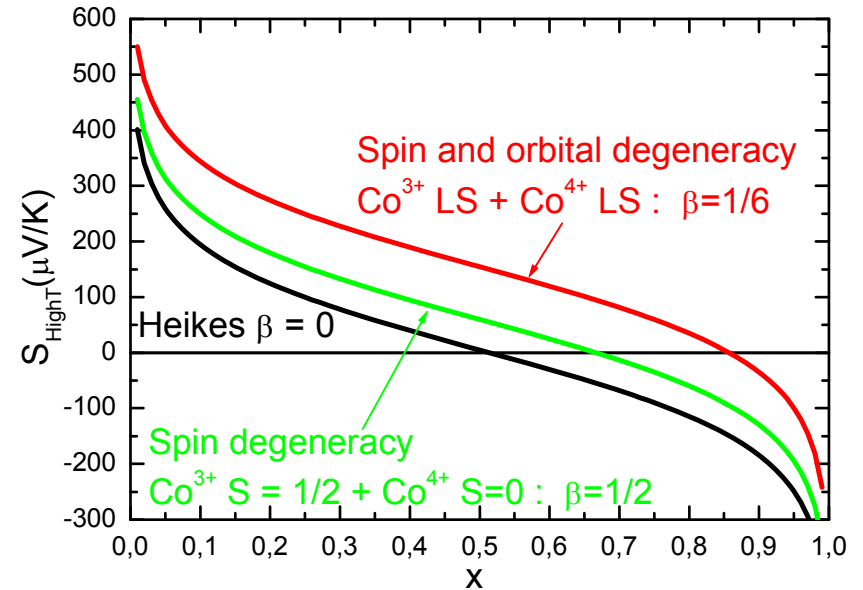
Heikes (S at 300K)	Hall effect
3.5 -3.7 for g_4 / g_3 = 6	3.05 -3.15

Na_xCoO_2
Misfits

Carrier concentration changes with misfit ratio b_1/b_2
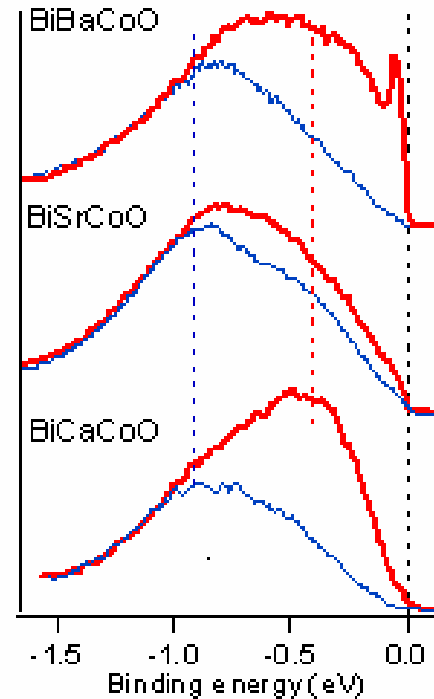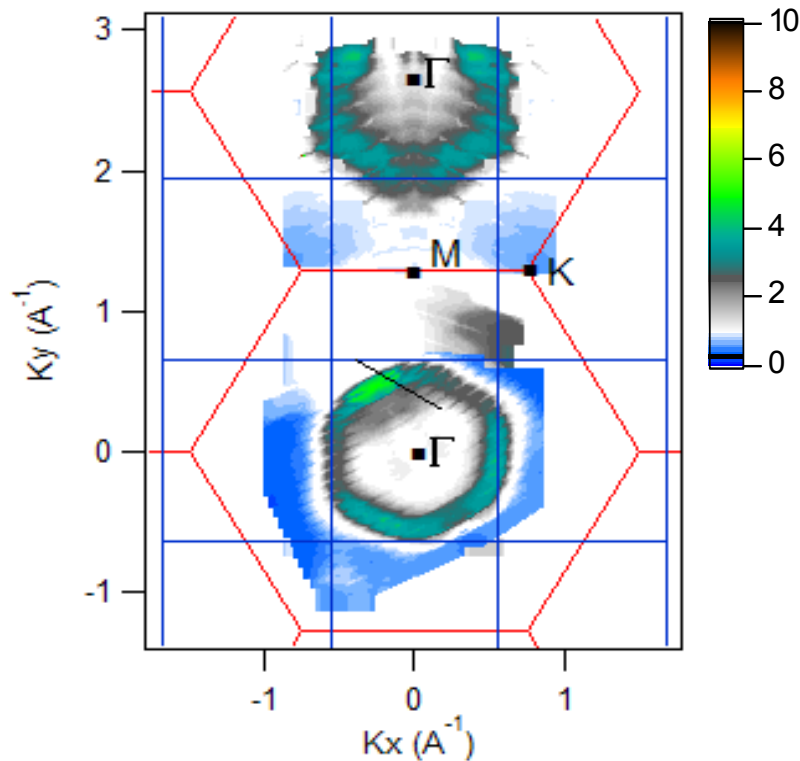
ARPES
Collaboration with

V. Brouet et al., LPS Orsay

Reliable data for v_{Co} are obtained for BiBaCoO

$$v_{Co} = 4 - \frac{\alpha}{b_1/b_2} \quad (\alpha = const)$$
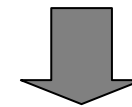
Co$^{3.2+}$ for BiSrCoO
Co$^{3.1+}$ for BiCaCoO

single hole-like fermi surface (a_{1g} character)

$k_F = 0.57 \pm 0.05$ Å^{-1} for BiBaCoO

→ similar to k_F of Na_xCoO_2 (x=0.7)

→ Co$^{3.3+}$ for BiBaCoO
   V. Brouet et al., PRB76, 100403 (2007)

Heikes formula

Na_xCoO_2
Misfits

$$S = -\frac{k_B}{e} \ln\left(\frac{g_3}{g_4} \frac{x}{1-x}\right)$$

Spin and orbital degeneracy
Co^{3+} LS + Co^{4+} LS : $\beta=1/6$

Heikes $\beta = 0$

Spin degeneracy
Co^{3+} S = 1/2 + Co^{4+} S=0 : $\beta=1/2$
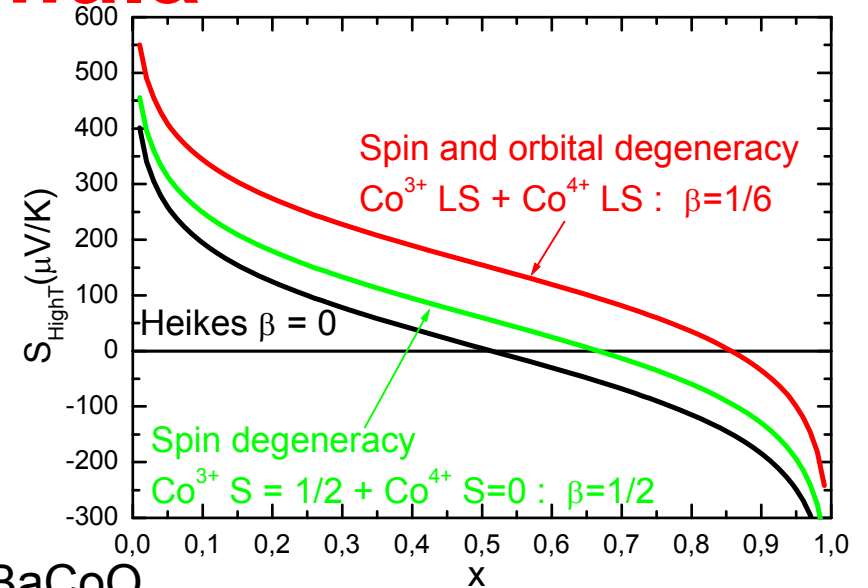
Valence du Co dans la famille BiCaCoO/ BiSrCoO / BiBaCoO

Heikes g_3/g_4 = 1/6 S à 300K	Seebeck avec S(H) g_3/g_4 = 1 BiCaCoO	Effet Hall	ARPES BiBaCoO	RMN	Susceptibilité BiCaCoO
3.5 -3.7	3.33 P. Limelette et al., PRL97, 046601 (2006)	3.05 -3.15 W. Kobayashi et al.	3.3 V. Brouet et al., PRB76, 100403 (2007)	3.1 -3.3 J. Bobroff et al., PRB76, 100407 (2007)	3.24 M. Pollet et al., JAP101, 083708 (2007)

g_3 / g_4 = 1/2 instead of 1/6

Confirms the results in BiCaCoO : v_{Co} = 3.24

M. Pollet et al., JAP101, 083708 (2007)

Na$_x$CoO$_2$ Misfits

Orbital filling in Na$_x$CoO$_2$ and misfit cobaltites with edge-shared CoO$_6$

LS Co^{3+}/Co^{4+} mixed-valency

↓

metallicity

MB Lepetit PHYSICAL REVIEW B **74**, 184507 (2006)
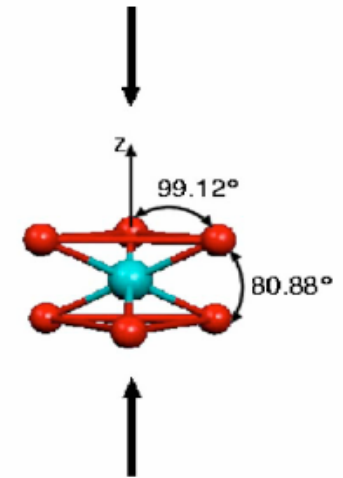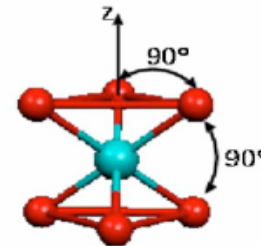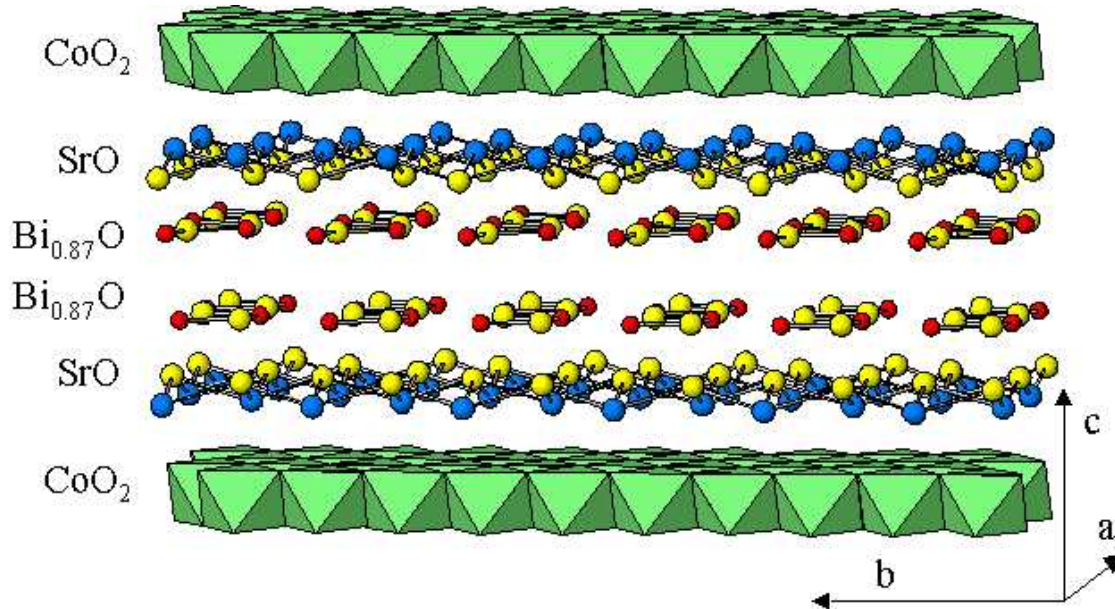
Ligand field splitting :
trigonal distortion

$\beta = 1/6$
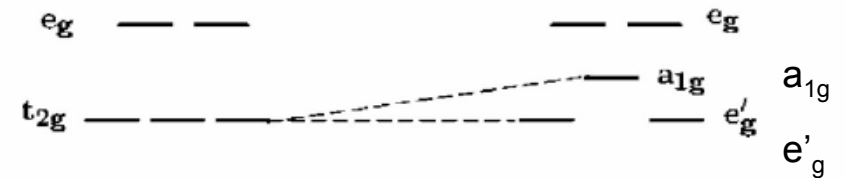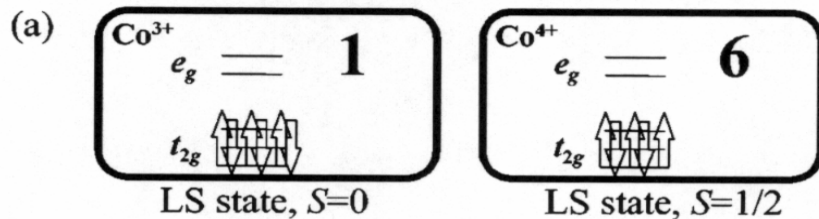
1 for Co^{3+} but 2 instead of 6 for Co^{4+}

$\beta = 1/2$

Na$_x$CoO$_2$
Misfits

Importance des corrélations électroniques

Pour T→0

$$q = \frac{S}{T}\frac{N_{Av}e}{\gamma} = cste$$

S ~ γT
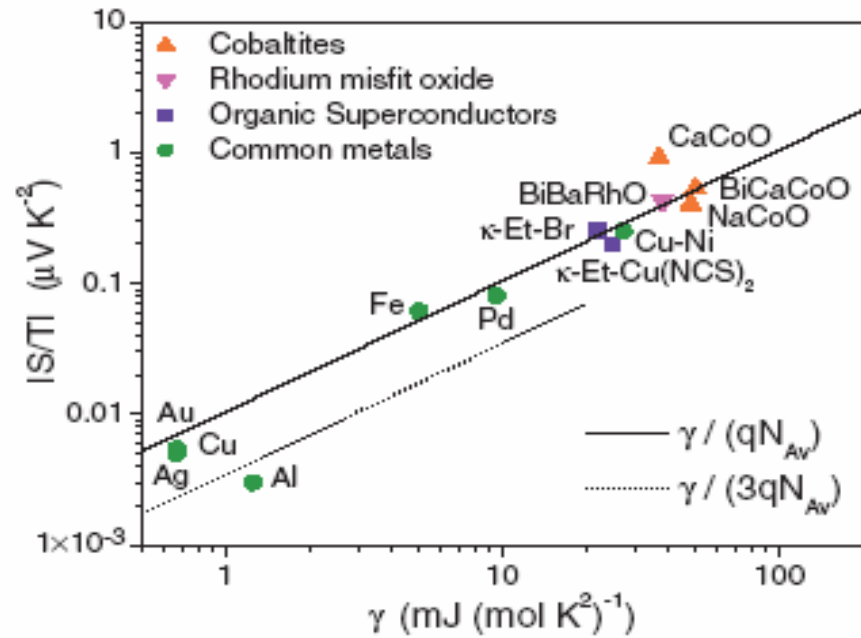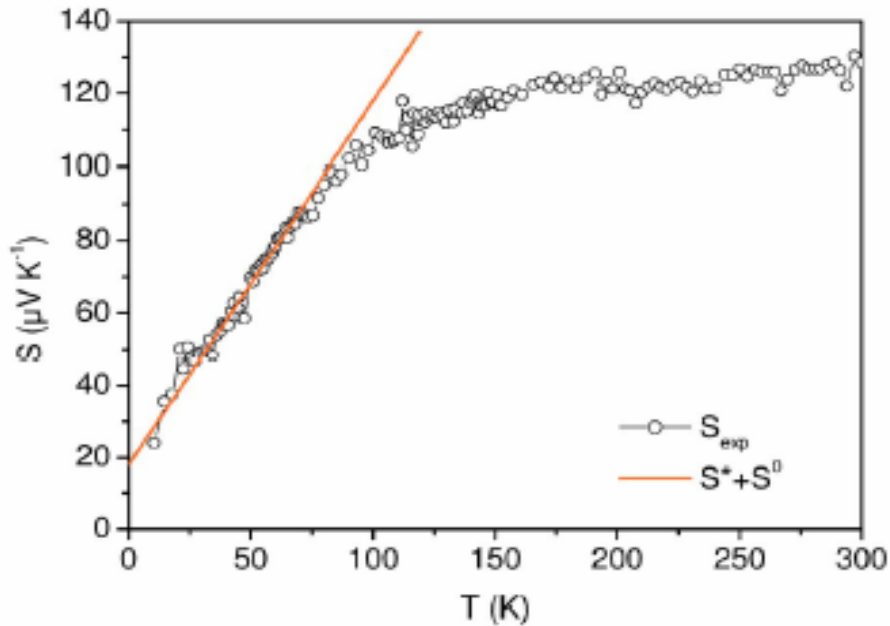
P. Limelette, PRB71, 233108 (2005)

P. Limelette, PRL97, 046601 (2006)

Low T : Spin entropy

BiCaCoO : excess of S at low T

A. Maignan et al., JPCM 15, 2711 (2003)
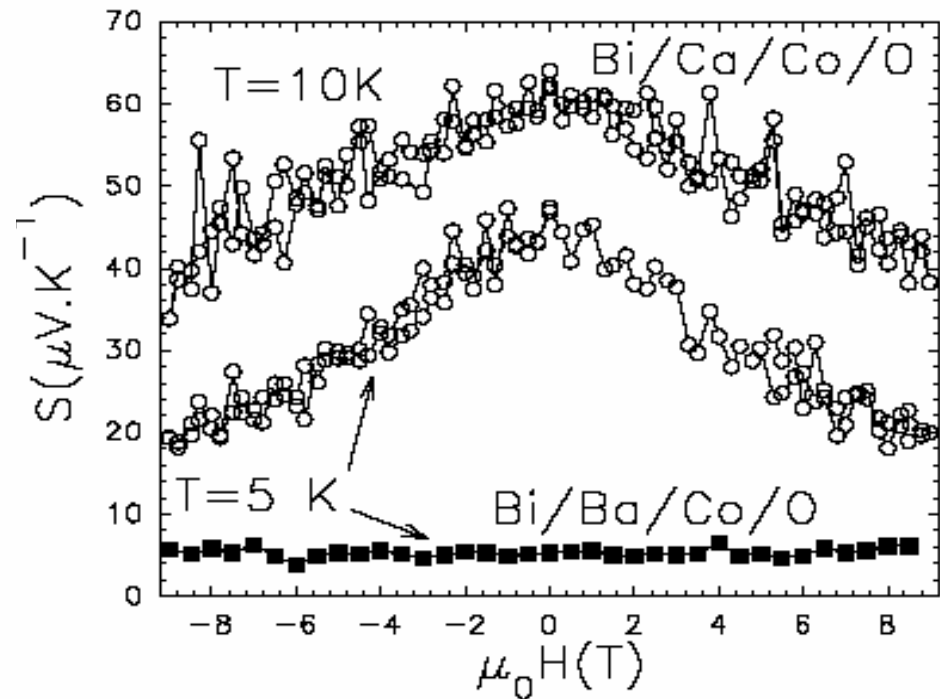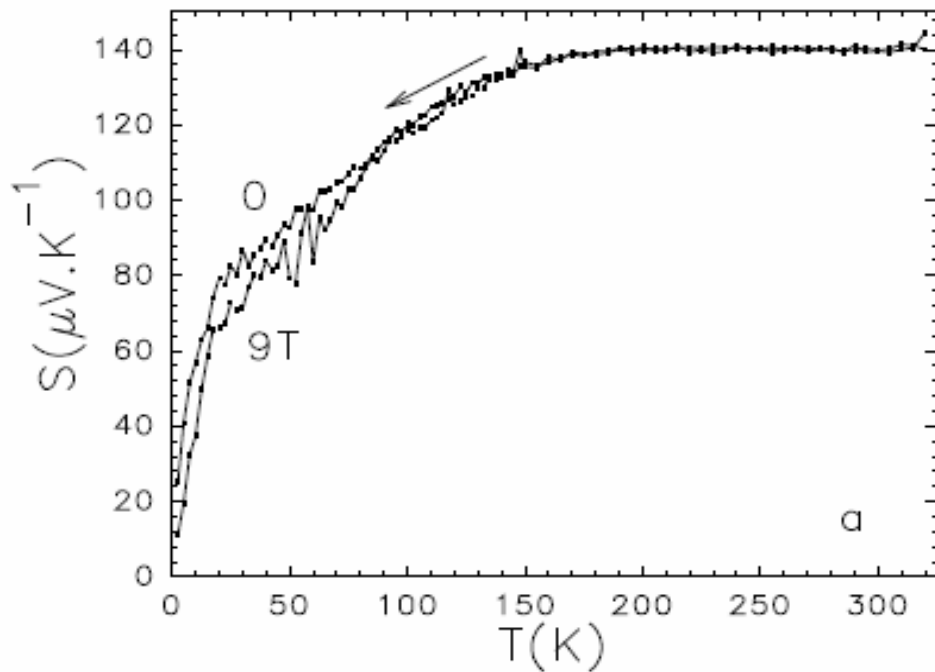
Observed also in Na$_x$CoO$_2$

[Wang et al. Nature 423, 425 (2003)]

Spin entropy at low T

Misfit BiCaCoO

A. Maignan et al., JPCM15, 2711 (2003)

Decrease of S under field at low T
Due to the alignement of paramagnetic spins
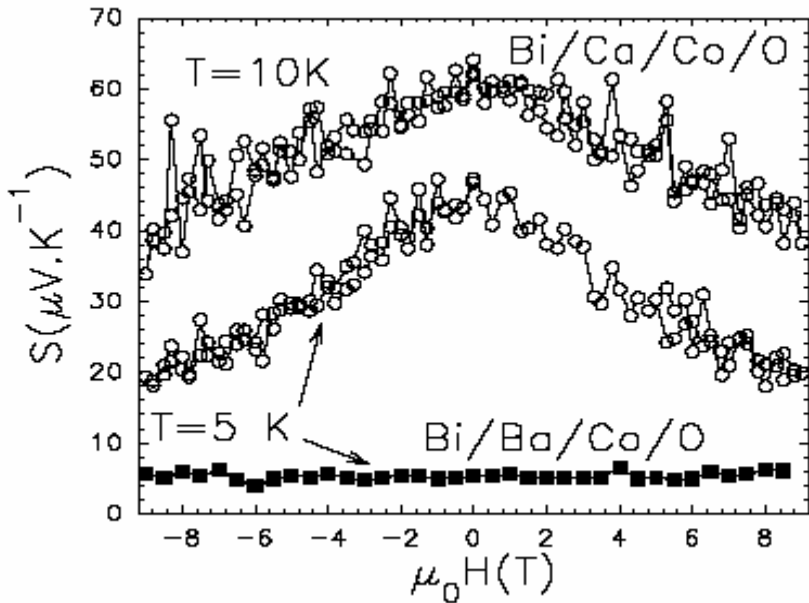
Peak of susceptibility

J. Bobroff et al., PRB76, 100407 (2007)
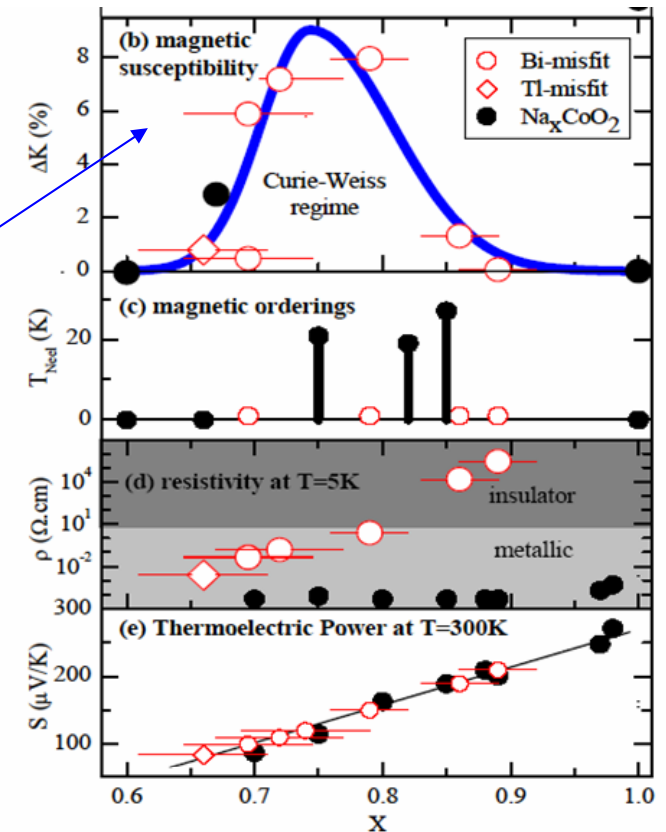
Scaling law for S(H) : paramagnetic spins S=1/2
Brillouin function

$$S(x)/S(0) = (\ln[2\cosh(x)] - x\tanh[x])/\ln(2).$$

$Na_{0.7}CoO_2$

P. Limelette et al., PRL97, 046601 (2006)

Y. Wang et al., Nature423, 425 (2003)

Na$_x$CoO$_2$
Misfits

Misfit oxides

NaCl-like triple layer (RS)
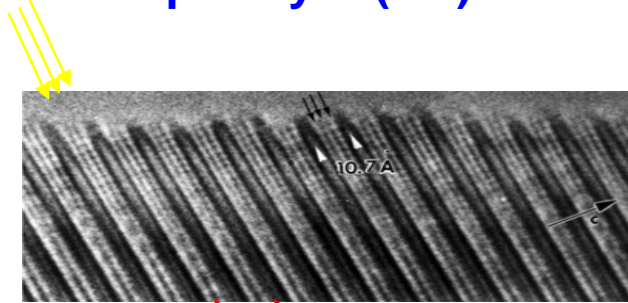
CoO$_2$ (type CdI$_2$)
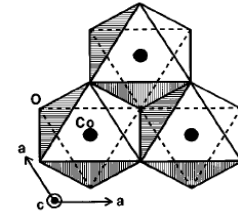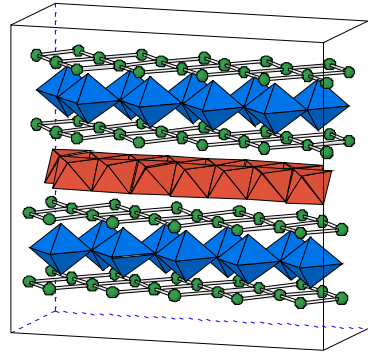
Co^{3+} (3d^6) / Co^{4+} (3d^5)
Low spin : t$_{2g}$ orbitals
+ triangular network
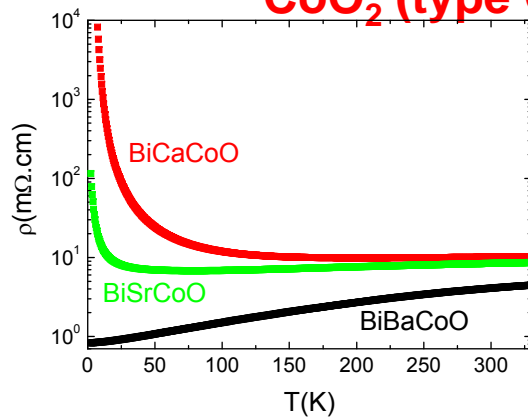
For T > 100K : metallicity + large S
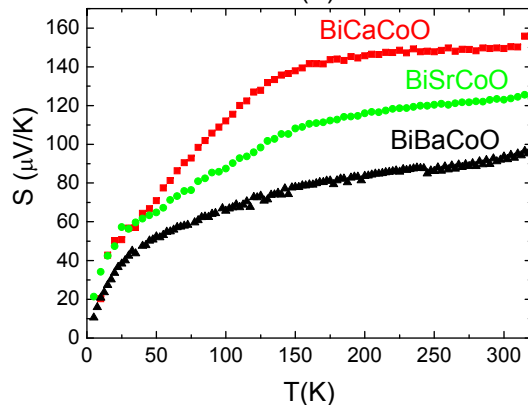
- **High T** : Seebeck depends on Co^{4+}
Heikes formula with spin / orbital degeneracy

- **Low T :** electronic correlations : S ~ γT
+ spin entropy depending on doping

- **High T limit** : small t from Hall effect.
Justifies the Heikes formula?

S. Hébert et al., PRB64, 172101 (2001), P. Limelette et al., PRL97, 046601 (2006), W. Kobayashi et al., JPCM21, 235404 (2009)

Thermoelectric power of misfits

High T Seebeck, depends on Co^{4+}
(Heikes formula with $\beta = 1/2$)

BiCaCoO

Spin entropy (depending on doping)
Electronic correlations : $S \sim \gamma T$

Power factor

enhancement for BiBaCoO and BiPbSrCoO

P is almost independent of carrier concentration

BiPbSrCoO

BiBaCoO

BiSrCoO

BiCaCoO

2.10^{-4} Wm^{-1}K^{-2} at 300K

Power Factor (μW/cmK^2)

Temperature (K)
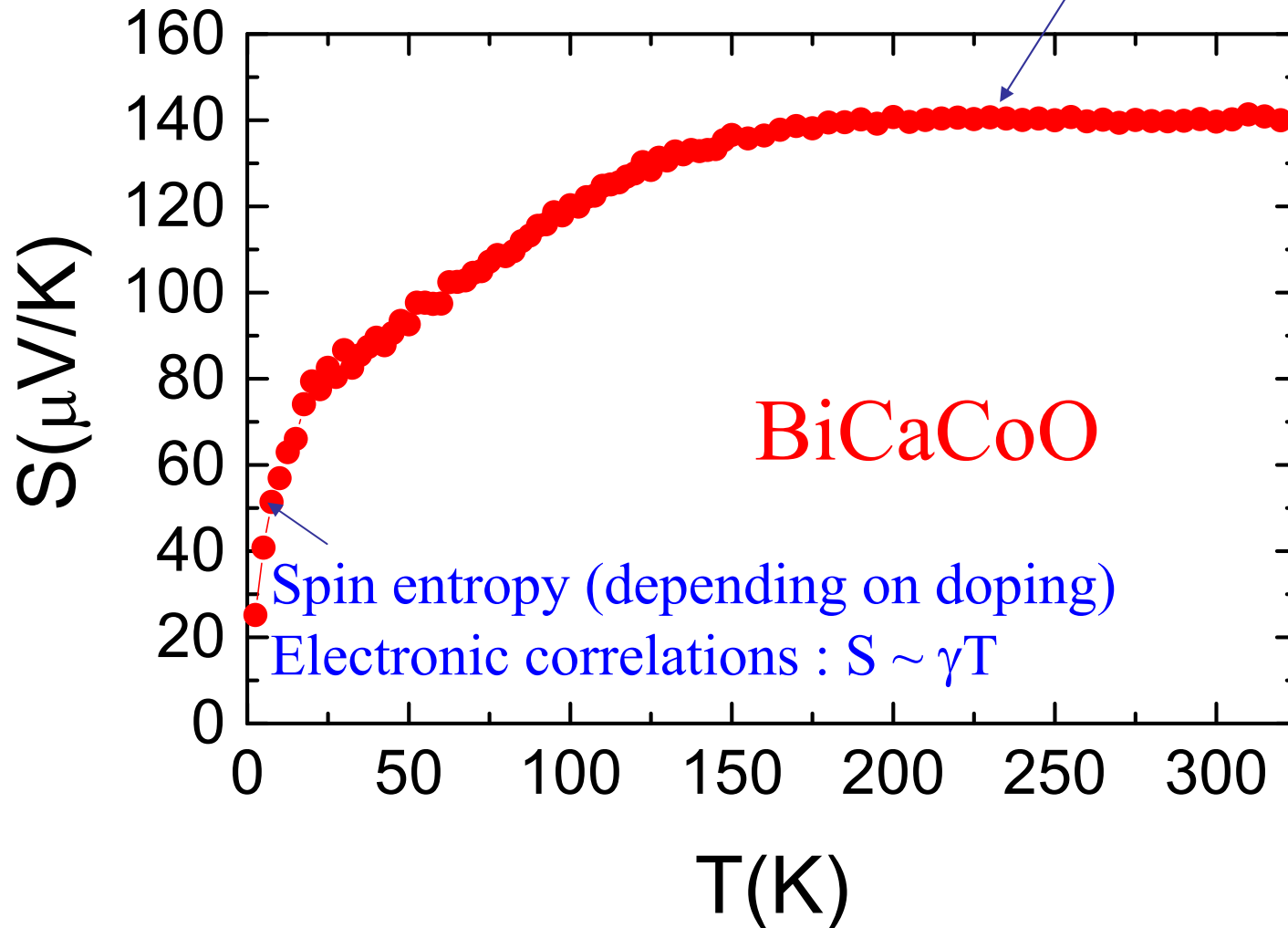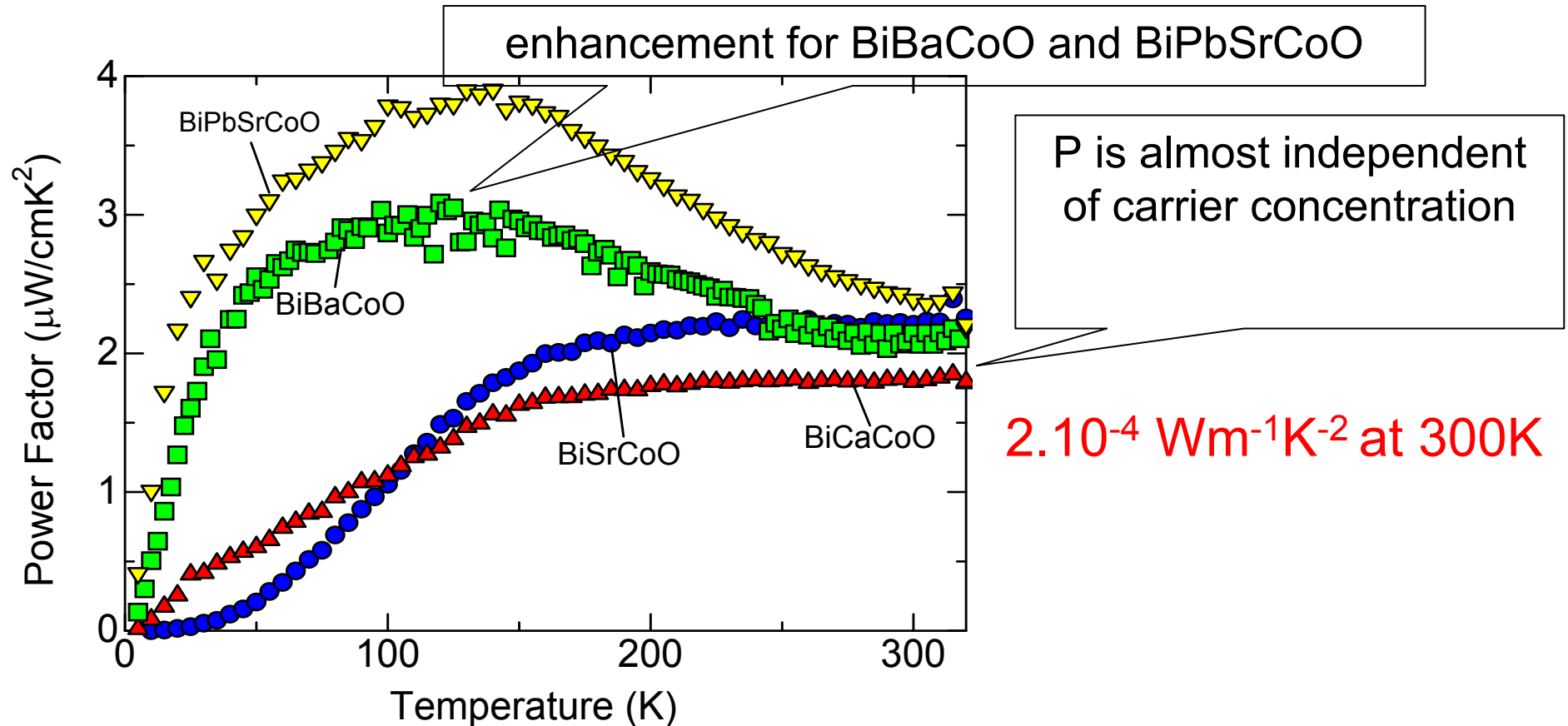
In conventional semiconducting thermoelectric material such as Bi$_2$Te$_3$, *n* is an important parameter to tune the properties.

How to modify the electronic properties?
Influence of the block layer?

Role of the block layer?
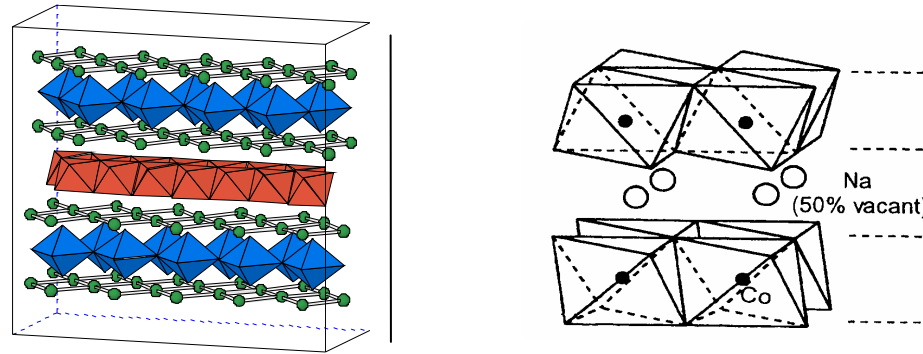
Curie-Weiss

• Role of Na$^+$: Curie-Weiss behavior obtained by introducing the electrostatic potential of Na$^+$ (Co^{3+} S = 0 / Co^{4+} S = 1/2)
C. Marianetti et al., PRL98, 176405 (2007)
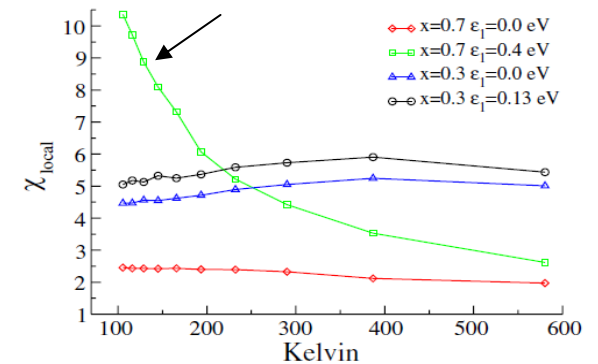
•Kagomé lattice in Na$_x$CoO$_2$ with x = 2/3 : strong electronic correlations
F. Lechermann et al., PRL107, 236404 (2011)
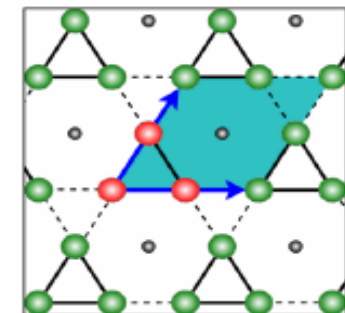
Thermal conductivity

Measurements of single crystals (Harman method)
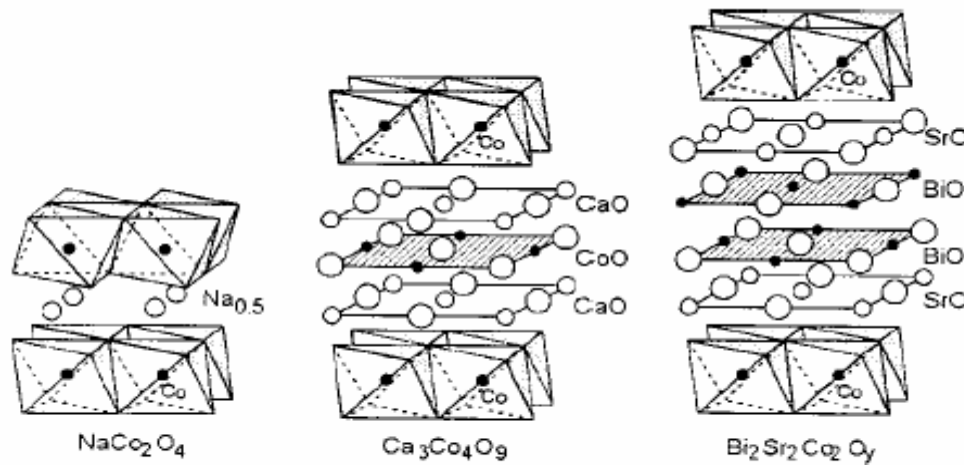
FIG. 1. Crystal structure of the layered cobalt oxides.

κ smaller in misfits

Influence of incommensurability?

A. Satake et al., JAP96, 931 (2004)
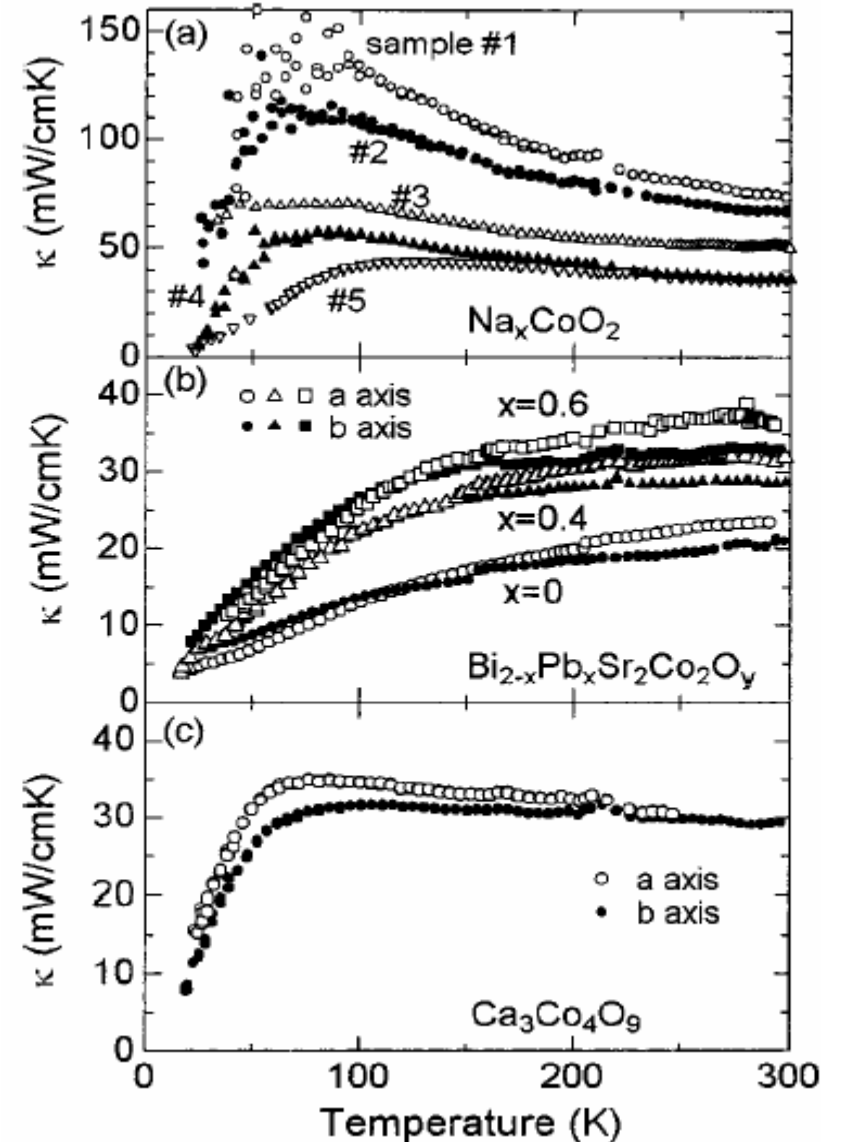
Conclusion

• Charge transfer between the layers :
S$_{300K}$ mostly depends on the ratio Co^{3+}/Co^{4+}

• Low T : electronic correlations influence (S ~ γT) + S(H) term

• Small κ

⇨ Power factor is constant : modification of the block layers?
⇨Influence on thermal conductivity?

Conclusion

ZT (n type) < ZT (p type)
Thermal conductivity : mostly coming from the lattice

- n type oxides : degenerate semi-conductors
Seebeck described in a first approach by Mott's formula
Polaronic transport

- p type oxides

Seebeck coefficient : **Major role of the**
spin and orbital term
Importance of electronic correlations

$$S = -\frac{k_B}{|e|} \ln(\beta \frac{1-x}{x})$$

How to enhance ZT??

↳Investigation of thermal conductivity

↳Microstructures to reduce thermal conductivity

↳ Low dimensional structures

↳Nanostructuration and electronic correlations?

↳Investigation of new families (pb of stability!)

↳ Anionic subsitutions (oxyselenides)

2D electron gas in SrTiO$_3$

H. Ohta et al., Nat. Mater. 6, 129 (2007)

SrTi$_{1-x}$Nb$_x$O$_3$

Nanostructuration :
Increase of S

$$\sigma_{eff.} = \sigma_{2DEG}/(1 + N_{barrier})$$

$$ZT_{eff.} = ZT_{2DEG}/(1 + N_{barrier})$$

'ZT' = 2.4!
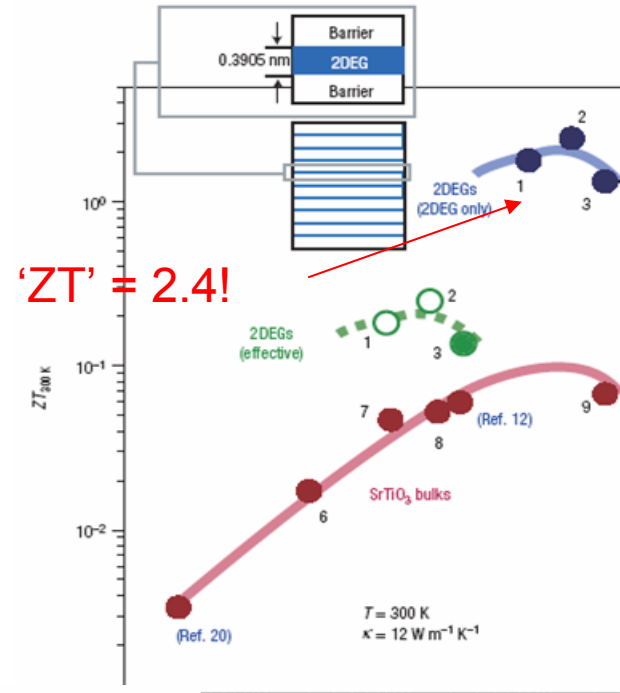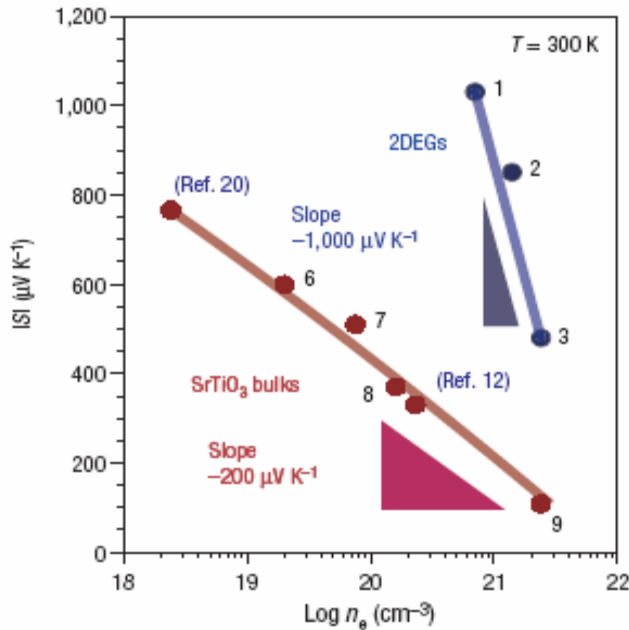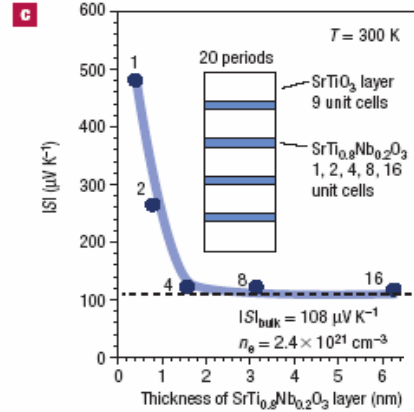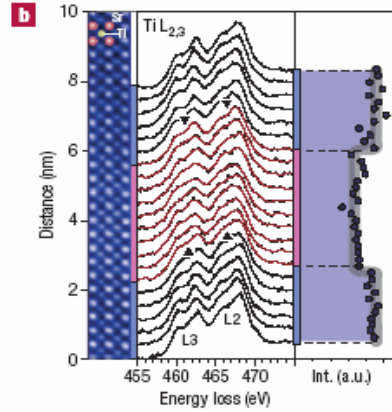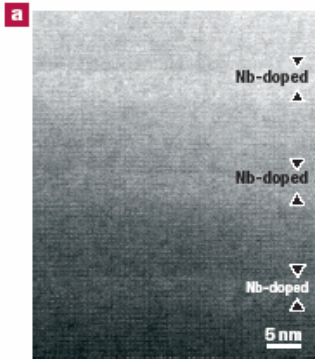
$$|S| = -k_B/e \cdot \ln 10 \cdot A \cdot (\log n_e + B)$$

κ of SrTiO$_3$ single crystals

Na$_x$CoO$_2$ nanowires

Sol-gel electrospinning

Same technique as for
Ca$_3$Co$_4$O$_9$
Lin et al., J. Phys.
Chem. C 114, 10061
(2010)

$\rho \sim \Omega.m$?
Resistivity
overestimated by 3
orders of
magnitude by the
measurement
technique?
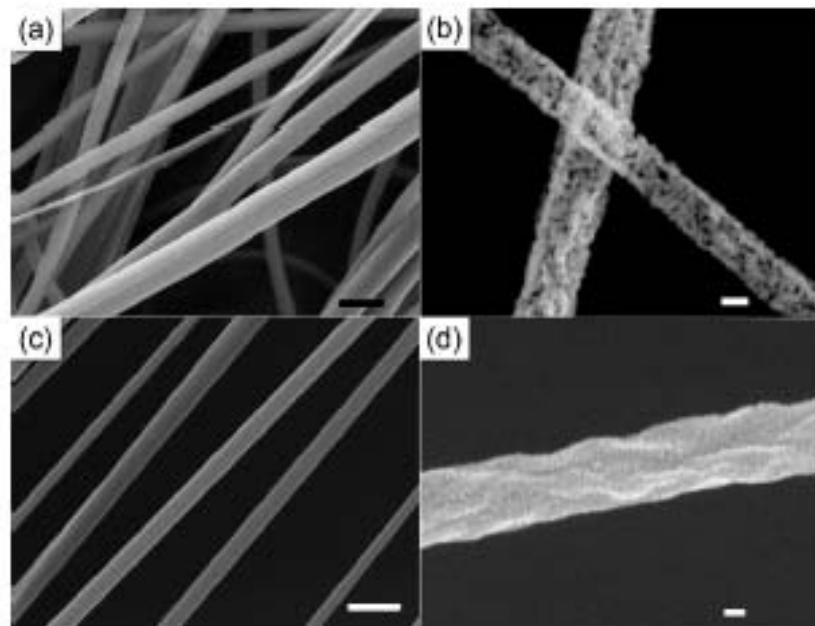
Figure 1. SEM image of NaCo$_2$O$_4$ nanofibers before and after annealing, synthesized with two different solvents; (a) and (b) methanol-based nanofibers before (a) and after (b) annealing; (c) and (d) water-based nanofibers before (c) and after (d) annealing; scale bars in (a) and (c) represent 1 μm, and in (b) and (d) represent 100 nm.

F. Ma et al., J. Phys. Chem. C 114, 22038 (2010)

Substitution anionique : BiSrCuSeO
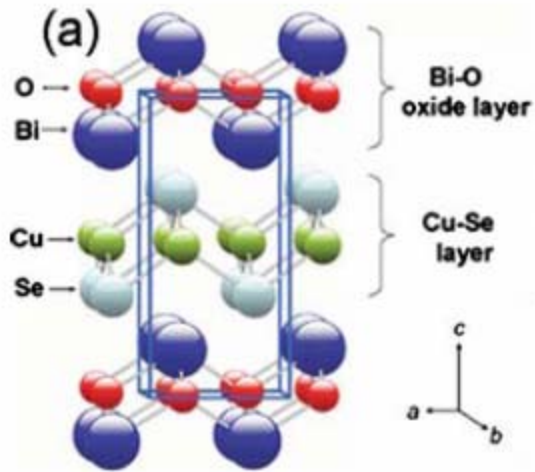
Augmentation de la covalence

⬇

Augmentation de la conductivité électrique
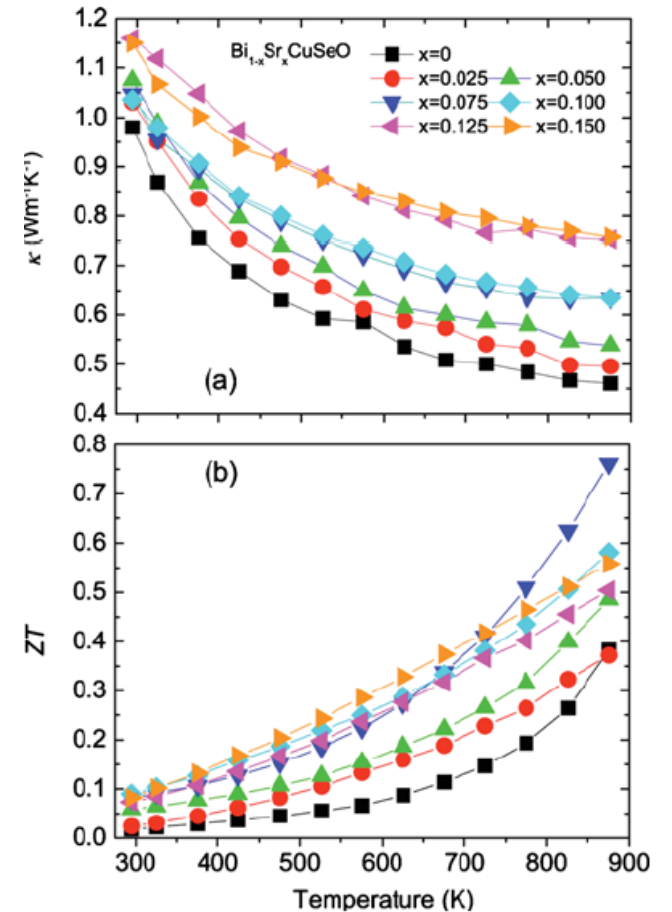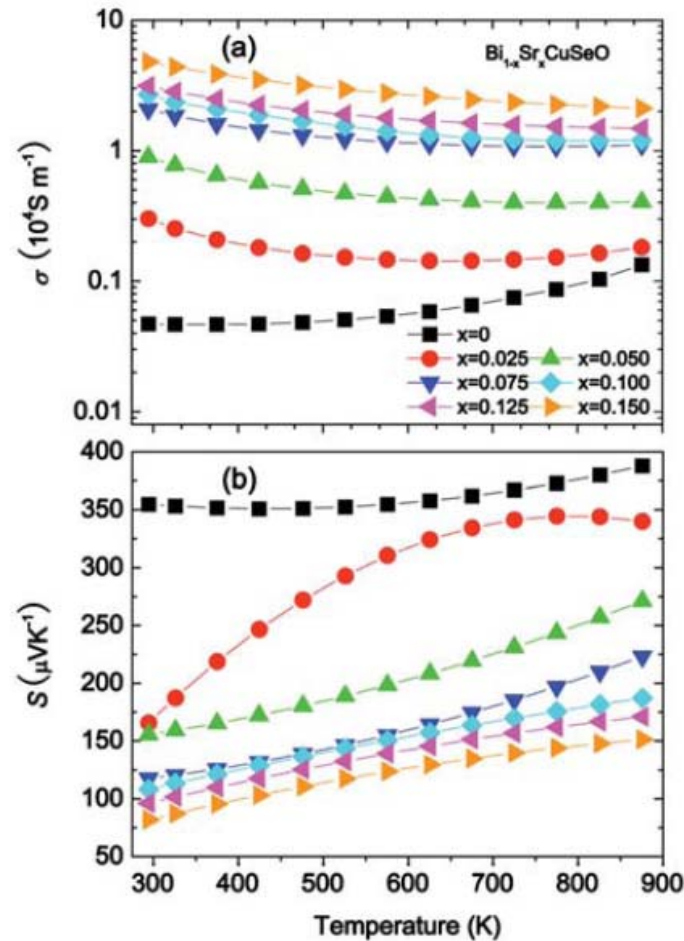
Dopage par des trous dans les couches $(Bi_2O_2)^{2+}$ via la substitution de Sr^{2+} par Bi^{3+}

L. D. Zhao et al., APL97, 092118 (2010)

Influence d'un déficit en Cu
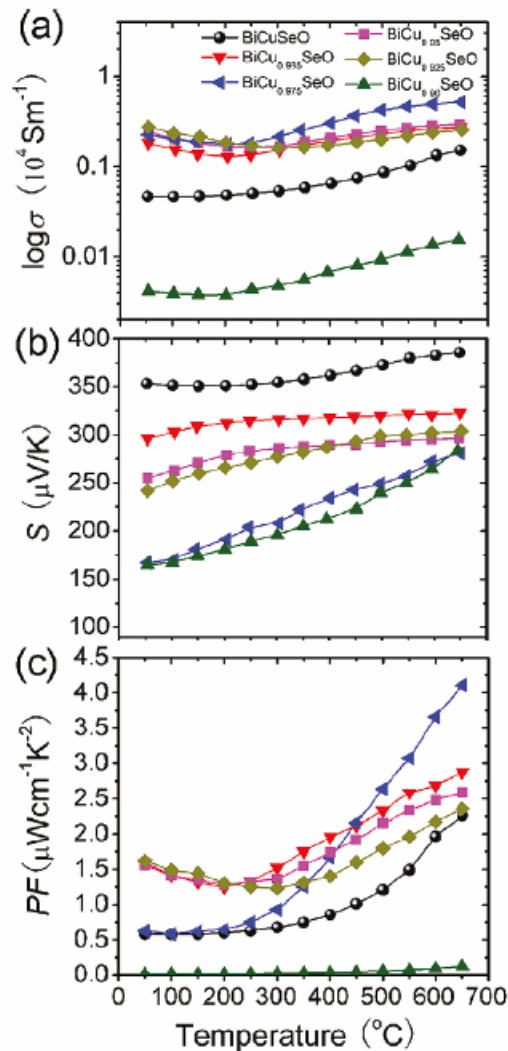
Figure 3. Temperature dependence of (a) electrical conductivity, (b) Seebeck coefficient, and (c) power factor of BiCu$_{1-x}$SeO ceramics.
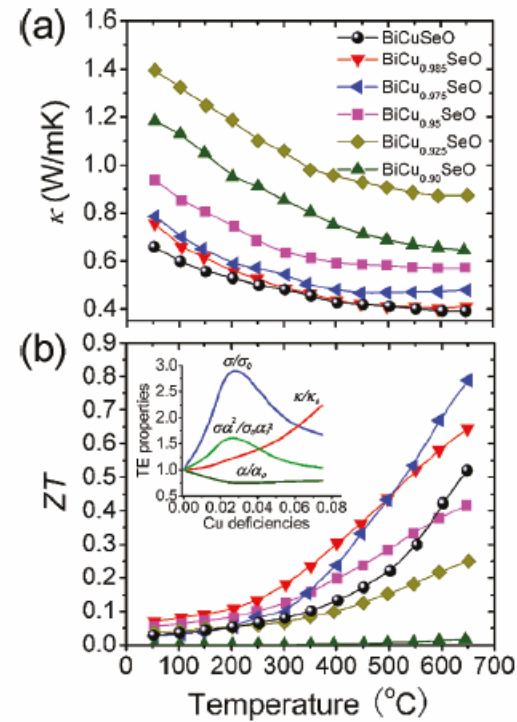
Figure 4. Temperature dependence of (a) thermal conductivity and (b) ZT of BiCu$_{1-x}$SeO samples. The inset in (b) shows the normalized TE properties of BiCu$_{1-x}$SeO samples at 650 °C as a function of x.

Cu deficiency in the (Cu$_2$Se$_2$)$^{2-}$ layer

L. Yong et al., JACS133, 20112 (2011)

Collaborators

Laboratoire CRISMAT
Wataru Kobayashi (Tsukuba), Hidefumi Takahashi (Nagoya),
Ramzy Daou, Raymond Frésard, Emmanuel Guilmeau,
Antoine Maignan, Christine Martin,
Denis Pelloquin, Olivier Perez

Patrice Limelette, GREMAN, Tours
Julien Bobroff, Véronique Brouet, LPS, Orsay

$Sr_xBa_{1-x}Nb_2O_{6-\delta}$ Ferroelectric-thermoelectrics: Crystal anisotropy, conduction mechanism, and power factor

Soonil Lee,[a] Rudeger H. T. Wilke, Susan Trolier-McKinstry, Shujun Zhang, and Clive A. Randall

Center for Dielectric Studies, Materials Research Institute, The Pennsylvania State University, University Park, Pennsylvania 16802, USA

+ Low thermal conductivity

Extremely reduced samples to get better conductivity
Stability?

Prototypes à base d'oxydes

1er prototype en 2000

n : $Ba_{0.4}Sr_{0.6}PbO_3$ Z = 2.10^{-4} K^{-1} à 673K (ZT = 0.13)
p : $Li_{0.025}Ni_{0.975}O$ Z = 0.75 10^{-4} K^{-1} à 1273K (ZT = 0.095)

a) Joining by sinter forging

p-type Li doped NiO
n-type (BaSr)PbO$_3$

b) Cutting junction

c) TE power factor measurement

A
junction
C
Air
Cold
Hot
MgO sheet
B
voltage leads
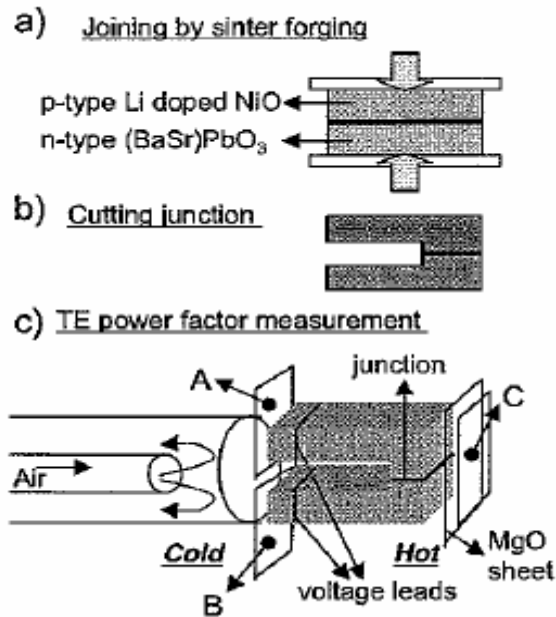
Pour chaque jambe : 4.8 ×4.9 × 17.5 mm^3

Une paire : 7.91mW
T_H = 987K
ΔT = 552K

W. Shin et al., JJAP39, 1254 (2000)

Dispositifs

Prototypes à base d'oxydes

$$n : Ca_{0.92}La_{0.08}MnO_3 / p : Ca_{2.75}Gd_{0.25}Co_4O_9$$
$$8 \text{ paires } 3 \times 5 \times 30 \text{ mm}^3$$
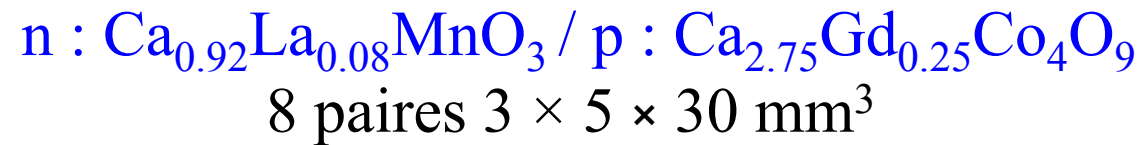
TABLE I. Thermoelectric power S, resistivity ρ, and power factor S^2/ρ of p and n legs used for fin-type device.

Materials	ρ-T	S (700 °C) μV/K	ρ (700 °C) mΩ cm	S^2/ρ (700 °C) 10^{-4}W m^{-1} K^{-2}
$Ca_{2.75}Gd_{0.25}Co_4O_9$ (p leg)	Semiconducting	185	7.8	4.8
$Ca_{0.92}La_{0.08}MnO_3$ (n leg)	Metallic	−120	6.6	2.2

$$T_h = 1046K , \Delta T = 390K,$$
$$P=63.5mW$$

TABLE II. Thermal conditions, open circuit voltage V_o, and maximum output power P_{max} for fin-type device with eight p−n couples.

Condition	T_h, °C	ΔT, °C	V_o, mV	P_{max}, mW
a	477	235	550	19.8
b	580	290	694	31.8
c	672	335	838	46.5
d	773	390	988	63.5

T_h: Hot side temperature.
ΔT: Temperature difference.

Stabilité

$T_C = 370°C$
$T_H = 650°C$

I. Matsubara et al., APL 78, 3627 (2001)

Dispositifs
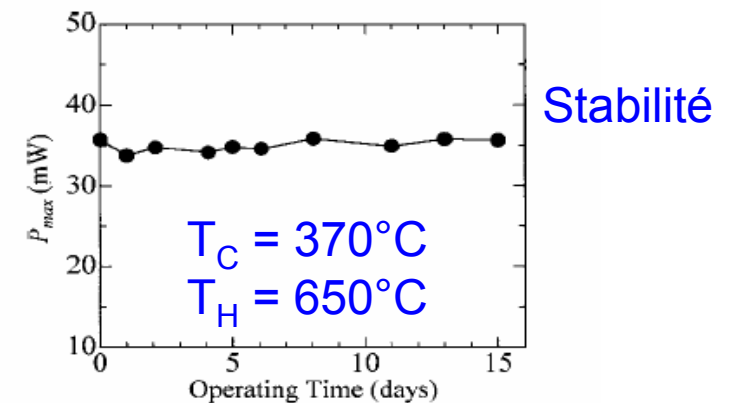
$La_{0.9}Bi_{0.1}NiO_3$ / $Ca_{2.7}Bi_{0.3}Co_4O_9$

n : $La_{0.9}Bi_{0.1}NiO_3$ / p : $Ca_{2.7}Bi_{0.3}Co_4O_9$
1 jonction : T_H = 1073K, ΔT = 500K, P = 94mW

140 paires
T_H = 1072K, ΔT = 551K

Module (interior)   Furnace
d.c.-d.c. converter
Mobile phone

FIG. 4. (Color) Comparative photographs of the oxide module and a mobile phone, and a demonstration of charging a lithium-ion battery in the mobile phone. Red LED on the mobile phone indicates charging of the lithium-ion battery is in progress.

Chargeur pour téléphone portable
T_H = 1072K!
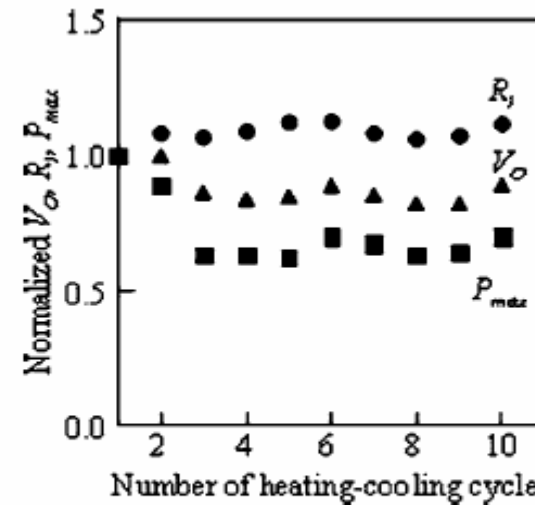
FIG. 3. Thermal resistance of the oxide module at T_H of ~723 K and ΔT of ~385 K. R_I (●), V_O (▲), and P_{max} (■) normalized by the values of the first trial are plotted against the number of heating-cooling cycles.

R. Funahashi et al., APL 85, 1036 (2004)
R. Funahashi et al., JAP99, 066117 (2006)

Dispositifs

$$Ca_3Co_4O_9/Ca_{0.95}Sm_{0.05}MnO_3$$

$4 \times 4 \times 5$ ou 10 mm^3
2 paires

$T_H = 1025K$, $\Delta T = 925K$, $P = 31.5mW$

E. Sudhakar Reddy et al., J. Phys. D Appl. Phys. 38, 3751 (2005)
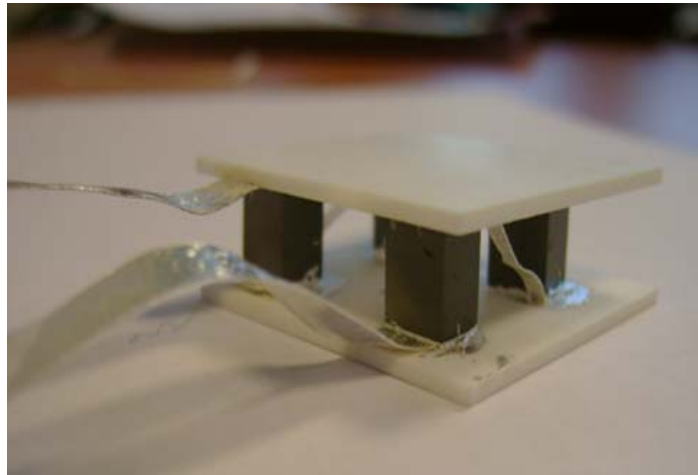
Prototype 'unileg'
 Un seul matériau (ici type n)

Choix du matériau avec le meilleur ZT
Diminution des contraintes mécaniques

C. Goupil, S. Lemonnier et al.

Comparaison des modules

Manufacturing factor
$$MF = R_{ideal} / R_{int},$$

Name	**Materials**	Type	Nb Couple	Power (W)	**MF**
Funahashi et al.	$Ca_{2.7}Bi_{0.3}Co_4O_9$ / $La_{0.9}Bi_{0.1}NiO_3$	PN	1	0.03	**0.15**
Shin et al.	(Li) NiO / (Ba, Sr) PbO_3	PN	2	0.034	**0.3**
Matsubara et al.	(Gd) $Ca_3Co_4O_9$ / (La) $CaMnO_3$	PN	8	0.089	**0.82**
Sudhakar et al.	$Ca_3Co_4O_9$ / $Ca_{0.95}Sm_{0.05}MnO_3$	PN	2	0.031	**0.57**
Present work	$Ca_{0.95}Sm_{0.05}MnO_3$/ $Ca_{0.95}Sm_{0.05}MnO_3$	N	2	0.016	**0.15**

Optimisation des contacts nécessaire!

S. Lemonnier, C. Goupil et al.

Modules et prototypes

Monolithic oxide–metal composite thermoelectric generators for energy harvesting

Shuichi Funahashi,[a)] Takanori Nakamura, Keisuke Kageyama, and Hideharu Ieki
Research Center for Next Generation Technology, Murata Manufacturing Co., Ltd., 2288 Ohshinohara, Yasu, Shiga 520-2393, Japan

Monolithic oxide–metal composite thermoelectric generators (TEGs) were fabricated using multilayer co-fired ceramic technology. These devices consisted of $Ni_{0.9}Mo_{0.1}$ and $La_{0.035}Sr_{0.965}TiO_3$ as p- and n-type thermoelectric materials, and $Y_{0.03}Zr_{0.97}O_2$ was used as an insulator, sandwiched between p- and n-type layers. To co-fire dissimilar materials, p-type layers contained 20 wt. % $La_{0.035}Sr_{0.965}TiO_3$; thus, these were oxide–metal composite layers. The fabricated device had 50 pairs of p–i–n junctions of 5.9 mm $\times$ 7.0 mm $\times$ 2.6 mm. The calculated maximum value of the electric power output from the device was 450 mW/cm^2 at $\Delta T = 360$ K. Furthermore, this device generated 100 μW at $\Delta T = 10$ K and operated a radio frequency (RF) transmitter circuit module assumed to be a sensor network system. © 2011 American Institute of Physics. [doi:10.1063/1.3599890]
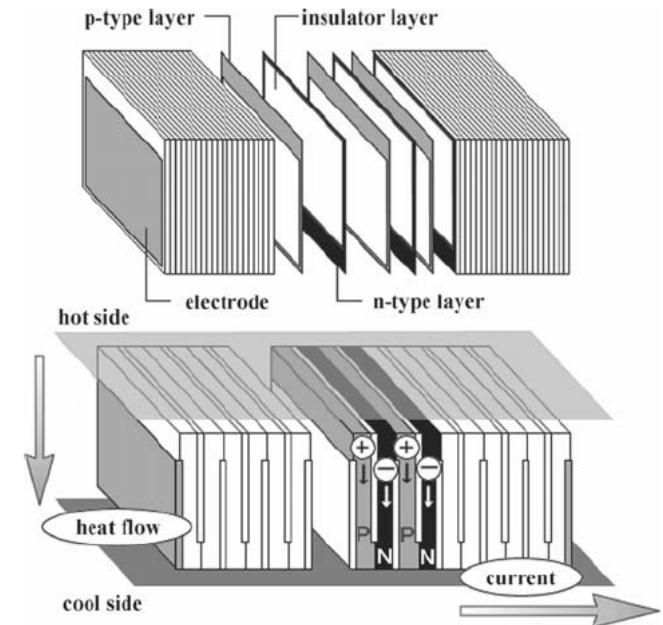

FIG. 1. Structure of the monolithic thermoelectric generator (TEG), based on multilayer ceramic capacitor (MLCC) technology. The p- and n-type layer printed insulators were stacked and co-fired.

Type n : $SrTiO_3$ dopé au La
450mW/cm^2 pour $\Delta T = 360$K